π-Conjugated Copolymers of Controlled Sequence

by

Jonas Robert Locke

A dissertation submitted in partial fulfillment
of the requirements for the degree of
Doctor of Philosophy
(Chemistry)
in The University of Michigan
2012

Doctoral Committee:

Assistant Professor Anne J. McNeil, Chair
Professor Brian J. Love
Professor John Montgomery
Associate Professor John P. Wolfe

2012

Acknowledgements

This work would not have been possible without the support and guidance of many people. Foremost are my mother and father, Annette and Steve Locke, who are a constant source of love and guidance. My love of science was fostered by your early introduction of telescopes, microscopes, and homemade chemistry kits to my life.

Thanks are due to my advisor Anne McNeil, who has given me guidance in meeting scientific and intellectual challenges these past five years.

Many thanks are due the friends and labmates who have managed to actually get work done alongside my hot mess; Cheryl Moy, Tracy Schloemer, Angela Gao, Kelsey King, Zack Bryan, Se Ryeon Lee and Jing Chen. I'd like to thank Chris Taylor for the good times we've had relieving some of the stress caused by this work.

Last, but most, I want to thank the person who has been instrumental in keeping me balanced and in perspective the past few years, Erica Lanni. We have been labmates, collaborators, friends, and partners. The support, comfort and love you have given has been invaluable in ordeals of grad school and I can't thank you enough.

Table of Contents

List of Figures

List of Tables

List of Schemes

List of Appendices

Abstract

Chapter 1 provides an introduction to π-conjugated copolymers. Conjugated polymers are an increasingly important class of materials because of their potential application in electronic devices. Little is known about the effect of copolymer constitutional sequence because these materials have been synthetically inaccessible. Now π-conjugated copolymers with varying sequences may be prepared through the newly discovered Ni-catalyzed living chain-growth polycondensation. Though several block and random copolymerizations have been reported, significant challenges remain in developing sophisticated π-conjugated copolymer architectures such as gradient copolymers. This thesis our details efforts in discovering and understanding controlled copolymerizations.

Chapter 2 describes the development of a living, chain-growth copolymerization of 3-hexylthiophene and 3-(hexyloxy)methylthiophene. Monomer reactivity ratios were measured and revealed that the growing polymer chain has little preference for either monomer. The first conjugated gradient copolymers were prepared. Random and block copolymers were also synthesized and the copolymer sequence was found to influence the solid-state properties of the copolymers.

Chapter 3 details studies on cross-propagation between 3-alkylthiophene and 2,5-dialkoxybenzene monomers to determine mechanisms of catalyst dissociation during copolymerization. The effect of ligand electronics on block copolymerization was investigated and found to have little influence on copolymerization. Small-molecule model reactions

indicated that catalyst dissociation does not occur due to a difference in π-binding affinity between 3-alkylthiophene and 2,5-dialkoxybenzene units.

Chapter 4 describes extension of controlled copolymerization to new monomer pairs. The Kumada coupling copolymerization of 9,9-dioctylfluorene and 2,5-(bishexyloxy)benzene was investigated and batch copolymerizaions were found to exhibit chain-growth behavior. However the large difference in monomer reactivity ratios limited the gradient copolymer sequences accessible by batch methods. Semi-batch copolymerizations proved to be challenging because chain-growth behavior was found to depend on the total concentration of monomer. $Ni(dppp)Cl_2$ catalyzed block copolymerizations of *N*-hexylpyrrole and 3-hexylthiophene displayed efficient cross-propagation. However, batch copolymerizations did not display chain-growth behavior.

Chapter 5 provides conclusion on the synthesis of conjugated copolymers and insights on controlled copolymerizations. The results reported herein suggest that improvements in catalyst and monomer design are necessary to increase the scope of controlled copolymerization.

Chapter 1
π-Conjugated Copolymers

π-Conjugated polymers are a class of materials that show great promise for applications such as thin-film solar cells[1] light-emitting diodes[2] and transistors.[3] These organic materials can find use in electronic applications due to the unique optical, electronic and redox properties that result from the delocalization of π-electrons along the polymer chain. The ability to synthetically tune these properties to meet specific needs is a key advantage and attraction of organic electronics. Synthetic modulation of polymer properties can be accomplished by designing new monomers or by copolymerizing two or more monomers.

Monomer design for π-conjugated polymers must take into account factors such as the energies of the molecular orbitals, planarity of the polymer backbone and crystallinity of the material.[4] The difference in energies of the molecular orbitals (bandgap) of conjugated polymers can be decreased by incorporating the following structural features into monomer design: aromatic units with low resonance energy; strongly coupled donor-acceptor substituents; large, coplanar π-systems; and highly regioregular and crystalline side chains.[4a] Incorporation of bulky side-chains and bulky conjugated units in the polymer backbone inhibit planarity of the polymer chain and reduce the effective conjugation length, increasing the bandgap, blue-shifting the absorption and emission and lowering charge mobility of the polymer. This effect has led to the development of monomers incorporating fused-ring systems, vinylidene linkers and five-membered aromatic rings within polymer backbones to maximize coplanarity.[5] Polymer crystallinity greatly impacts phase behavior, morphology, and solubility of the material and is primarily modified by the length and linearity of the monomer side chain. Design of new monomers for π-conjugated polymers has resulted in a plethora of new materials, however prediction of all the relevant polymer properties before actually preparing the material remains elusive.

Copolymerization of two existing monomers is an alternative approach to synthetically tuning polymer properties. The order of comonomers in the polymer chain, or sequence, can also influence the optical, physical and phase behavior of a material. Copolymerization of two monomers with different HOMO and LUMO energies alters the molecular orbitals of the resultant π-conjugated polymer due to orbital mixing along the polymer chain. This approach has led to the development of low-bandgap materials, which capture a large range of the solar spectrum for polymer solar cells.[6] Bandgap tuning via copolymerization is also utilized to modify the emission wavelength of fluorescent polymers used in polymer light-emitting diodes. Changing the molecular orbital energy levels of the polymer via copolymerization tends to be most efficient with random and alternating copolymers to maximize orbital overlap and mixing within the effective conjugation length. Typical cross-coupling syntheses of π-conjugated polymers proceed through step-growth mechanisms, making it difficult to control the copolymer sequence, which can be important for determining the solid-state and thin-film properties of a material.

The development of living, chain-growth polymerizations (Figure 1.1) for π-conjugated polymers by Ni-catalyzed polycondensation stimulated interest in using this method to create new, defined materials with reproducible molecular weights and polydispersities. Controlled polymerizations enable the synthesis of materials with a molecular weight dependence on the ratio of monomer to nickel and narrow polydispersity. In addition, controlled copolymerizations enable control over the sequence of a copolymer with knowledge of monomer reactivity ratios and manipulation of monomer concentrations. Copolymerizations utilizing living, chain-growth methods could lead to new, defined materials with unique properties. Since 2004, a number of monomers including: thiophene derivatives[7] (**1**), (2,5-bishexyloxy)phenylene[8] (**2**), 9,9-dioctylfluorene[9] (**3**), *N*-hexylpyrrole[10] (**4**), 3-hexylselenophene[11] (**5**) 3-(methoxyethoxyethoxy)pyridine[12] (**6**), and N-octylcarbazole[9b] have been shown to undergo chain-growth polymerizations with various degrees of living character. Chain-growth behavior is proposed arise from formation of nickel-polymer π-complex between the nickel initiator and polymer chain after reductive elimination. Subsequent intra-complex oxidative addition results in successive monomer addition to the polymer chain

end (Scheme 1.1). Interestingly, recent investigations have suggested that Ni^0 is able to "walk" along the polymer chain before oxidative addition.[13] Consequently, polymerizations initiated with nickel dihalide complexes can undergo propagation from both ends of the polymer. This behavior makes it difficult to control copolymer sequence and can be prevented with the use of nickel aryl halide initiators (Scheme 1.2)

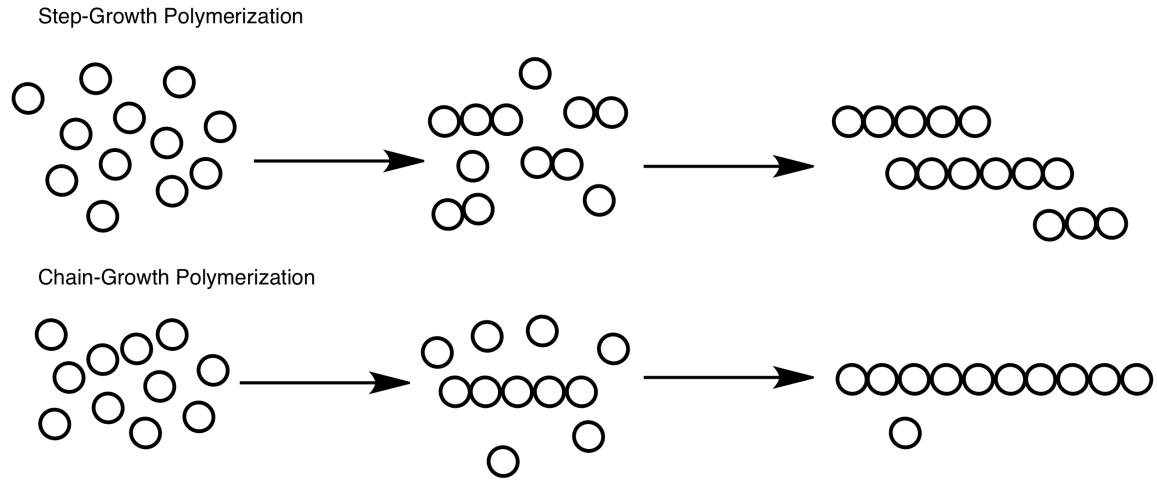

Figure 1.1 Step-growth and chain-growth polymerization comparison

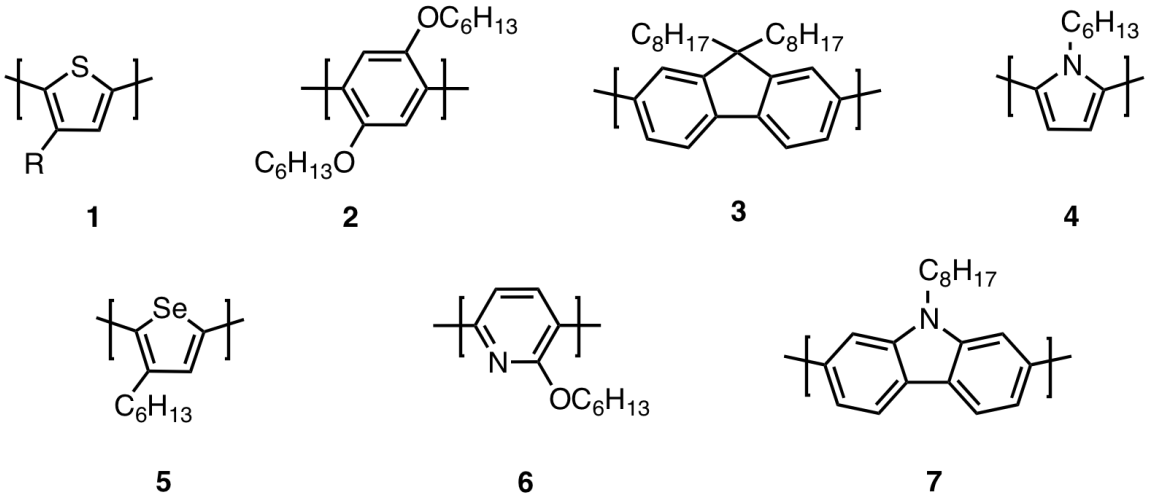

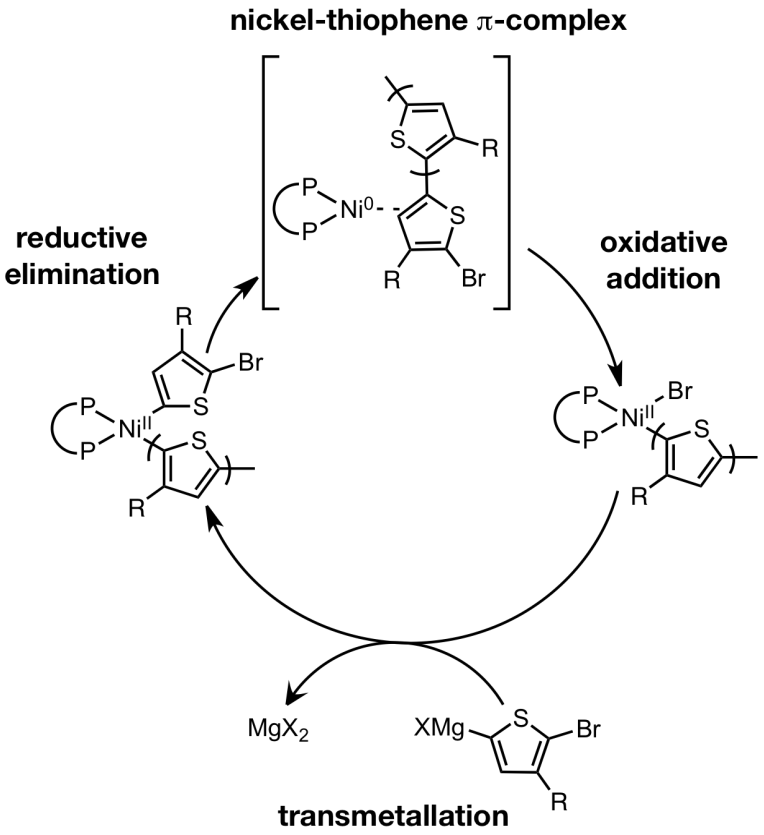

Scheme 1.1 Proposed chain-growth mechanism

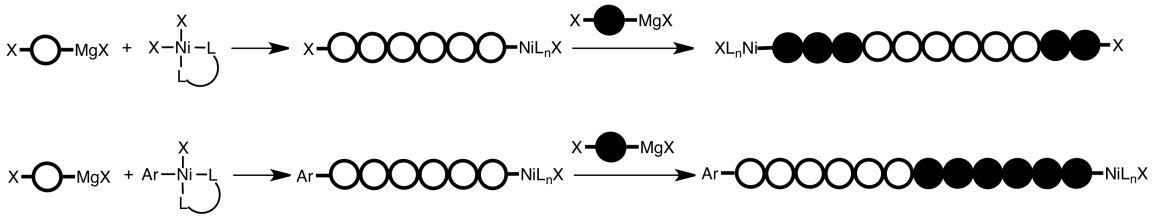

Scheme 1.2 Ni "ring-walking" and its impact on copolymer sequence

All-conjugated block copolymers, which possess a sequence consisting of two or more homopolymers covalently bound to one another (Figure 1.2), display exploitable phase separation behavior that may be advantageous for many solution-processed devices. Block copolymers can be prepared using step-growth polymerizations by a grafting-to method, where appropriately end-functionalized polymers are attached to one another (Figure 1.3).[14] However, "grafting to" methods often result in mixtures of ungrafted homopolymers and block copolymers. These mixtures can be difficult to separate and are difficult to reproduce from batch to batch. Living, chain-growth copolymerizations, wherein each initiator begins a single polymer chain, enable the

production of all-conjugated block copolymers by the grafting-from method.[15] This procedure takes advantage of the continued association of the Ni catalyst with the polymer chain after the first batch of monomer has been consumed (Figure 1.3). Addition of a second monomer extends the polymer from the active chain end to form a block copolymer.

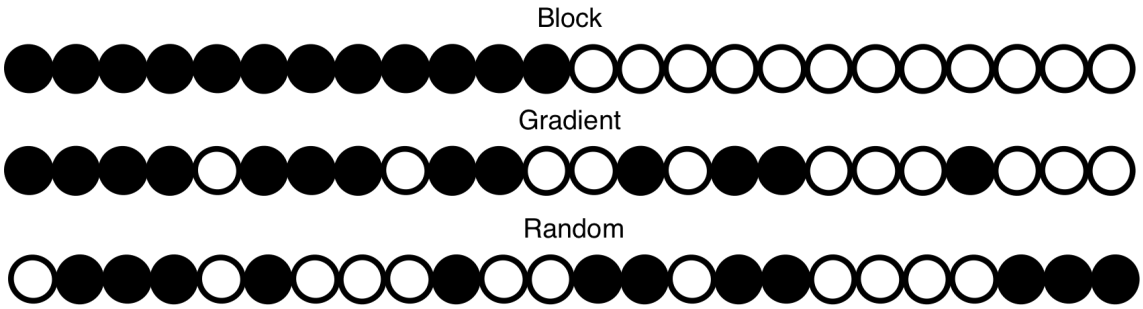

Figure 1.2 Copolymer Sequences

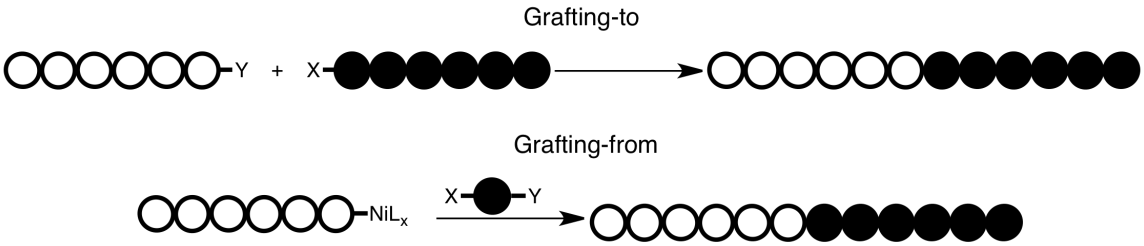

Figure 1.3 Synthetic approaches to all-conjugated block copolymers

The grafting-from procedure has been widely used for the block copolymerization of thiophene derivatives.[16] The phase behavior of these rod-rod block copolymers has been investigated for their potential application in polymer solar cell devices. For example, it was found that the introduction of an amorphous 3-(2-ethylhexyl)thiophene block to poly(3-hexylthiophene) (**8**) induced the formation of a microphase-separated nanostructure with enhanced crystallinity in the poly-(3-hexylthiophene) block.[16f] Enhanced crystallinity typically leads to increased charge mobility in conjugated polymers. Higashihara and coworkers reported that 3-hexylthophene-3-(2-(2-(2-methoxyethoxyethoxy)methylthiophene block copolymers (**9**) self-assemble into vertically oriented lamellae.[16b] In another example, block copolymers of 3-hexylthiophene and 3-thiophene hexylacetate (**10**) demonstrated a lowered HOMO relative to poly-(3-hexylthiophene) and displayed microphase separation in thin-films which could be controlled by the percentage of 3-thiophene hexylacetate in the

polymer.[17] Control over polymer microphase separation could lead to more efficient charge separation in polymer solar cells. These and related studies demonstrate the possibility of creating defined nanostructures through phase-separation of all-conjugated thiophene block copolymers.

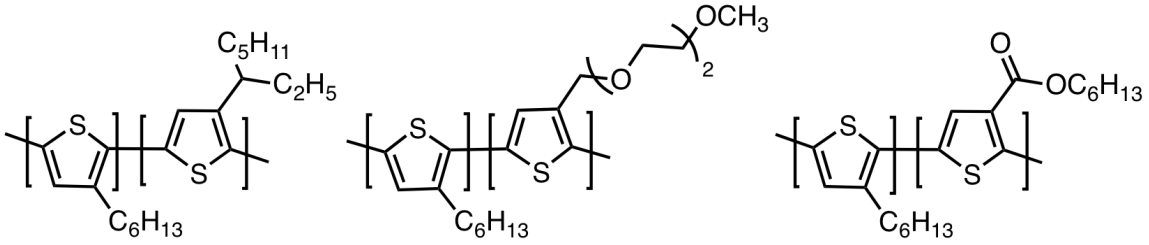

8 **9** **10**

Block copolymerization utilizing Ni-catalyzed chain-growth polycondensation has also been extended to monomer pairs including phenylene-thiophene (**11**),[18] thiophene-fluorene (**12**),[19] phenylene-fluorene (**13**),[19] phenylene-pyrrole (**14**),[10] and thiophene-selenophene (**15**).[15a] These copolymerizations have been somewhat more difficult to develop than all-thiophene systems because the conditions required for chain-growth hompolymerizations are often different and must be reconciled for successful copolymerization. For example, the polymerization of 3-hexylthiophene is best initiated by Ni(bis(diphenylphosphino)propane)Cl_2 (Ni(dppp)Cl_2) whereas the polymerization of (2,5-bishexyloxy)benzene is best carried out with Ni(bis(diphenylphosphino)ethane)Cl_2 (Ni(dppe)Cl_2). The order of polymerization has also proven to be critical for block copolymer formation (Scheme 1.3).[19] McCullough and coworkers observed that when the polymerization of 9,9-dioctylfluorene was followed by 2,5-(bishexyloxy)benzene, the GPC elution profile revealed a bimodal molecular weight distribution. This result suggested the presence of side reactions, such as chain termination or transfer, which prevented efficient cross-propagation to the phenylene monomer. However, the opposite order of monomer addition resulted in successful block copolymer formation. Dependence of block copolymer formation on monomer addition order has also been observed in the thiophene-phenylene,[18] thiophene-fluorene,[19] and phenylene-pyrrole[10] copolymerizations. The observed effect of monomer addition order is hypothesized to be due to a difference in π-binding ability between the monomers. However, there is lack of a clear model for copolymerization behavior. There exists a need for an increased

understanding of the mechanism of Ni-catalyzed copolymerizations and development of more general polymerization conditions. Inefficient cross-propagation between monomers also makes construction of statistical and gradient copolymers difficult as each chain-termination and transfer event leads to sequence heterogeneity in the polymers formed.

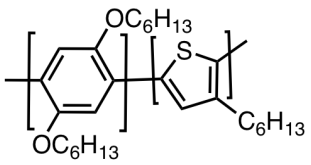

11

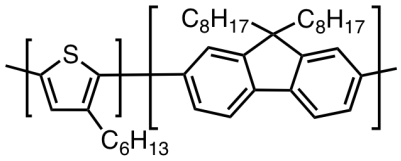

12

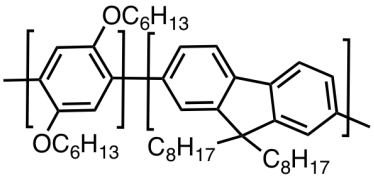

13

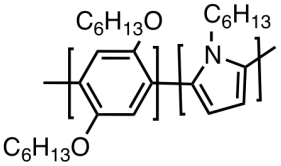

14

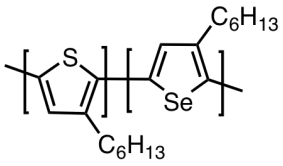

15

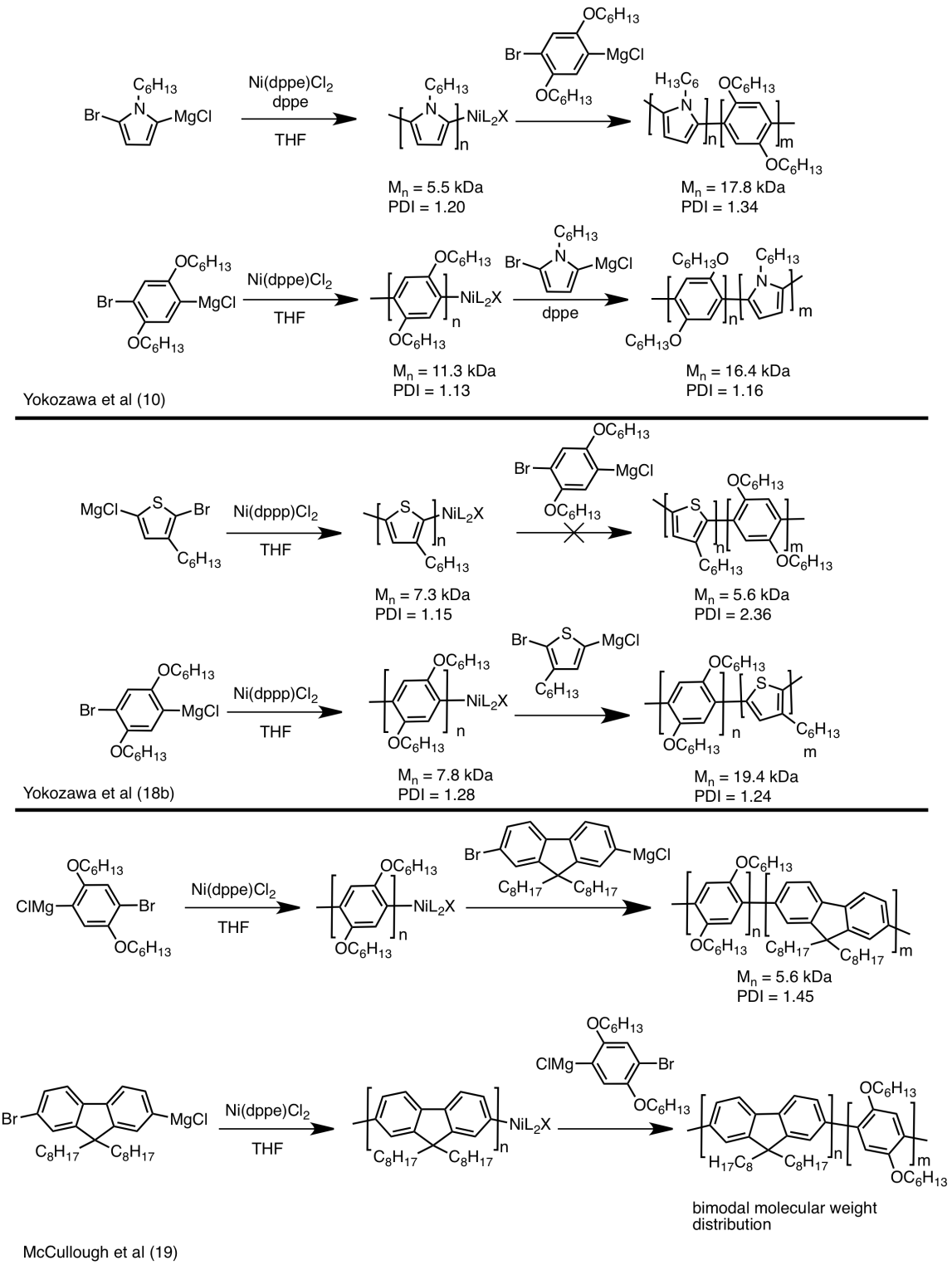

Scheme 1.3 Inefficient catalyst-transfer in block copolymerizations of dissimilar monomers.

In comparison to block copolymers, there have been far fewer studies focused on the synthesis and properties of all-conjugated statistical or random copolymers (Figure 1.1). This lack of attention is likely because random copolymers are believed to not form well-defined nanostructures, which reduces their utility in many device applications. Random copolymers of 3-butylthiophene and 3-octylthiophene (**16**) were shown to have melting and crystallization temperatures that varied with copolymer composition.[20] Bulk heterojunction cells fabricated from these random copolymers and phenyl-C_{71}-butyric acid methyl ester ($PC_{71}BM$) displayed increased power conversion efficiency compared to devices fabricated from the corresponding homopolymers. This improvement was attributed to the increased solubility of the copolymers, which allowed for slow polymer crystallization during casting and resulted in worm-like nanoscale structures during device fabrication. Random (**17**) and block (**18**) copolymers consisting of 3-hexylthiophene and thiophene containing fullerene-substituted alkyl chains were synthesized and displayed differences in solubility and phase separation.[21] The random copolymer was shown transfer charge more efficiently to the fullerene acceptor than the analogous block copolymer, however the random copolymer also formed larger phase-separated domains than the block copolymer. Large phase domains decrease the interfacial area between donor and acceptor and lower overall device efficiency.

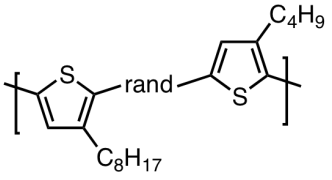

16

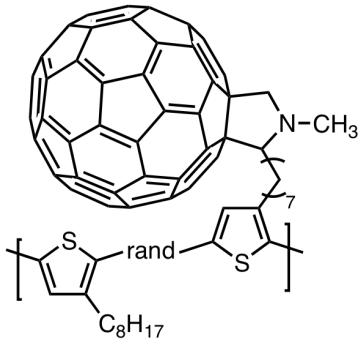

17

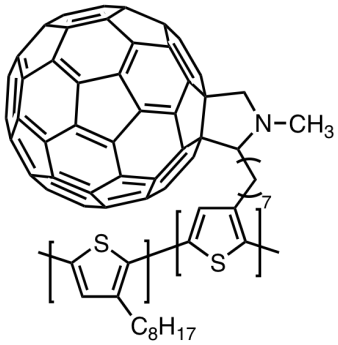

18

Gradient copolymers, a copolymer architecture where the monomer composition varies continuously along the polymer chain, are class of polymers accessible only through controlled copolymerizations. Gradient copolymers occupy the compositional space between block and random sequences (Figure 1.2). The preparation of gradient copolymers requires a controlled, chain-growth mechanism as well as knowledge of the

monomer reactivity ratios. These conditions are necessary to achieve a continuous change in monomer composition along the entire polymer chain and prevent the formation of homopolymer mixtures. We have recently utilized controlled Ni-catalyzed copolymerization to synthesize the first all-conjugated gradient copolymers. Using 3-hexylthiophene and 3-((hexyloxy)methyl)thiophene as the co-monomers, a series of gradient copolymers were prepared via Ni-catalyzed controlled copolymerization (Scheme 1.4).[22] These gradient copolymers were shown to undergo phase transitions that were different than analogous block and random copolymers. These results indicate that it is possible to finely tune polymer properties simply by changing the copolymer sequence.

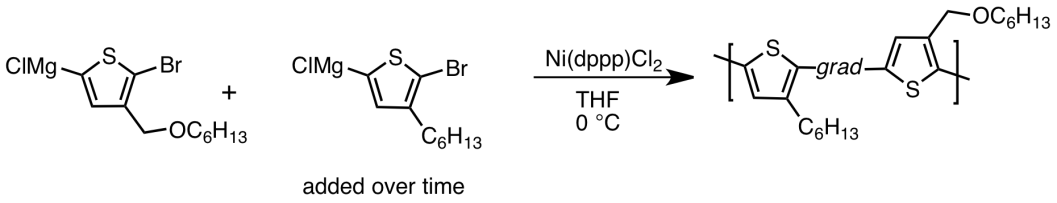

Scheme 1.4 Synthesis of poly(3-hexylthiophene-grad-3-((hexyloxy)methyl)thiophene)

This dissertation details my work on the synthesis and characterization of all π-conjugated copolymers with gradient sequences. Chapter 2 will describe the first gradient π-conjugated copolymers of 3-hexylthiophene and 3-((hexyloxy)methyl)thiophene prepared via Ni-catalyzed chain-growth copolymerization. Chapter 3 will describe studies undertaken to better understand cross-propagation between 3-alkylthiophene and 2,5-(bisalkoxy)benzene monomers. Chapter 4 will detail efforts to develop Ni-catalyzed chain-growth copolymerizations between structurally different monomers including 9,9-dioctylflourene and 2,5-(bisalkoxy)benzene as well as 3-hexylthiophene and *N*-hexylpyrrole. In total, this work demonstrates the feasibility and current limitations of controlling copolymer sequence via Ni-catalyzed chain-growth copolymerizations.

References Cited

(1) (a) Dennler, G.; Scharber, M. C.; Brabec, C. J. *Adv. Mater*. **2009**, *21*, 1323-1338. (b) Hoppe, H.; Sariciftci, N. S. Advances in Polymer Science. In *Photoresponsive Polymers II;* Marder, S.R.; Lee, K-S, Eds; Springer Berlin: Heidelberg, 2008; Vol. 214; p. 1-86.

(2) Grimsdale, A. C.; Chan K. L.; Martin, R. E.; Jokisz, P. G.; Holmes, A. B. *Chem. Rev.* **2009**, *109*, 897-1091.

(3) Arias, A. C.; MacKenzie, J. D.; McCulloch, I.; Rivnay, J.; Salleo, A. *Chem. Rev.* **2010**, *110*, 3-24.

(4) (a) Facchetti, A. *Chem. Mater.* **2011**, *23*, 733–758. (b) Bilby, D.; Kim, B.G.; Kim, J. *Pure Appl. Chem.* **2011**, *83*, 127-139. (c) Roncali, J. *Chem. Rev.* **1997**, *97*, 173−205.

(5) Cheng, Y-J; Yang, S-H.; Hsu C-S. *Chem. Rev*. **2009**, *109*, 5868–5923.

(6) Liang, Y.; Yu, L. *Polymer Reviews* **2010**, *50*, 454–473.

(7) (a) Benanti, T. L.; Kalaydjian, A.; Venkataraman, D. *Macromolecules* **2008**, *41*, 8312-8315. (b) Ouhib, F.; Dkhissi, A.; Iratçabal, P.; Hiorns, R. C.; Khoukh, A.; Desbrières, J.; Pouchan, C.; Dagron-Lartigau, C. *J. Polym. Sci., Part A: Polym. Chem*. **2008**, *46*, 7505-7516. (c) Li, Y.; Xue, Y.; Xia, H.; Xu, B.; Wen, S.; Tian, W. *J. Polym. Sci., Part A: Polym. Chem*. **2008**, *46*, 3970-3984. (d) Vallat, P.; Lamps, J.-P.; Schosseler, F.; Rawiso, M.; Catala, J.-M. *Macromolecules* **2007**, *40*, 2600-2602. (e) Adachi, I.; Miyakoshi, R.; Yokoyama, A.; Yokozawa, T. *Macromolecules* **2006**, *39*, 7793-7795. (f) Koeckelberghs, G.; Vangheluwe, M.; Van Doorsselaere, K.; Robijns, E.; Persoons, A.; Verbiest, T. *Macromol. Rapid Commun*. **2006**, *27*, 1920-1925. (g) Sheina, E. E.; Khersonsky, S. M.; Jones, E. G.; McCullough, R. D. *Chem. Mater.* **2005**, *17*, 3317-3319.

(8) Miyakoshi, R.; Shimono, K.; Yokoyama, A.; Yokozawa, T. *J. Am. Chem. Soc*. **2006**, *128*, 16012-16013.

(9) (a) Huang, L.; Wu, S.; Qu, Y.; Geng, Y.; Wang, F. *Macromolecules* **2008**, *41*, 8944-8947. (b) Stefan, M. C.; Javier, A. E.; Osaka, I.; McCullough, R. D. *Macromolecules* **2009**, *42*, 30-32.

(10) Yokoyama, A.; Kato, A.; Miyakoshi, R.; Yokozawa, T. *Macromolecules* **2008,** *41*, 7271-7273.

(11) Heeney, M.; Zhang, W.; Crouch, D. J. *Chem. Commun.* **2007**, *47*, 5061-5063.

(12) Nanashima, Y.; Yokoyama, A.; Yokozawa, T. J. *Polym Sci. Part A: Polym. Chem.* **2012**, *50*, 1054-1061.

(13) Tkachov, R.; Senkovskyy, V.; Komber, H.; Sommer, J.-U.; Kiriy, A. *J. Am. Chem. Soc.* **2010**, *132*, 7803-7810.

(14) (a) Woody, K.B.; Leever, B.J.; Durstock, M.F.; Collard, D.M. *Macromolecules* **2011**, *44*, 4690-4698. (b) Scherf, U.; Gutacker, A.; Koenen, N. *Acc. Chem. Res.* **2008**, *41,* 1086-1097.

(15) (a) Hollinger, J.; Jahnke, A. A.; Coombs, N.; Seferos, D. S. *J. Am. Chem. Soc*. **2010**, *132*, 8546-8547. (b) Van den Bergh, K.; Cosemans, I.; Verbiest, T. Koeckelberghs, G. *Macromolecules* **2010**, *43*, 3794–3800. (c) Miyakoshi, R.; Yokoyama, A.; Yokozawa, T. *Chem. Lett.* **2008**, *37*, 1022-1023.

(16) (a) Kim, J.; Siva, A.; Song, I.Y.; Park, T. *Polymer* **2011**, *52*, 3704-3709. (b) Higashihara, T.; Ohsimimizu, K.; Ryo, Y.; Sakurai, T.; Takahashi, A.; Nojima, S.; Ree, M.; Ueda, M. *Polymer* **2011**, *52,* 3687-3695. (c) Ge, J.; He, M.; Qiu, F.; Yang, Y. *Macromolecules* **2010**, *43,* 6422-6428. (d) Van den Bergh, K.; Cosemans, I.; Verbiest, T.; Koeckelberghs, G.; *Macromolecules* **2010**, *43*, 3794-3800. (e) Clément, S.; Meyer, F.; De Winter, J.; Coulembier, O.; Vande Velde, C. M. L.; Zeller, M.; Gerbaux, P.; Balandier, J.-Y.; Sergeyev, S.; Lazzaroni, R.; Geerts, Y.; Dubois, P. *J. Org. Chem*. **2010**, *75*, 1561-1568. (f) Zhang, Y.; Tajima, K.; Hashimoto, K.; *Macromolecules* **2009**, *42*, 7008-7015. (g) Wu, P.-T.; Ren, G.; Li, C.; Mezzenga, R.; Jenekhe, S. A. *Macromolecules* **2009**, *42*, 2317-2320. (h) Ouhib, F.; Khoukh, A.; Ledeuil, J.-B.; Martinez, H.; Desbrières, J.; Dagron-Lartigau, C. *Macromolecules* **2008**, *41*, 9736-9743. (f) Ohshimizu, K.; Ueda, M. *Macromolecules* **2008**, *41*, 5289-5294. (i) Ouhib, F.; Hiorns, R. C.; de Bettignies, R.; Bailly, S.; Desbrières, J.; Dagron-Lartigau, C.; *Thin Solid Films* **2008**, *516*, 7199-7204. (j) Zhang, Y.; Tajima, K.; Hirota, K.; Hashimoto, K. *J. Am. Chem. Soc*. **2008**, *130*, 7812-7813. (k) Van den Bergh, K.; Huybrechts, J.; Verbiest, T.; Koeckelberghs, G. *Chem. Eur. J.* **2008**, *14*, 9122-9125. (l) Yokozawa, T.; Adachi, I.; Miyakoshi, R.; Yokoyama, A. *High Perform. Polym*. **2007**, *19*, 684-699. (m) Iovu, M. C.;

Sheina, E. E.; Gil, R. R.; McCullough, R. D. *Macromolecules* **2005**, *38*, 8649-8656.

(17) Ho, C-C.; Liu, Y-C.; Lin, S-H.; Su, W-F. *Macromolecules*, **2012**, *45*, 813-820.

(18) (a) Wu, S.; Bu, L.; Huang, L.; Yu, X.; Han, Y.; Geng, Y.; Wang, F. *Polymer*, **2009**, *50*, 6245-6251. (b) Miyakoshi, R.; Yokoyama, A.; Yokozawa, T. *Chem. Lett.* **2008**, *37*, 1022-1023.

(19) Javier, A. E.; Varshney, S. R.; McCullough, R. D. *Macromolecules* **2010**, *43*, 3233-3237.

(20) Wu, P-T.; Ren, G.; Jenekhe, S.A. *Macromolecules* **2010**, *43*, 3306-3313.

(21) Ouhib, F.; Khoukh, A.; Ledeuil, J.-B.; Martinez, H.; Desbrières, J.; Dagron-Lartigau, C. *Macromolecules* **2008**, *41*, 9736-9743.

(22) Locke, J.R.; McNeil, A. J. *Macromolecules* **2010**, *43,* 8709-8710.

Chapter 2[1]

Syntheses of Gradient π-Conjugated Copolymers of Thiophene

Organic π-conjugated polymers are an increasingly important class of materials because of their widespread application in electronic devices.[1] Although there have been extensive studies aimed at controlling their physical and optoelectronic properties through synthetic modifications,[2] processing conditions,[3] and device designs,[4] little is known about the effect of copolymer sequence because these materials have been synthetically inaccessible. Now π-conjugated copolymers with varying sequences can be prepared through the newly discovered Ni-catalyzed chain-growth polymerization.[5,6,7] The ability to tailor properties by simply altering the copolymer sequence should provide a powerful new design strategy for preparing the next-generation of tunable organic materials. We targeted *gradient* π-conjugated copolymers, which exhibit continuously changing composition along the polymer chain, because their anticipated phase-compatibilizing abilities may solve a long-standing problem in polymer-based solar cells by providing access to stable, nanostructured polymer blends.[8] Herein we report the first syntheses and characterization of gradient π-conjugated copolymers.

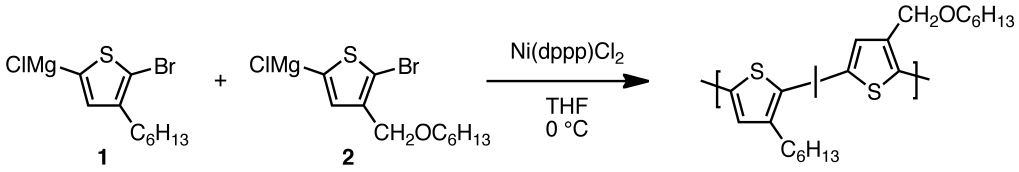

(1)

Thiophene-based monomers were chosen because they have been successfully used to prepare block copolymers,[6] which suggests that cross-propagation can readily occur between these monomers.[9] Moreover, polythiophenes are one of the most widely studied and utilized π-conjugated polymers because of their good hole mobility and long wavelength absorption.[10] We began by evaluating whether the Ni-catalyzed copolymerization of monomers **1**[5a] and **2**[11] followed a chain-growth mechanism (eq 1).

---

(1) Reproduced with permission from Locke, J. R.; McNeil, A. J. "Syntheses of Gradient π-Conjugated Copolymers of Thiophene" *Macromolecules* **2010,** *43,* 8709-8710. Copyright 2010 American Chemical Society.

Both monomers were prepared in situ by magnesium-halogen exchange[12] using a mixed halogen precursor (I/Br) to regioselectively generate the Grignard reagents (Appendix 1). All copolymerizations were run at 0 °C to prevent monomer decomposition via reaction with *i*-PrI generated in the metathesis reaction.[13] When $Ni(dppe)Cl_2$ and $Ni(dppp)Cl_2$ were used as initiators, a linear increase in the number-average molecular weight (M_n) as a function of conversion was observed, consistent with a chain-growth mechanism (Figure 2.1A).[14] Other commercially available Ni catalysts, such as $Ni(dppf)Cl_2$ and $Ni(PPh_3)_2Cl_2$, did not exhibit chain-growth behavior in the copolymerizations (Appendix 1). Given that $Ni(dppp)Cl_2$ produced copolymers with the lowest polydispersity (PDI), it was selected for the gradient copolymer syntheses.

A series of batch polymerizations were performed, wherein the initial molar ratio of **1**:**2** was varied, forming copolymers with different final compositions (**P1**-**P3**, Figure 2.1B). During these experiments it became apparent that there was little difference in the relative reactivity of **1** and **2**, which is not surprising given their similar steric and electronic properties.[9] To quantify these differences, the monomer reactivity ratios were determined through a series of experiments wherein the initial concentrations of **1** and **2** were varied and the rates of monomer consumption were followed for the first 10% conversion (SI). These data were then fit to the copolymerization equation via least-squares regression.[15] In total, 17 experiments at different initial concentrations were simultaneously fit to determine the reactivity ratios. Consistent with our qualitative observations, monomer **1** gave a reactivity ratio (r_1) of 1.12 ± 0.04 while monomer **2** gave a reactivity ratio (r_2) of 1.09 ± 0.02. These values indicate that the growing polymer chain has little preference for either monomer. Thus, the copolymers synthesized using this batch method have a random sequence.

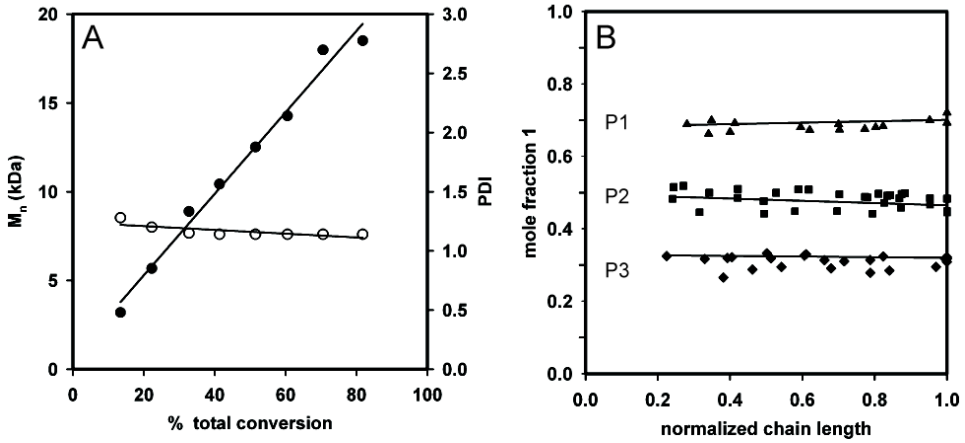

Figure 2.1. (A) Plot of M_n (●) and PDI (○) versus conversion for a batch copolymerization of **1** and **2** in THF at 0 °C ([**1**] = [**2**] = 0.04 M; [Ni(dppp)Cl_2] = 0.002 M). (B) Plot of the cumulative mole fraction of **1** in the copolymer versus the normalized chain length for the batch copolymerizations (**1**:**2** = 67:33 (**P1**, ▲); 50:50 (**P2**, ■); 33:67 (**P3**, ◆)).

Because r_1 and r_2 are approximately equal to 1, the semi-batch method is required to synthesize gradient copolymers. In semi-batch copolymerizations, one monomer is gradually added to the reaction over time via syringe pump. One advantage of this technique is that gradient copolymers with varying composition profiles can be prepared by using different rates of monomer addition. Herein, monomer **1** was added to the reaction at varying rates to generate gradient copolymers **P4**-**P8** (Figure 2.2A).[16] Ni(dppp)Cl_2 was used to prepare gradient copolymers **P4**-**P7**. Given that propagation was recently shown to occur at both chain ends in the Ni(dppe)Cl_2-catalyzed synthesis of poly(3-hexylthiophene),[17] gradient copolymer **P8** was synthesized using a functionalized Ni(dppe)ArBr initiator, which can only propagate from one chain end (see Appendix 1). To elucidate the copolymer sequence, aliquots were taken during polymerization and analyzed by ^{1}H NMR spectroscopy and GPC to determine the mole fraction incorporation of each monomer as a function of chain length. Representative data is shown in Figure 2.2A, where the rate of monomer addition determines its mole fraction distribution along the copolymer chain.[18]

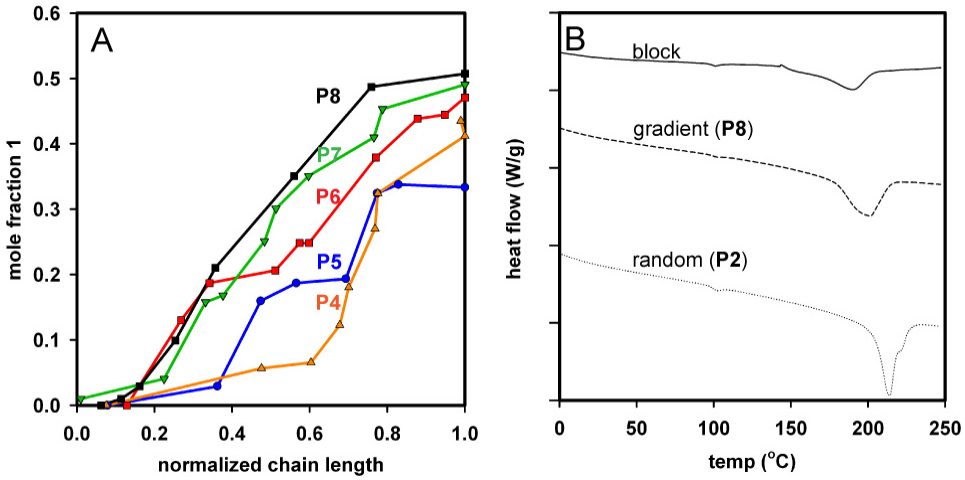

Figure 2.2. (A) Plot of the cumulative mole fraction of **1** in the copolymer versus the normalized chain length for the semi-batch copolymerizations (**1** addition rates (mmol/min) = 0.12 (**P4**, ▲); 0.20 (**P5,** ●); 0.28 (**P6**, ■); 0.40 (**P7**, ▼); 0.48 (**P8,** ■)). (B) DSC data for selected copolymers.

The influence of copolymer sequence on the optical and physical properties was investigated. For comparison, the results for the block, random, and gradient copolymers with the same molar composition (1:1) are presented in Table 2.1, along with the homopolymer data. The spectroscopic studies revealed similar spectra for all three copolymers in solution. The emission maxima resemble those of P3HT, suggesting efficient energy transfer to oligothiophene moieties within the polymer chains. In contrast, thin-film spectroscopic studies revealed some differences among the copolymers (Appendix 1). In addition, each copolymer exhibited a unique thermal transition (Figure 2B and Appendix 1). These results indicate that there are sequence-dependent changes in the solid-state organization, which is reflected in the different thin film optical and physical properties. As a result, these gradient copolymers might be useful not only for their potential phase-compatibilizing abilities but also for tailoring solid-state properties.

					soln ($CHCl_3$)	
	M_n (kDa)	**PDI**	**T_c (°C)**	**T_m (°C)**	**Abs λ_{max} (nm)**	**Em λ_{max} (nm)**
P3HT	18.5	1.1	--	240	445	568
P3HOMT	16.5	1.1	240	--	425	556
Block	22.1	1.1	--	190	451	572
Random (P2)	16	1.3	--	213	449	574
Gradient (P8)	10.3	1.1	--	200	445	568

Table 2.1. Copolymer Characterization Data

In summary, we prepared the first gradient π-conjugated copolymers via Ni-catalyzed chain-growth copolymerization of 3-hexylthiophene and 3-((hexyloxy)methyl)thiophene. Because rate studies indicated little difference in monomer reactivities, one monomer was gradually added to the polymerization over time to form gradient copolymers. Now that controlled sequence π-conjugated copolymers can be synthesized, the next goal is to identify their unique properties, including phase-compatibilizing abilities in homopolymer blends. Preliminary data reported herein suggests that the solid-state optical and physical properties are influenced by the copolymer sequence. Finally, although the Ni-catalyzed copolymerizations are chain-growth under the conditions reported herein, our preliminary attempts to expand the substrate scope by examining the copolymerization of monomers with varying steric and electronic properties has highlighted[18] a need for developing improved catalysts.

References Cited

(1) For recent reviews, see: (a) Li, C.; Liu, M.; Pschirer, N. G.; Baumgarten, M.; Müllen, K. *Chem. Rev.* [Online early access]. DOI: 10.1021/cr100052z. Published Online: June 29, 2010. (b) Arias, A. C.; MacKenzie, J. D.; McCulloch, I.; Rivnay, J.; Salleo, A. *Chem. Rev.* **2010**, *110*, 3-24. (c) Grimsdale, A. C.; Chan, K. L.; Martin, R. E.; Jokisz, P. G.; Holmes, A. B. *Chem. Rev.* **2009**, *109*, 897-1091.

(2) For recent reviews, see: (a) Heeger, A. J. *Chem. Soc. Rev.* **2010**, *39*, 2354-2371. (b) Kroon, R.; Lenes, M.; Hummelen, J. C.; Blom, P. W. M.; de Boer, B. *Polym. Rev.* **2008**, *48*, 531-582.

(3) For recent reviews, see: (a) Tsao, H. N.; Müllen, K. *Chem. Soc. Rev.* **2010**, *39*, 2372-2386. (b) Groves, C.; Reid, O. G.; Ginger, D. S. *Acc. Chem. Res.* **2010**, *43*, 612-620. (c) Yang, X.; Loos, J. *Macromolecules* **2007**, *40*, 1353-1362.

(4) For a recent review, see: Slota, J. E.; He, X.; Huck, W. T. S. *Nano Today* **2010**, *5*, 231-242.

(5) (a) Yokoyama, A.; Miyakoshi, R.; Yokozawa, T. *Macromolecules* **2004,** *37,* 1169-1171. (b) Miyakoshi, R.; Yokoyama, A.; Yokozawa, T. *J. Am. Chem. Soc.* **2005**, *127*, 17542-17547. (c) Sheina, E. E.; Liu, J.; Iovu, M. C. Laird, D. W.; McCullough, R. D. *Macromolecules* **2004**, *37*, 3526-3528. (d) Iovu, M. C.; Sheina, E. E.; Gil, R. R.; McCullough, R. D. *Macromolecules* **2005**, *38*, 8649-8656.

(6) For recent examples of block copolymers, see: (a) Hollinger, J.; Jahnke, A. A.; Coombs, N.; Seferos, D. S. *J. Am. Chem. Soc*. **2010**, *132*, 8546-8547. (b) Van den Bergh, K.; Cosemans, I.; Verbiest, T. Koeckelberghs, G. *Macromolecules* **2010**, *43*, 3794–3800.

(7) For a recent example of a random copolymer, see: Ouhib, F.; Khoukh, A.; Ledeuil, J.-B.; Martinez, H.; Desbrières, J.; Dagron-Lartigau, C. *Macromolecules* **2008**, *41*, 9736-9743.

(8) For recent examples, see: (a) Wang, R.; Li, W.; Luo, Y.; Li, B.-G.; Shi, A.; Zhu, S. *Macromolecules* **2009**, *42* 2275–2285. (b) Kim, J.; Sandoval, R. W.; Dettmer, C. M.; Nguyen, S. T.; Torkelson, J. M. *Polymer* **2008**, *49*, 2686-2697.

(9) Attempts at copolymerizing phenylene and fluorene were largely unsuccessful because we could not identify catalysts with chain-growth behavior under semi-batch conditions. For other examples of challenging copolymerizations, see: (a) Miyakoshi, R.; Yokoyama, A.; Yokozawa, T. *Chem. Lett.* **2008**, *37*, 1022-1023. (b) Yokoyama, A.; Kato, A.; Miyakoshi, R.; Yokozawa, T. *Macromolecules* **2008**, *41*, 7271-7273.

(10) *Handbook of Thiophene-based Materials: Applications in Organic Electronics and Photonics*; Perepichka, I. F.; Perepichka, D. F., Eds.; Wiley & Sons: New York, 2009; Vols 1 and 2.

(11) Adachi, I.; Miyakoshi, R.; Yokoyama, A.; Yokozawa, T. *Macromolecules* **2006**, *39*, 7793-7795.
(12)For a review, see: Knochel, P.; Dohle, W.; Gommermann, N.; Kneisel, F. F.; Kopp, F.; Korn, T.; Sapountzis, I.; Vu, V. A. *Angew. Chem., Int. Ed.* **2003**, *42*, 4302-4320. For a recent example, see: Shi, L.; Chu, Y.; Knochel, P.; Mayr, H. *Org. Lett.* **2009**, *11,* 3502–3505.

(13) Hauk, D.; Lang, S.; Murso, A. *Org. Process Res. Dev.* **2006**, *10*, 733-738.

(14) The non-zero y-intercept in the Mn versus conversion plot arises because these polymerizations are initiated by pre-treating Ni(dppp)Cl2 with several equiv of monomer. For reference, see: Lanni, E. L.; McNeil, A. J. *J. Am. Chem. Soc.* **2009**, *131*, 16573-16579.

(15) (a) Odian, G. Chain Copolymerization. In *Principles of Polymerization*, 4th ed.; John Wiley & Sons: Hoboken, 2004; pp 466-469. (b) Tidwell, P. W.; Mortimer, G. A. *J. Polym. Sci., Part A* **1965**, *3*, 369-387.

(16) Note that for these studies it was necessary to generate **1** from the dibromo precursor to avoid monomer decomposition at rt (Appendix 1). Although an approximately 80:20 mixture of regioisomers is generated via this method, the minor regioisomer is unreactive during polymerization. See ref 14.

(17) Tkachov, R.; Senkovskyy, V.; Komber, H.; Sommer, J.-U.; Kiriy, A. *J. Am. Chem. Soc.* **2010**, *132*, 7803-7810.

(18) Although all gradient copolymer compositions were intended to have a final composition of 1:1 (**1**:**2**), as the monomer **1** addition rate decreased, the incorporation of monomer **1** into the copolymer also decreased, possibly due to increased amounts of quenched monomer.

Chapter 3

Cross-propagation in Ni-catalyzed copolymerizations of 3-alkylthiophenes and 2,5-dialkoxybenzenes

Introduction

The recent advances in nickel-catalyzed chain-growth polycondensations have created a powerful means of synthesizing well-defined and uniform π-conjugated polymers.[1] The chain-growth behavior is hypothesized to be due to the formation of a Ni-polymer π-complex, which maintains association of the Ni catalyst with the polymer throughout the polymerization. A particularly attractive use of this method is the synthesis of copolymers with new sequences. The first example of an all-conjugated block copolymer with structurally distinct monomers prepared by this method was demonstrated by Yokozawa in the block copolymerization of 2,5-(bishexyloxy)benzene and 3-hexylthiophene monomers by successive monomer addition to form a diblock copolymer.[2] It was found that the order of monomer addition was critical to the success of block copolymer formation.[2,3] Specifically, when the polymerization of 3-hexylthiophene monomer (**1a**) was followed by the addition of 2,5-bis(hexyloxy)benzene monomer (**2a**), the polydispersity of the block copolymer was significantly greater than the 3-hexylthiophene macroinitiator (Scheme 3.1). This result suggested that the transfer of the Ni-catalyst from the thiophene prepolymer to the active phenylene chain-end was inefficient. However, block copolymer formation was successful when the phenylene monomer was polymerized before the thiophene monomer. The order of monomer addition has also been shown to determine copolymerization success in the thiophene-fluorene,[4] fluorene-phenylene,[4] and phenylene-pyrrole[5] block copolymerizations.

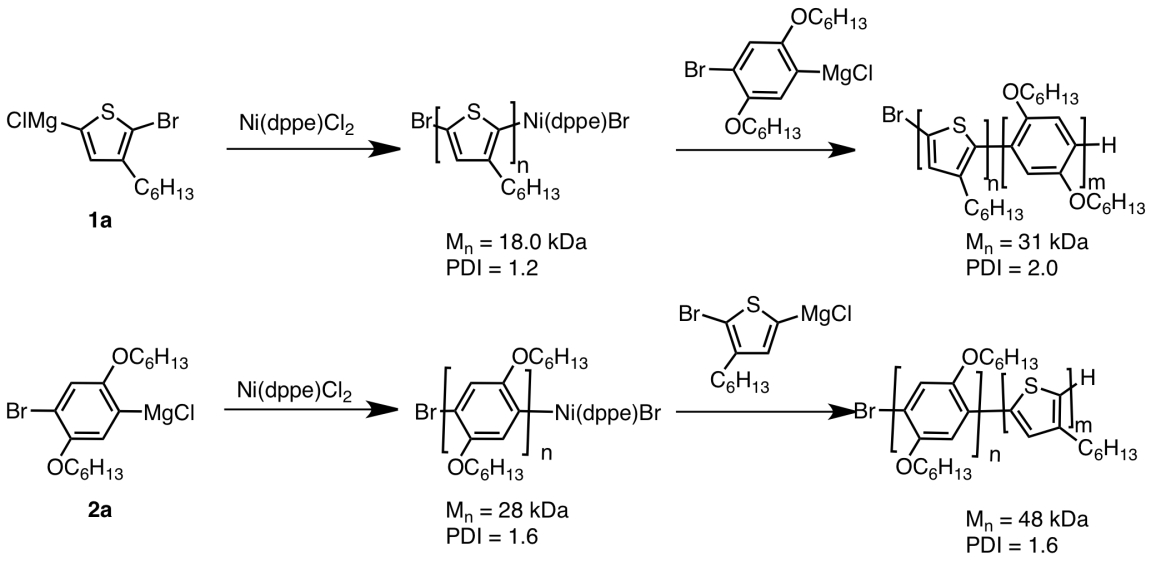

Scheme 3.1 Impact of copolymerization order on cross-propagation

The importance of monomer addition order on copolymerization success is hypothesized to be due to a difference in π-binding ability between poly(2,5-bis(hexyloxy)benzene) and poly(3-hexylthiophene).[2] The Ni catalyst is hypothesized to remain associated with the poly(3-hexylthiophene) segment after the first addition of arene monomer (Scheme 3.2). If the poly(3-hexylthiophene) segment irreversibly ligates the Ni catalyst and prevents it from migrating to the terminal arene C-Br bond of the polymer, chain termination pathways, such as Ni dissociation, can become competitive with propagation. At this point, Ni^0 may dissociate from the polymer through ligand exchange, possibly to monomer, leading to initiation of a new polymer chain. While inefficient cross-propagation due to different π-binding ability can be circumvented by judicious choice of monomer addition order in block copolymerizations, construction of more complex copolymer sequences, such as statistical and gradient copolymers, requires multiple cross-propagation events. To access more sophisticated copolymer sequences it is necessary to better understand the limitations of cross-propagation in these Ni-catalyzed polycondensations and develop controlled copolymerizations.

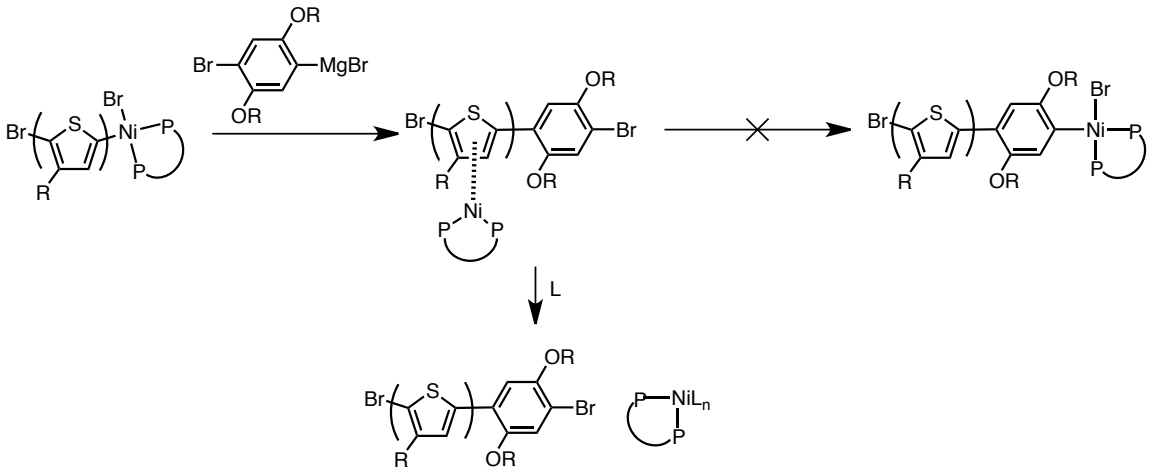

Scheme 3.2 Proposed mechanism of Ni dissociation during cross-propagation.

We recently developed the Ni-catalyzed living, chain-growth copolymerization of 3-hexylthiophene and 3-(hexyloxy)methylthiophene and used this method to create the first gradient conjugated copolymers.[6] Controlled copolymerization was also used to synthesize block and random copolymers of 3-hexylthiophene and 3-(hexyloxy)methylthiophene. Comparison of copolymers with different sequences revealed that copolymer sequence impacted the solid-state organization of the copolymers. However our efforts to expand the scope of controlled copolymerizations to comonomers that were not both thiophene derivatives, described in Chapter 4, were stymied by breakdown of living polymerization behavior during cross-propagation.

In our effort to expand the scope of controlled copolymerizations we undertook studies on cross-propagation of 3-alkylthiophene and 2,5-dialkoxybenzene monomers. These co-monomers were chosen because they undergo controlled homopolymerization but do not copolymerize via a living mechanism. We hypothesized that changing the ligand environment around the Ni center can improve catalyst-transfer between monomers. Previous investigations on the role of ligand steric properties in Ni-catalyzed polycondensations showed no significant difference in cross-propagation in copolymerizations initiated with Ni(bis(diethylphosphino)ethane)Cl_2 (Ni(depe)Cl_2) relative to those from Ni(dppe)Cl_2(Scheme 3.3).[7] This result was surprising since we had hypothesized that increased electron donation from bis(diethylphosphino)ethane relative to bis(diphenylphosphino)ethane would stabilize the proposed Ni-polymer intermediate, leading to less dissociation of Ni from the polymer. While these studies did not find a

difference in cross-propagation we were encouraged by recent[8] results from our laboratory which indicate that electron-rich ligands with identical steric properties lead to lower polymer polydispersities in the homopolymerization of 2,5-(bishexyloxy)benzene. It is thought that this effect is the result of greater backbonding in the Ni-π intermediate due to increased electron density at Ni. Increased stability of the Ni-π complex could result in more efficient cross-propagation between different monomers by suppression of π-complex dissociation. Alternatively, decreasing electron density at the Ni center may decrease the difference in π-affinity of the Ni catalyst for the thiophene monomer relative to the arene monomer and promote catalyst-transfer to the arene. By testing both orders of monomer addition to the block copolymerization we can determine whether cross-propagation is affected by ligand electronics. To further shed light on catalyst-transfer we conducted batch copolymerizations while varying ligand electronics. Batch copolymerizations involve multiple cross-propagations during the polymerization, increasing any difference in the continued association of Ni catalyst with growing polymer chains. Next, we investigated catalyst-transfer and dissociation in a series of small-molecule model reactions and examined ligand electronic effects on Ni-π complex lifetime relative to dissociation.

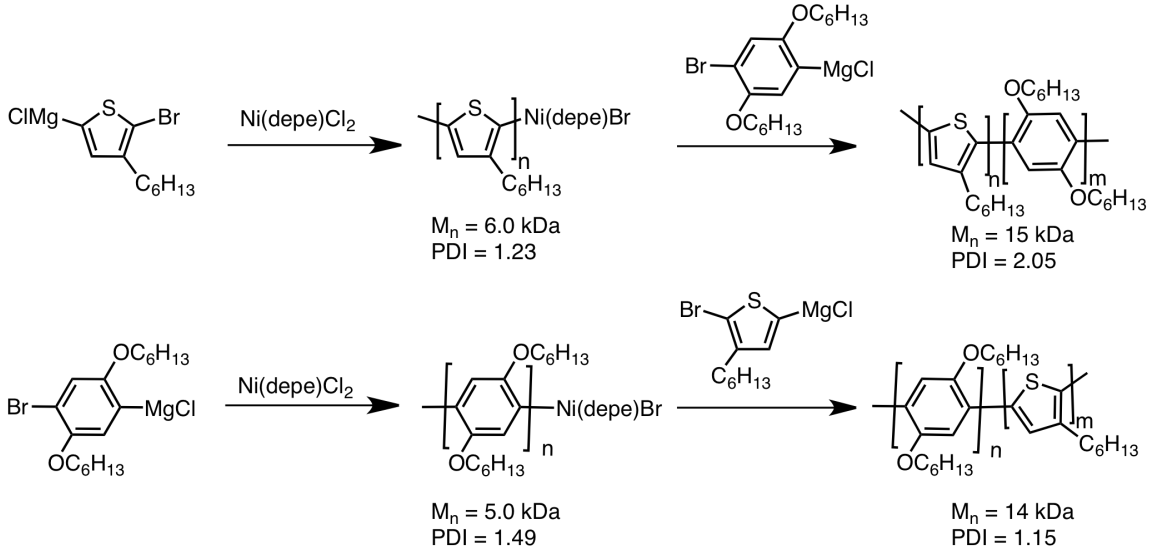

Scheme 3.3 Block copolymerizations initiated by Ni(depe)Cl_2

Results and Discussion

Block copolymerizations

We probed the effect of ligand electronic properties on cross-propagation efficiency in diblock copolymerizations of monomers **1a** and **2a** (Scheme 3.4) using both orders of monomer addition. To test these possibilities, we synthesized Ni initiators **3a-c** via oxidative addition of ortho-bromoanisole to $Ni(cod)_2$ in the presence of two equivalents of triphenylphosphine (PPh_3), followed by ligand exchange with the appropriate bis(diarylphosphino)ethane (Scheme 3.5).[9,10] The o-anisyl group incorporated in the Ni initiator serves to solubilize and stabilize the initiator as well ensure the polymer will propagate from only one chain end.[11] We subsequently used these Ni complexes to initiate copolymerizations of **1a** and **2a.**

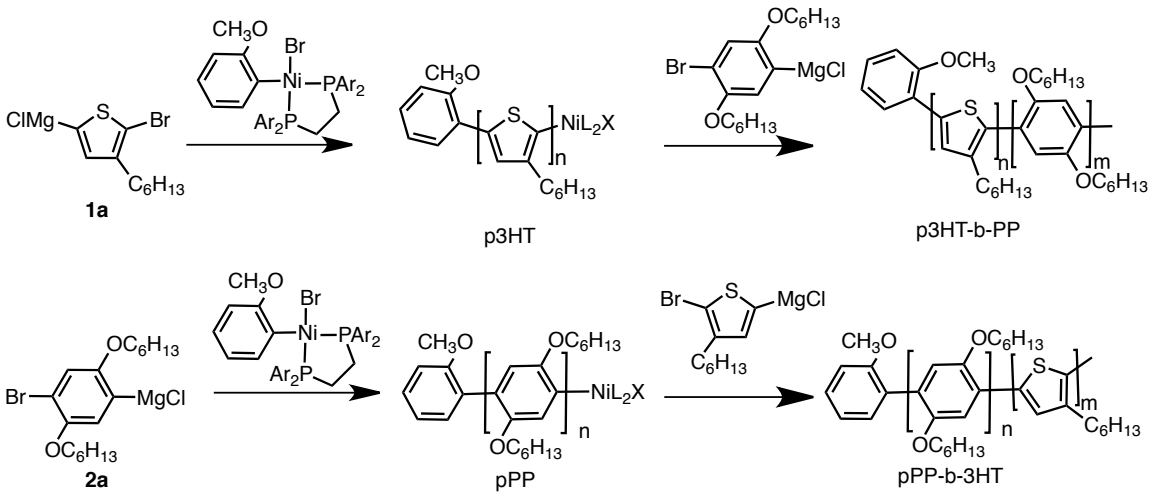

Scheme 3.4 Block copolymerizations with Ni initiators **3a-c.**

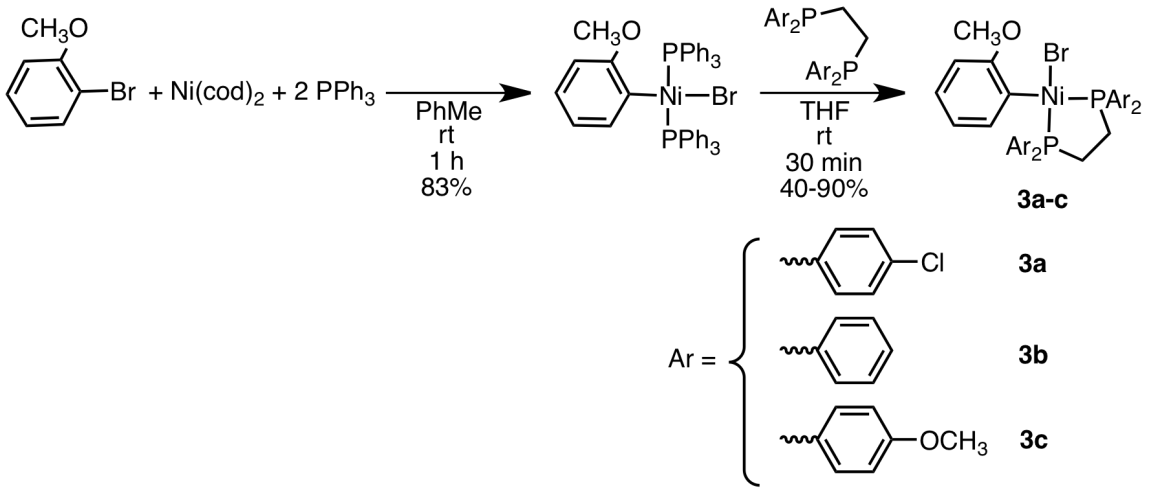

Scheme 3.5 Synthesis of Ni-anisyl initiators **3a-c**

Analysis of the block copolymerization data indicates differences in the copolymerization behavior of the electronically differentiated Ni initiators **3a-c** (Table 3.1). There is an increase in the number average molecular weight (M_n) after addition of the second monomer in all copolymerizations, indicating that there is a degree of catalyst transfer to the second monomer. Catalyst transfer from the thiophene macroinitiator (p3HT) to phenylene remains inefficient for all initiators, but it is clear that electron-poor **3a** has the highest degree of catalyst dissociation from the prepolymer. In addition, the more electron-rich catalyst **3c** resulted in lower polydispersities (PDI), suggesting that increasing electron density at Ni promotes continued association of the Ni-polymer intermediate. Comparison of representative GPC profiles of the polyphenylene (pPP) and p3HT macroinitiators (Figure 3.1) display unimodal distributions of molecular weight; although the polyphenylene displays evidence of "peak tailing" in the lower molecular weight region. This tailing may be due to a slow rate of initiation relative to propagation[6,12] or catalyst quenching during the polymerization. Catalyst transfer from p-PP to the 3-hexylthiophene monomer is efficient for all initiators as shown by the maintenance of low copolymer PDI and unimodal molecular weight distributions for poly(2,5-bishexyloxybenzene)-*block*-3-hexylthiophene (pPP-b-3HT) (Figure 3.1A). The poly(3-hexylthiophene)-*block*-2,5-(bishexyloxy)benzene (p3HT-b-PP) (Figure 3.1B) GPC profile is clearly bimodal for all initiators, indicating that a significant portion of the p-3HT macroinitiator failed to incorporate 2,5-(bishexyloxy)benzene monomer into the polymer. These studies indicate that electron-rich **3c** performs best in the block

copolymerizations, suggesting that the cross-propagation event is facilitated with these ligands due to a robust association between the catalyst and polymer chain. To provide support for this hypothesis, multiple cross-propagation events were further probed using batch copolymerizations.

Table 3.1 Summary of block copolymerization data

Initiator	pPP M_n (kDa)	pPP PDI	pPP-b-3HT M_n (kDa)	p-PP-b-3HT PDI
3a	28.3	2.02	48.0	1.96
3b	26.5	1.29	57.8	1.55
3c	31.2	1.33	59.5	1.31
	p3HT M_n (kDa)	**p3HT PDI**	**p3HT-b-PP M_n (kDa)**	**p3HT-b-PP PDI**
3a	31.5	1.12	39.7	2.44
3b	25.4	1.07	41.5	1.68
3c	27.9	1.04	38.2	1.71

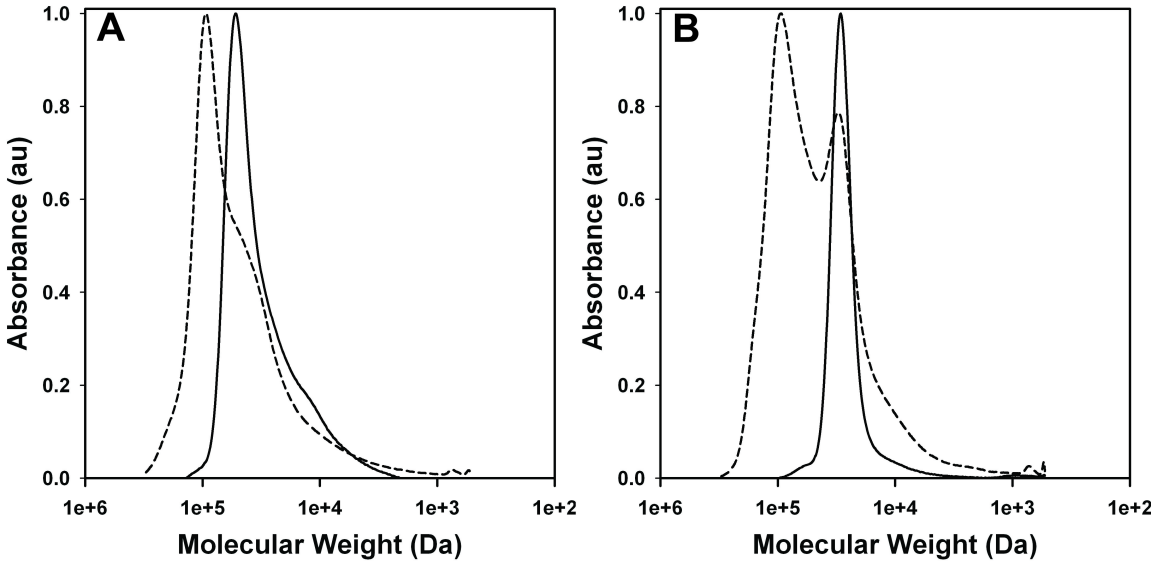

Figure 3.1 (A) GPC profile of p-PP (solid line) and pPP-b-3HT (dashed line) initiated by **3c** ([**1a**] = [**2a**] = 0.10 M [**Ni**] = 0.001 M). (B) GPC profile of p3HT (solid line) and p3HT-b-PP (dashed line) initiated by **3c** ([**1a**] = [**1a**] = 0.10 M [**Ni**] = 0.001 M)

Batch Copolymerizations

We next investigated the behavior of batch copolymerizations of **1a** and **2a** initiated by **3a-c** (Scheme 3.6). Batch copolymerizations, where both monomers are present throughout the polymerization and their inclusion into the growing polymer is dictated by their relative reactivity and concentration, feature multiple cross-propagation events. Having multiple catalyst-transfers during the polymerization will increase

differences in the behavior of the electronically differentiated catalysts. Monitoring the conversion of **1a** and **2a** over the course of the polymerization initiated by **3b** revealed that **1a** is incorporated into the copolymer faster than **2a** (Figure 3.2A) and both monomers are incorporated into the copolymer. Analysis of the polymer molecular weight as a function of total monomer conversion indicated that as **2a** is consumed the chain-growth behavior of the copolymerization ceases, as evidenced by the increase in PDI and nonlinear increase in M_n as conversion and the number of catalyst transfers from one monomer to the other increases (Figure 3.2B).

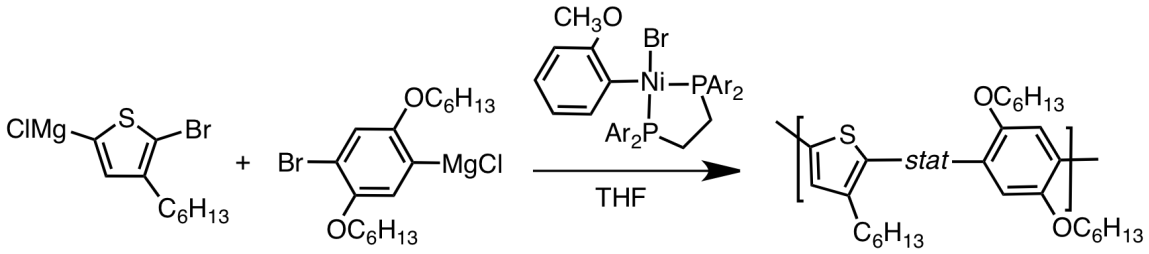

Scheme 3.6 Batch copolymerizations of **1a** and **2a** with Ni initiators **3a-c.**

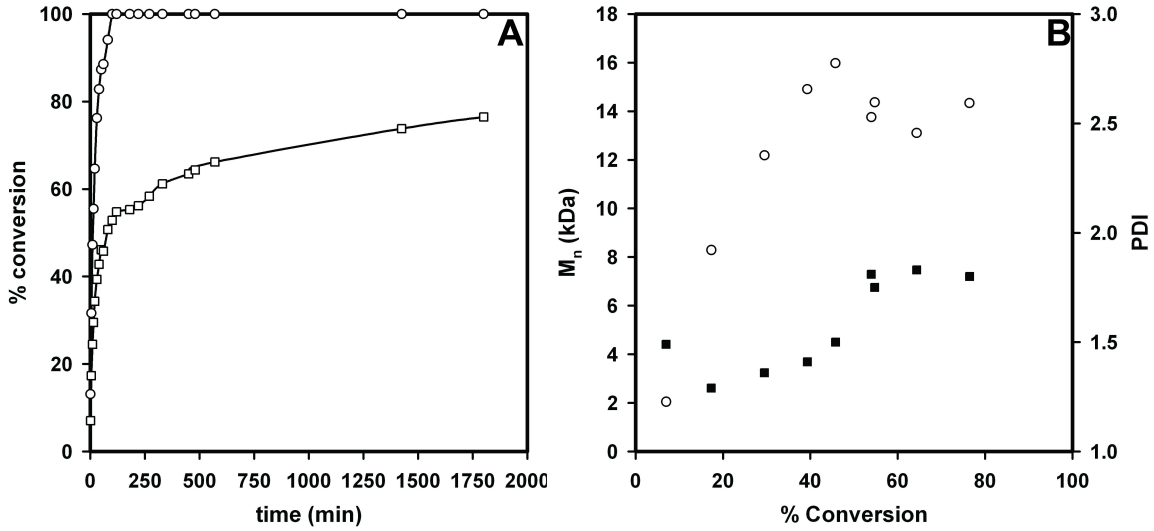

Figure 3.2 (A) Plot of conversion versus time for the batch copolymerization of **1a** (○) and **2a** (□) initiated by **3b** ([**1a**] = [**2a**] = 0.10 M [**3b**] = 0.0025 M). (B) Plot of M_n (○) and PDI (■) versus time for the copolymerization of **1a** and **2a** initiated by **3b** ([**1a**] = [**2a**] = 0.10 M [**3b**] = 0.0025 M).

Batch copolymerizations were conducted at varying ratios of monomer-to-initiator to test whether chain-transfer would increase as the number of propagation events increase. In a living, chain-growth polymerization, the end molecular weight of the polymer is determined by the amount of monomer relative to initiator. If the Ni-

catalyst is dissociating from the initially formed polymer chains during cross-propagation then the PDI of the copolymerization should broaden as the ratio of monomer to initiator increases. From these experiments it is evident that as the degree of polymerization increases the polydispersity also increases (Figure 3.9). As the monomer-to-initiator ratio increases the end molecular weight also increases, as expected from a chain-growth polymerization. However, it is clear that copolymers from initiator **3a** are shorter than those from **3b** or **3c**, indicating that more chain-termination and transfer is occurring with the more electron-poor catalyst. Copolymers from electron-rich initiator **3c** displayed the lowest PDIs, suggesting that electron-rich Ni centers promote continued association with the polymer during cross-propagation. GPC profiles of the polymers from the batch copolymerizations (Figure 3.10) also indicate that fewer copolymers initiated by electron-rich initiator **3c** do not undergo catalyst dissociation, as evidenced by the greater proportion of high molecular weight polymer at higher monomer to initiator ratios.

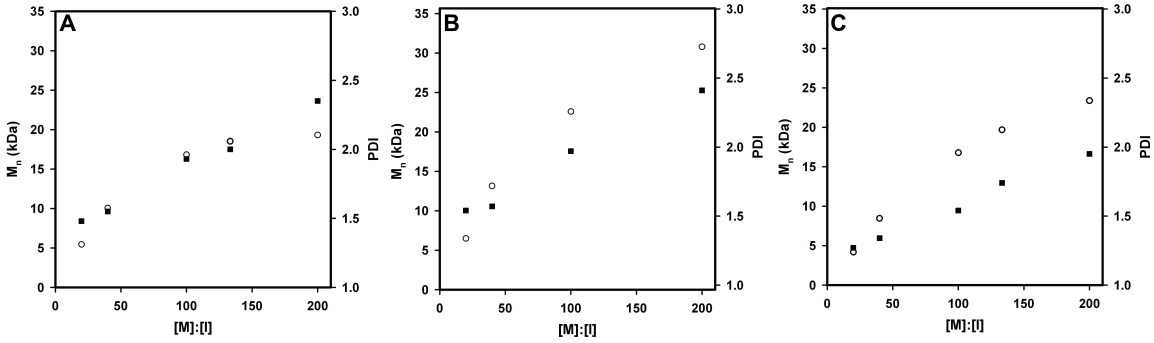

Figure 3.3 Plot of M_n (○) and PDI (■) versus monomer-to-initiator ratio (M:I) for the batch copolymerization of **1a** and **2a** initiated by (A) **3a** (B) **3b** (C) **3c** ([**1a**] = [**2a**] = 0.04 M).

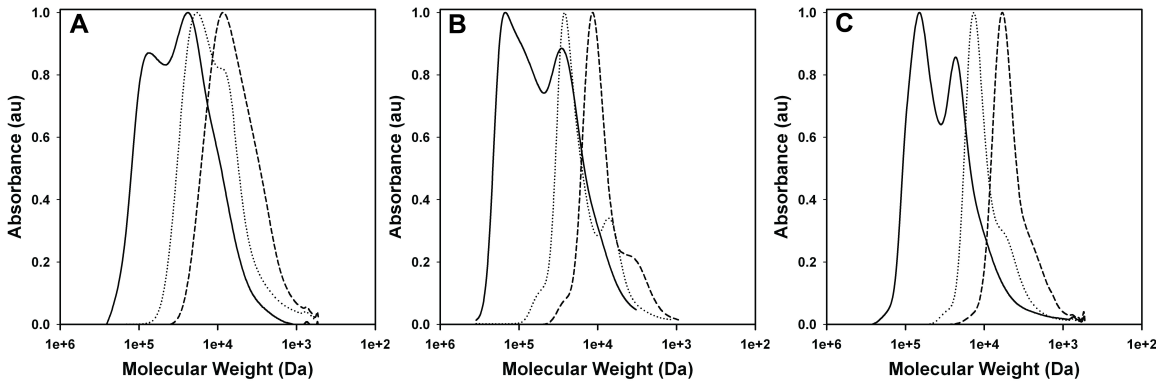

Figure 3.4 GPC profiles of batch copolymerizations of **1a** and **2a** initiated by (A) **3a** (B) **3b** (C) **3c** ([**1a**] = [**2a**] = 0.04 M, [**Ni**] = 0.4 mM (solid line), 2 mM (dotted line), 4 mM (dashed line)).

Small-molecule block copolymerization model

We next sought to determine if the improved copolymerization behavior we observed with electron-rich catalysts was due to a difference in π-binding affinities as well as test whether Ni^0 irreversibly complexes to a thiophene monomer when two different monomers are present. Small molecule cross-over experiments (Scheme 3.7) were designed to model the transition from a thiophene polymer to a 2,5-dialkoxybenzene monomer. This model study was designed to create a Ni-thiophene-arene intermediate similar to what is formed in the block copolymerization of 3-alkylthiophene and 2,5-dialkoxybenzene during the transfer from a polythiophene block to the phenylene monomer.

Starting with Ni complexes **4a-c**, transmetallation of thiophene monomer model **1b** followed by reductive elimination would generate the proposed Ni-thiophene-arene complex. This complex is analogous to that formed at the first crossover event during the poly(3-hexylthiophene)-block-(2,5-(bishexyloxy)phenylene) polymerization. At this stage, Ni^0 can undergo a ligand exchange reaction to dissociate from the π-complex or migrate to the aryl C-Br bond and undergo oxidative addition. Our initial hypothesis, based on results from block copolymerization experiments, was that some Ni^0 would preferentially bind to the thiophene π-system and eventually undergo ligand exchange with solvent or an equivalent of monomer. In this way the Ni^0 would not transfer to the arene monomer and undergo oxidative addition. An equivalent of trapping ligand was

added to the reactions to prevent "free" Ni^0 from further reaction with dissociated aryl bromide.[13] After hydrolysis of organometallic species the reactions were analyzed for the amounts of products **5**, **6** and **7** by gas chromatography. Products **5** and **6** arise from a pathway where Ni^0 remains associated with **7** until oxidative addition whereas **7** results from dissociation of Ni^0 from the arene-thiophene complex. Results from these studies are given in Table 3.2 where % associative is the ratio of products from continued association of Ni to **7** over all products (e.g. (**5** + **6**)/(**5** + **6** + **7**).

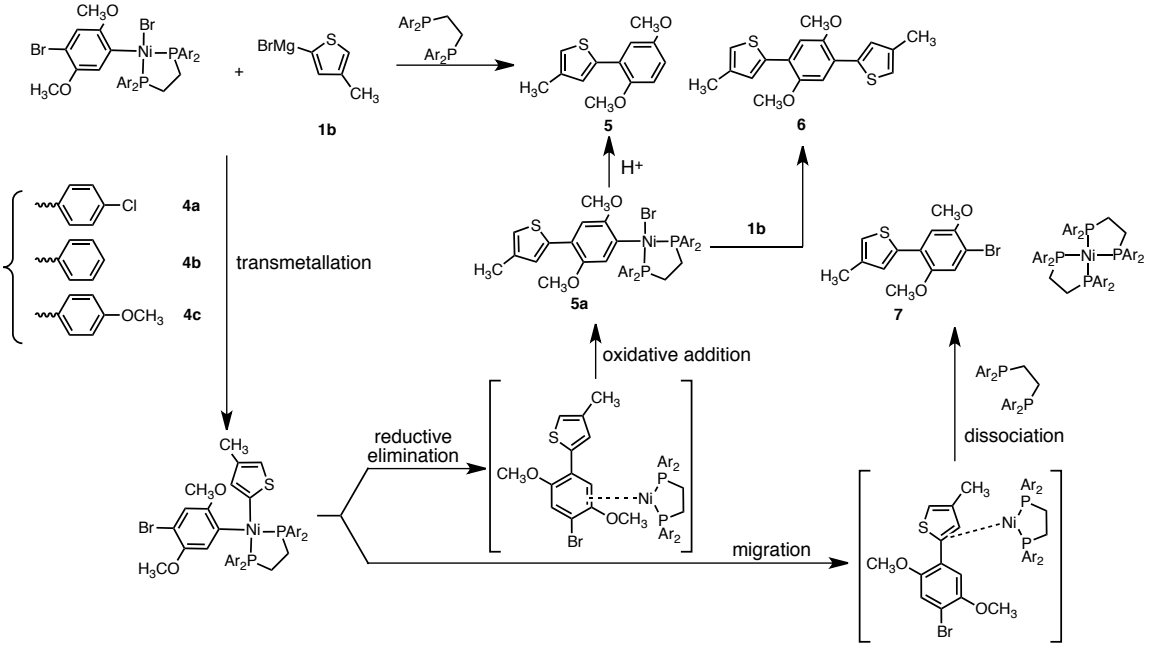

Scheme 3.7 Block copolymerization model study design

Table 3.2 Summary of crossover studies

catalyst	% associative
4a	94 ± 6
4b	90 ± 5
4c	93 ± 4

During these crossover experiments we were surprised to observe a high degree of continued association of the Ni catalyst with **7**, as evidenced by predominant formation of **5** and **6** in the cross-couplings. Unlike copolymerizations, where it appears that a significant fraction of Ni^0 does not transfer from a poly(thiophene) segment to a phenylene monomer, the Ni-aryl associated complex appears to not undergo a significant amount of dissociation during catalyst transfer. As a comparison, we designed an

analogous chain extension experiment to model the stability of the Ni-π complex in a homopolymerization (Scheme 3.8). From these results (Table 3.3) there appears to be no difference in the ability of the Ni-diarene or Ni-arene-thiophene complex to undergo oxidative addition.

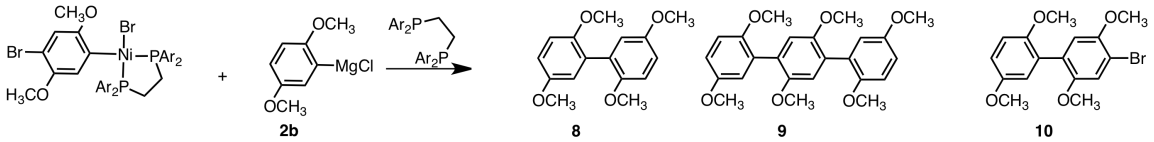

Scheme 3.8 Chain extension model design

Table 3.3 Summary of chain extension model studies

catalyst	% associative
4a	94 ± 3
4b	91 ± 7
4c	91 ± 7

π-Competition experiments

We next turned our attention to determining the difference in π-affinity of the Ni^0 intermediate for 3-alkylthiophene and 2,5-dialkoxybenzene monomers (Scheme 3.9). A Ni-arene-thiophene intermediate was designed that placed aryl-Br and thienyl-Br bonds in direct competition for oxidative addition. Our hypothesis was that the π-system with greater affinity for Ni^0 would undergo oxidative addition to a greater extent due to proximity of Ni^0 with the reactive bond. To test this hypothesis, we utilized Ni complexes **4a-c** and thiophene monomer **1c**, which contains a thienyl-Br bond. Transmetallation of **2c** to **4a-c** and reductive elimination generates a Ni-arene-thiophene complex. Ni^0 can then equilibrate between the different π-systems and undergo oxidative addition. Subsequent hydrolysis of the organometallic species yields **7** and **11**, which we quantified by gas chromatography. In these studies we observed solely products arising from oxidative addition into the thienyl-Br bond for all Ni catalysts. No products resulting from dissociation of the Ni-arene-thiophene π-intermediate were observed in these reactions.

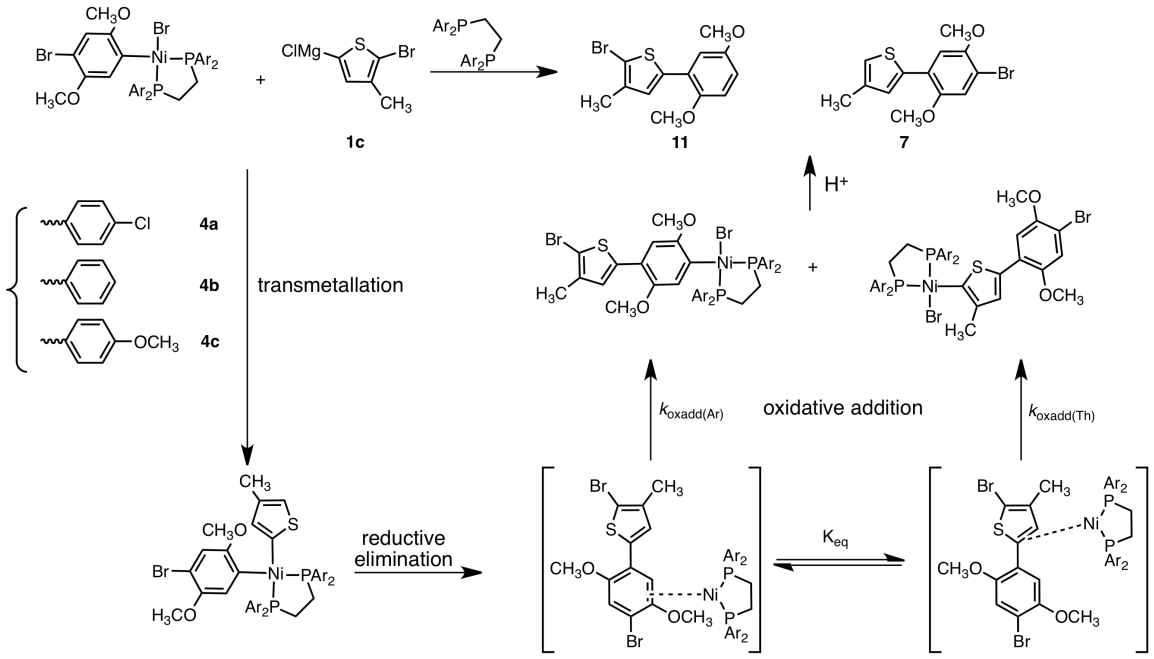

Scheme 3.9 π-competition model study design

We had hypothesized that the ratio of **5**:**7** would be largely determined by the equilibrium between the two the Ni-arene-thiophene π-intermediates (K_{eq}). However, the relative rates of oxidative addition ($k_{oxadd(Ar)}$, $k_{oxadd(Th)}$) also impact the product ratio. These relative rates were determined by a different experiment wherein 1 equivalent of Ni^0 was treated with one equivalent each of a 2-bromo-3-methylthiophene and bromo-2,5-dimethoxybenzene (Scheme 3.10). Product ratios and conversion were determined by ^{31}P NMR spectroscopy (Figure 3.5) and gas chromatography. From this experiment it was determined that **11**:**12** is approximately 1:50. Since oxidative addition is preceded by association of π–binding of Ni^0 to the aryl and thienyl halide it is difficult to directly determine $k_{oxadd(Ar)}$: $k_{oxadd(Th)}$. This experiment suggests it is possible that the results from the π-affinity studies are solely determined by the fast rate thiophene of oxidative addition relative to the arene monomer, instead of being a reflection of which π-system ligates Ni^0.

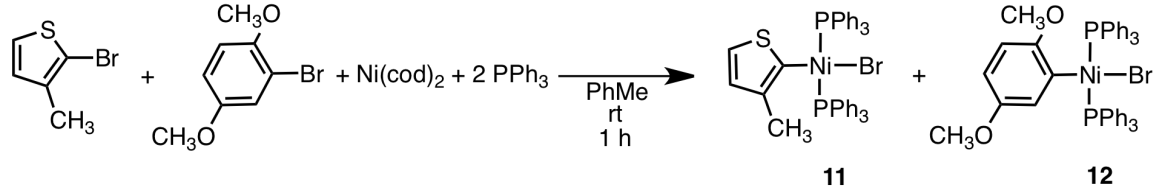

Scheme 3.10 Competitive oxidative addition to Ni^0 model study

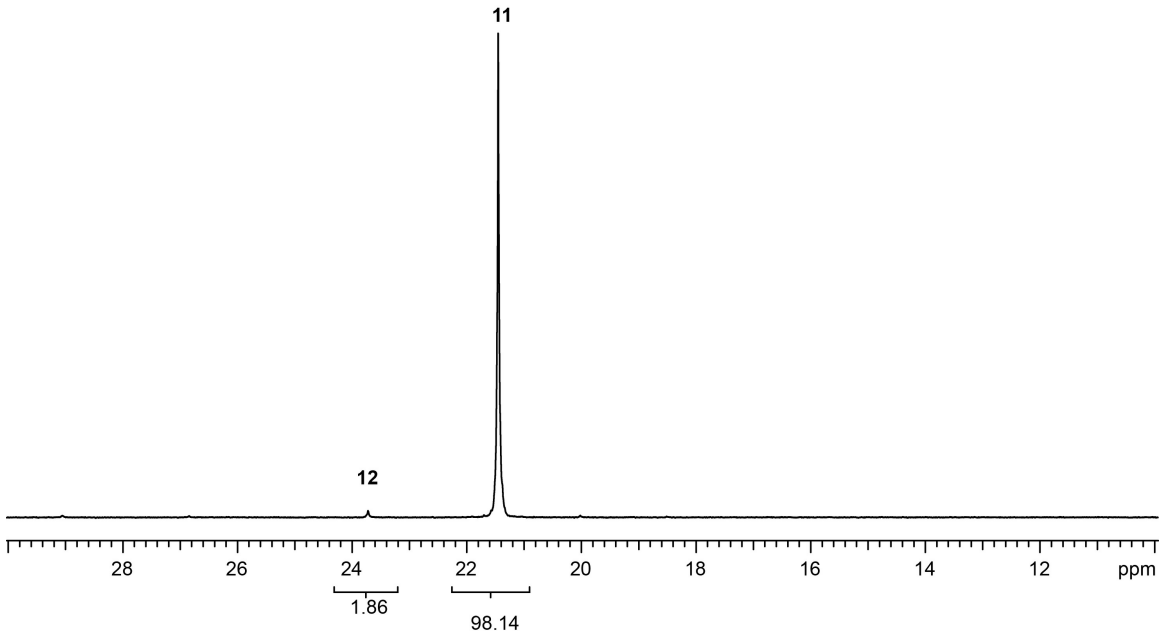

Figure 3.5 ^{31}P NMR spectrum of products from competitive oxidative addition.

Conclusions

Our investigations into cross-propagation of 3-alkylthiophene and 2,5-dialkoxybenzene monomers have yielded some insights into cross-propagation in Ni-catalyzed Kumada coupling copolymerizations. From the block copolymerization experiments it is clear that catalyst-transfer from poly(thiophene) to the phenylene monomer results in a significant amount of catalyst dissociation from the polymer, leading to chain termination and transfer. The amount of chain-transfer increased as the number of cross-propagations increased, as in a batch copolymerization. However, this dissociation cannot simply be due to breakdown of Ni-arene-thiophene π-complex due to different binding affinities of the arene and thiophene monomers because the amount of catalyst dissociation from our small molecule arene-thiophene system is comparable to that of the biaryl system. A possible alternative explanation in the difference between the copolymerizations and our model system may lie in recent observations of catalyst "ring-walking" across the length of a polymer (Scheme 3.11).[11] If the Ni catalyst has a greater degree of association with the 3-alkylthiophene segment than the arene then it will preferentially ring-walk away from the reactive chain-end. Ni^0 can then be intercepted via ligand exchange.

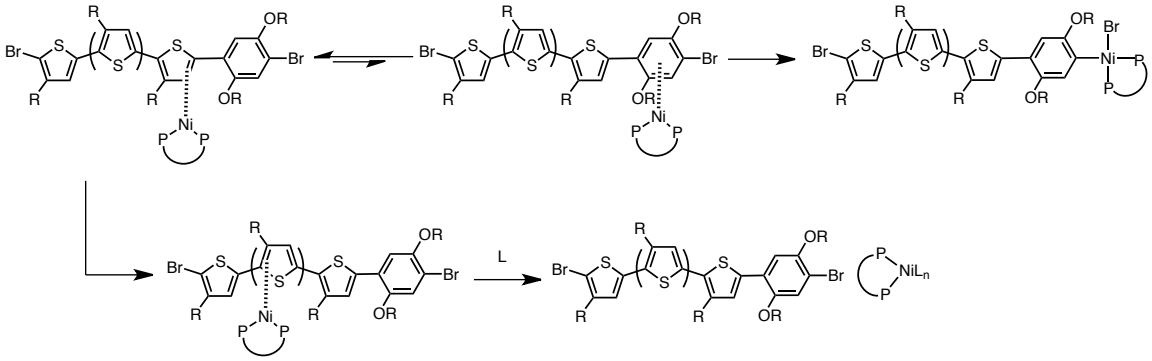

Scheme 3.11 Ni-ring-walking during copolymerization

Although electron-rich 1,2-bis(bis(4-methoxyphenyl)phosphino)ethane catalysts preformed the best in copolymerizations, our investigations into the effect of ligand electronics on cross-propagation did not yield a usefully more effective catalyst for the copolymerization of 3-alkylthiophenes and 2,5-dialkoxybenzenes. From these results it is clear that continued improvement of catalysts and reaction conditions is necessary to broaden the scope of living-chain-growth copolymerizations. Development of more electron-donating ligands, such as bidendate phosphites or diimines,[14] may decrease the amount of chain-transfer during cross-propagation. Alternatively, additives that may stabilize the Ni-polymer intermediate and prevent dissociation could be employed, as suggested in a recent report[15] of acetylacetone stabilized homopolymerization. Regardless of method, challenges in monomer cross-propagation must be overcome before a broader range of conjugated gradient copolymers can be prepared.

References Cited

(1) (a) Yokozawa T.; Yokoyama, A. *Chem. Rev.* **2009**, *109*, 5595-5619. (b) Osaka, I.; McCullough, R. D. *Acc. Chem. Res*. **2008**, *41*, 1202-1214. (c) Miyakoshi, R.; Yokoyama, A.; Yokozawa, T. *J. Poly. Sci., Part A: Polym. Chem*. **2008**, *46*, 753-765. (d) Yokoyama, A.; Miyakoshi, R.; Yokozawa, T. *Macromolecules* **2004**, *37*, 1169-1171. (e) Miyakoshi, R.; Yokoyama, A.; Yokozawa, T. *Macromol. Rapid Commun*. **2004**, *25*, 1663-1666. (f) Sheina, E. E.; Liu, J.; Iovu, M. C.; Laird, D. W.; McCullough, R. D. *Macromolecules* **2004**, *37*, 3526-3528.

(2) Miyakoshi, R.; Yokoyama, A.; Yokozawa, T. *Chem. Lett.* **2008**, *37*, 1022-1023.

(3) Wu, S.P.; Bu, L. J.; Huang, L.; Yu, X.H.; Han, Y.C.; Geng, Y.H.; Wang, F.S. *Polymer* **2009**, *50*, 6245−6251.

(4) Javier, A. E.; Varshney, S. R.; McCullough, R. D. *Macromolecules* **2010**, *43*, 3233-3237.

(5) Yokoyama, A.; Kato, A.; Miyakoshi, R.; Yokozawa, T. *Macromolecules* **2008,** *41*, 7271-7273.

(6) Locke, J.R.; McNeil, A. J. *Macromolecules* **2010**, *43,* 8709-8710.

(7) Lanni, E.L.; Locke, J.R.; Gleave, C.M.; McNeil, A.J. *Macromolecules*, **2011**, *44,* 5136–5145.

(8) Lee, S. R.; Bryan, Z. J.; Wagner, A. M.; McNeil, A. J. *Chem. Sci.* **2012**, *3*, 1562-1566.

(9) Chatt, J.; Hussain, W.; Leigh, G. J.; Ali, H. M.; Pickett, C. J.; Rankin, D. A. *Dalton Trans*, **1985**, 1131-1136.

(10) (a) Marshall, N.; Sontag, S. K.; Locklin, J. *Chem. Commun*. **2011**, *47*, 5681-5689. (b) Doubina, N.; Paniagua, S. A.; Soldatova, A. V.; Jen, A. K. Y.; Marder, S. R.; Luscombe, C. K. *Macromolecules* **2011**, *44*, 512-520. (c) Tkachov, R.; Senkovskyy, V.; Oertel, U.; Synytska, A.; Horecha, M.; Kiriy, A. *Macromol. Rapid Commun*. **2010**, *31*, 2146-2150.

(11) Tkachov, R.; Senkovskyy, V.; Komber, H.; Sommer, J.-U.; Kiriy, A. *J. Am. Chem. Soc.* **2010**, *132*, 7803-7810.

(12) Lanni, E.L; Locke, J.R.; Gleave, C.M.; McNeil, A.J. *Macromolecules* **2011**, *44*, 5136-5145.

(13) The increased reactivity of thienyl bromide towards oxidative addition relative to aryl bromide necessitated the use of diphosphine ligands.

(14) (a) Magurudeniya, H.D.; Sista, P.; Westbrook, J.K.; Ourso, T.E.; Nguyen, K.; Maher,M.C.; Alemseghed, M.G.; Biewer, M.C.; Stefan, M.C. *Macromol. Rapid Commun.* **2011**, *32*, 1748–1752. (b) Sheina, E.E.; Iovu, M.C.; McCullough, R. D. *Polym. Prepr. (Am. Chem. Soc., Div. Polym. Chem.)* **2005**, *46*, 1070-1071.

(15) Sui, A.; Shi, X.; Wu, S.; Tian, H.; Geng, Y.; Wang, F. *Macromolecules* [online early access] DOI: 10.1021/ma3009299. Published online: June 22, 2012. http://pubs.acs.org (accessed June 22, 2012).

Chapter 4

Challenges in Ni-catalyzed Controlled Copolymerizations

The development of controlled polymerizations for π-conjugated polymers presents an opportunity to synthesize and study new, defined materials.[1] Controlled polymerization behavior is proposed to arise from formation of nickel-polymer π-complex between the nickel initiator and polymer chain after reductive elimination (Scheme 4.1). Subsequent intra-complex oxidative addition results in successive monomer addition to the polymer chain end. Controlled polymerizations enable the synthesis of materials with a molecular weight dependence on the ratio of monomer to nickel, defined end-groups, and narrow polydispersity. Broadening the scope of living, chain-growth polymerizations to copolymerization would pave the way toward the production of π-conjugated copolymers with defined sequences such as block, gradient or random copolymers. Controlling the sequence of conjugated copolymers offers a means of adjusting the nanoscale morphology exhibited in polymer electronic devices.[2]

Efforts towards developing controlled copolymerizations of monomers which homopolymerize in a controlled manner have been frustrated by inefficient catalyst transfer during cross-propagation between the monomers. For example, in the block copolymerization of 3-hexylthiophene and 2,5-bis(hexyloxy)benzene, the Ni catalyst was efficiently transferred from the poly(phenylene) macroinitiator to the thiophene monomer.[3] However the opposite order of polymerization resulted in a significant amount of catalyst dissociation from the initially formed poly(thiophene). This dependence of block copolymer formation on monomer addition order has been observed in the phenylene-fluorene,[4] thiophene-fluorene,[2] and phenylene-pyrrole[5] copolymerizations. The termination of controlled polymerization behavior during cross-propagation is proposed to result from the monomer with higher π-binding ability binding with Ni^0 and preventing the initiator from migrating to the reactive chain end. This hypothesis was tested in Chapter 3, where it was found that monomer differences in π-binding ability are not the sole factor for catalyst dissociation. Inefficient catalyst transfer

during cross-propagation restricts the types of π-conjugated copolymer sequences that can be synthesized via Ni-catalyzed polycondensations.

We are especially interested in studying π-conjugated gradient copolymers, which can only by synthesized via living, chain-growth copolymerization. Gradient copolymers are an attractive target because they may allow for control of the nanoscale phase separation in conjugated polymer blends used in organic electronic devices. Chapter 2 described our development of controlled copolymerization of thiophene monomers with different side chains and observations of sequence-dependent changes in the solid-state organization of the copolymers.[6] However, controlled copolymerization remains limited to 3-alkylthiophene[7], 3-arylthiophene[8] and 3-alkylselenophene[9] monomers. To further our goal of synthesizing new π-conjugated gradient copolymers we investigated the copolymerizations of several new monomer pairs as well as homopolymerization of new monomers. In these investigations we examined several Ni complexes with different steric and electronic properties as initiators of the polymerization (Scheme 4.2).

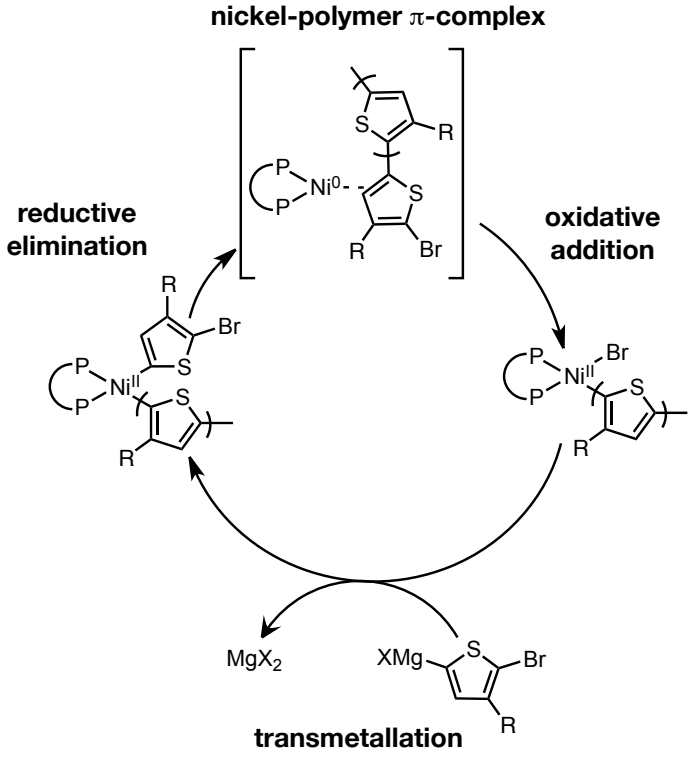

Scheme 4.1 Proposed mechanism of controlled cross-coupling polymerization

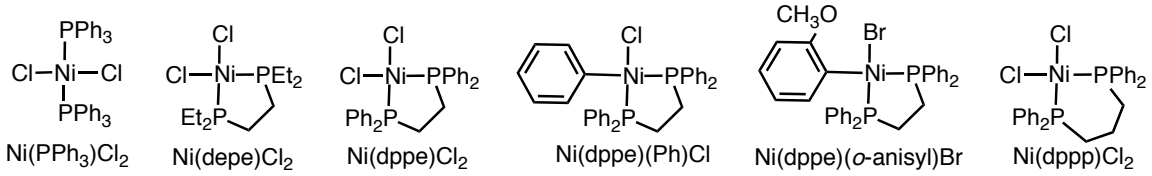

Scheme 4.2 Ni initiators used in these studies

Copolymerizations of 2,5-(bishexyloxy)benzene and 9,9-dioctylfluorene

We began by evaluating whether the Ni-catalyzed copolymerization of monomers **1**[10] and **2**[11] followed a chain-growth mechanism (eq 4.1). These monomers were chosen because each was reported to give a chain-growth homopolymerization and their polymers are commonly used in polymer light-emitting diodes.[12] Both monomers were prepared in situ by LiCl promoted magnesium-halogen exchange.[13] During the copolymerization the conversion of **1** and **2** were simultaneously monitored using in situ IR spectroscopy at 1330 and 810 cm^{-1}, respectively. Aliquots were taken over the course of the polymerization and analyzed by gel permeation chromatography to determine the number average molecular weight (M_n) and polydispersity (PDI).

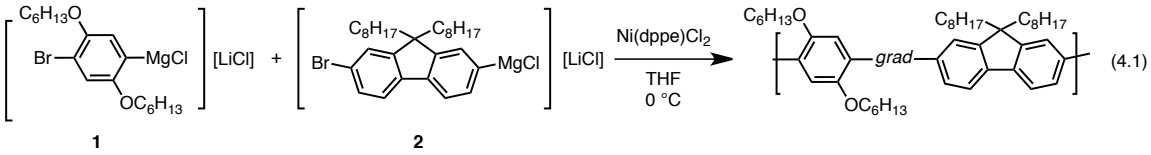

1 2

When $Ni(dppe)Cl_2$ was used as the initiator, a linear increase in M_n as a function of conversion was observed, suggesting a chain-growth mechanism (Figure 4.1A). Although the PDI of the resulting polymer is high for a chain-growth process, it decreases throughout the polymerization. This result suggests that the broad molecular weight distribution is due to a relatively slow and inefficient initiation, which leads to an initial large difference in polymer molecular weights that becomes less important as polymer chain length increases. Other Ni catalysts reported to give chain-growth homopolymerizations, such as $Ni(dppp)Cl_2$[14] and $Ni(PPh_3)_2Cl_2$,[15] did not exhibit chain-growth behavior in the copolymerizations (Appendix 3). Thus, $Ni(dppe)Cl_2$ was selected as the optimum catalyst for preparing gradient copolymers. The copolymerizations were run at 0 °C because the rt reactions resulted in copious amounts of Ni black and $Ni(dppe)_2$. These decomposition products may be due to competitive ligand exchange and

disproportionation during initiation. These processes remove unknown amounts of Ni catalyst from the polymerization and lead to uncontrolled conditions.

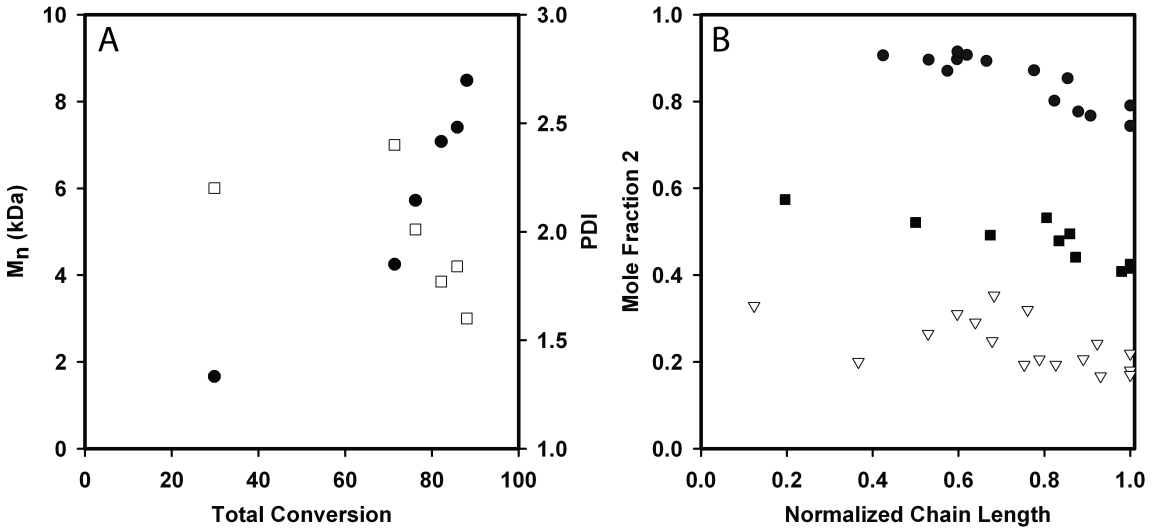

Figure 4.1 (A) Plot of M_n (●) and PDI (□) versus conversion for Ni(dppe)Cl_2-catalyzed batch copolymerization of **1** and **2** at 0 °C ([**1**]=[**2**] = 0.15 M, [Ni] = 3 mM). (B) Plot of the mole fraction **2** in the copolymer versus the normalized chain length from the batch copolymerizations. (**1:2**; P1 = 25:75 ●; P2 = 50:50 ■; P3 = 25:75 ▽)

A series of batch polymerizations were carried out wherein the initial molar ratio of **1:2** was varied, forming copolymers with different sequences and final compositions (Figure 4.1B). During these experiments it became apparent that there was a large difference in the reactivities of **1** and **2**. For example, a copolymerization using an initial equal molar ratio of **1:2** showed complete conversion of **2** within 42 min while monomer **1** was consumed after 336 min. To quantify these differences, the monomer reactivity ratios were determined through a series of experiments wherein the initial concentrations of **1** and **2** were varied. The rates of monomer consumption were followed for the first 30 % conversion by IR spectroscopy. These data were then fit to the integrated copolymerization equation[16] via least-squares regression (Appendix 3). In total, over 40 experiments at 8 different initial concentrations were simultaneously fit to determine the reactivity ratio. Interestingly, monomer 1 gave a reactivity ratio (r_1) of 0.35 ± 0.03 while monomer **2** gave a reactivity ratio (r_2) of 10 ± 1, consistent with our qualitative observations. These values indicate that the growing polymer chain prefers to add **2** over **1** regardless of the identity of the previously added monomer unit. Given that the two monomers are competing for the catalyst during the transmetallation step of the catalytic

cycle, the steric interactions between the *ortho*-substituted arene (**1**) and the catalyst may be more severe, leading to a diminished rate. As a result of large difference in reactivity ratios for **1** and **2**, batch copolymerizations create tapered block copolymers (Figure 4.2)

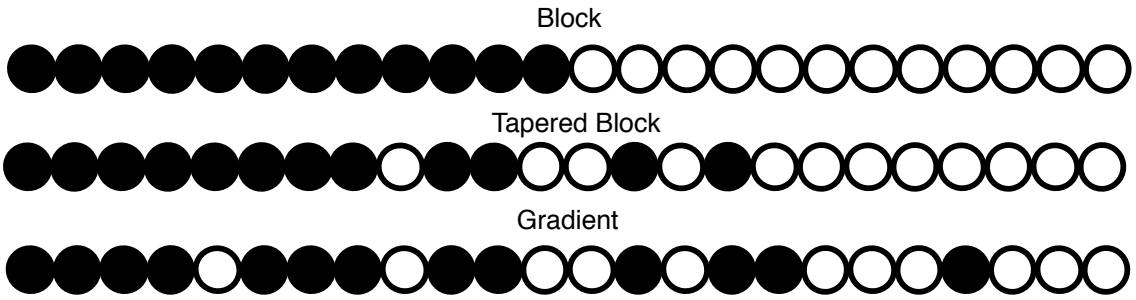

Figure 4.2 Copolymer sequences

Next, copolymers with a more gradual rate of compositional change were synthesized using the semi-batch method, wherein the more reactive monomer (**2**) is added to the reaction gradually over time. One advantage of this technique is that gradient copolymers with varying composition profiles can be prepared by using different rates of addition. These studies proved challenging, however, because the chain-growth behavior was found to depend on the total monomer concentration. For example, a linear increase in M_n was observed until the [monomer] reached approximately 0.02 M, at which point the increase in M_n slowed dramatically and a concomitant increase in PDI was observed (Figure 4.3B). This result is consistent with a change to a step-growth mechanism at high dilution or chain-transfer becoming competitive with propagation. When we conducted polymerizations at higher initial [monomer] the growing polymer chains precipitated at moderate chain-lengths, effectively removing active catalyst from the reaction. Ultimately, the [monomer]-dependent behavior of the copolymerization limited the gradient sequences that could be obtained by this method (Figure 4.3A).

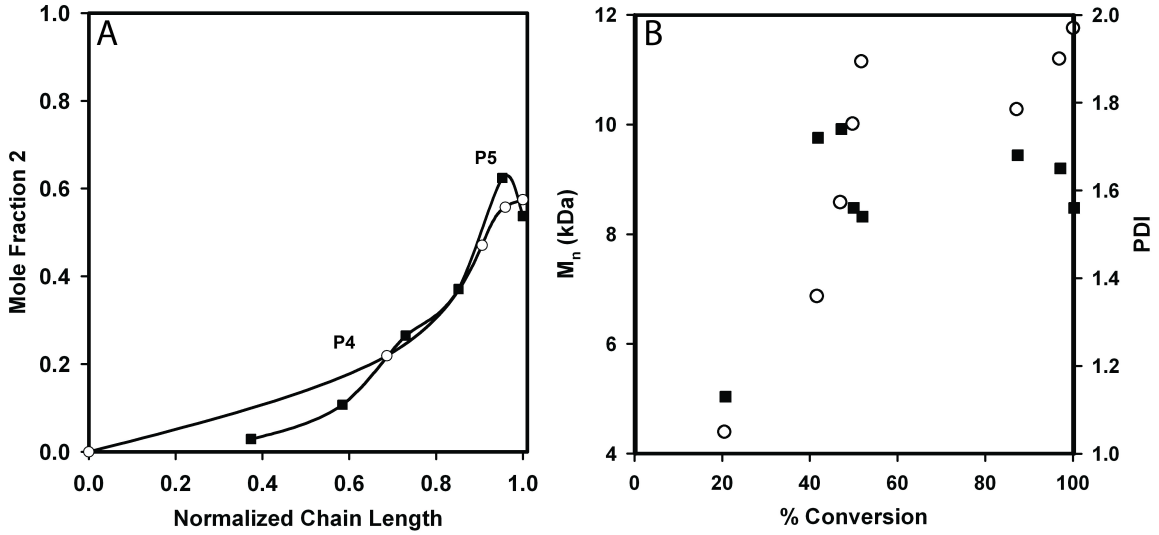

Figure 4.3. (A) Plot of semi-batch copolymerization mole fraction **2** versus normalized chain length at different rates of addition of **2** (**P4** = 0.47 mmol/h ○; **P5** = 0.32 mmol/h ■). (B) Plot of M_n (○) and PDI (■) versus conversion for Ni(dppe)Cl_2-catalyzed semibatch copolymerization of **1** and **2** at 0 °C ([**1**] 0.15 M, d[**2**]/dt = 0.34 mmol/h, [Ni] = 3 mM).

The solution phase and thin-film spectral properties of the tapered block copolymers prepared via the batch copolymerization method are shown in Figure 4.3. The tapered block copolymers absorb similar wavelengths to blends of the homopolymers in both solution and thin films. Surprisingly, the emission spectra predominantly show maxima at 430 nm, which corresponds to emission from polyfluorene. This result suggests that energy transfer along the tapered block π-conjugated copolymer backbone is highly efficient, even in dilute solutions.

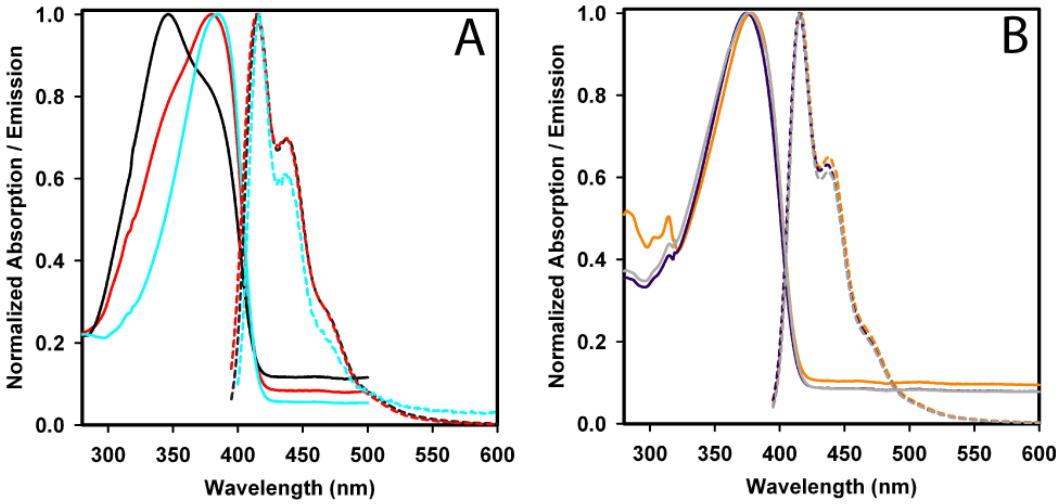

Figure 4.4. Absorption and emission spectra of batch copolymers in $CHCl_3$ solution (1.0 x 10^{-4} M) (A) **P1** blue: **P2** red: **P3** black (B) **P4** purple; **P5** gray

Copolymerizations of 3-hexylthiophene and N-hexylpyrrole

We next decided to investigate the copolymerization of 2-bromo-3-hexylthienyl magnesium chloride (**3**)[17] and (5-bromo-1-hexyl-1*H*-pyrrol-2-yl)magnesium chloride (**4**)[5] monomers. These monomers have been reported to undergo living, chain-growth homopolymerizations, but their copolymerization behavior had not been investigated. Monomer **3** was synthesized by bromination of 3-hexylthiophene followed by magnesium-bromine exchange (Appendix 3). Monomer **4** was prepared via N-alkylation of pyrrole, followed by bromination and LiCl promoted magnesium-halogen exchange (Appendix 3). Copolymers of thiophene and pyrrole monomers could potentially be useful in applications such as polymer transistors, due to the high charge mobility and conductivity of polythiophene and polypyrrole.

We began by evaluating the block copolymerization of **3** and **4** using both orders of monomer addition catalyzed by Ni dihalide salts that effect living, chain-growth homopolymerizations (Scheme 4.3). Block copolymerizations were initially chosen so that difficulties in catalyst-transfer between the monomers could be readily identified. Block copolymerizations of **3** and **4** initiated by Ni(dppe)Cl_2 and Ni(depe)Cl_2 showed evidence of catalyst dissociation during cross-propagation, reflected in an increase in the PDI of the copolymers (p3HT-*b*-Py, pPy-*b*-3HT) relative to the initial macroinitiator (p3HT, pPy) (Table 4.1) as well as bimodal distribution of molecular weights in the gel

permeation chromatogram. However, block copolymerizations initiated by Ni(dppp)Cl_2 displayed relatively small increases in PDI and maintained reasonably unimodal GPC profiles after polymerization of the second monomer for both sequences of monomer addition (Figure 4.4). Encouraged by this result, we conducted batch copolymerizations of **3** and **4** to confirm their living copolymerization behavior. During the batch copolymerizations it became apparent that there was a significant degree of catalyst dissociation as evidenced by a lack of a trend in M_n versus time (Figure 4.6A).[18] M_n ceases to increase as the amount of cross-propagation from **3** to **4** increases (Figure 4.6B). As shown in Chapter 3, multiple cross-propagations increase the amount of catalyst dissociation in uncontrolled copolymerizations. This result may not have been evident in the block copolymerizations, which feature a single cross-propagation event. The fact that a single cross-propagation between **3** and **4** was relatively efficient whereas batch copolymerizations failed to remain chain-growth supports the hypothesis that ring-walking during catalyst transfer, rather than differences in π-binding affinity between co-monomers, may be leading to catalyst dissociation. These uncontrolled copolymerizations are unsuitable for the synthesis of gradient copolymers.

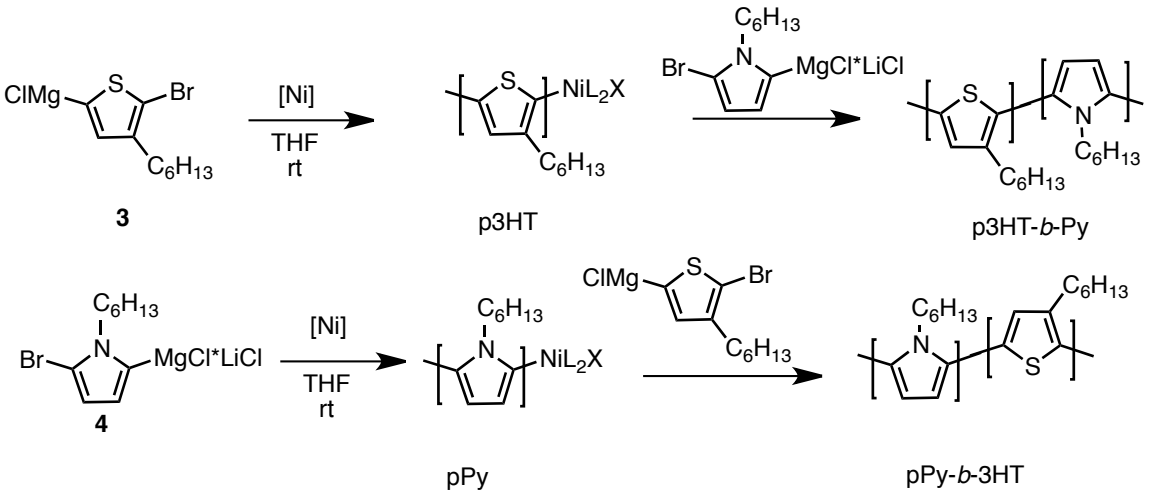

Scheme 4.3 Block copolymerizations of 3-hexylthiophene and *N*-hexylpyrrole ([**3**] = [**4**] = 0.1 M, [Ni] = 1.5 mM).

Table 4.1 Summary of block copolymerization data for the copolymerization of **3** and **4**

	p3HT		**p3HT-*b*-Py**	
[Ni]	**M_n (kDa)**	**PDI**	**M_n (kDa)**	**PDI**
$Ni(dppe)Cl_2$	8.7	1.4	13.9	1.6
$Ni(dppp)Cl_2$	5.5	1.3	14.0	1.6
$Ni(depe)Cl_2$	5.7	1.2	6.8	1.3
	pPy		**pPy-*b*-3HT**	
	M_n (kDa)	**PDI**	**M_n (kDa)**	**PDI**
$Ni(dppe)Cl_2$	8.7	1.4	8.7	1.7
$Ni(dppp)Cl_2$	6.3	1.3	10.5	1.4
$Ni(depe)Cl_2$	8.4	1.3	6.2	1.5

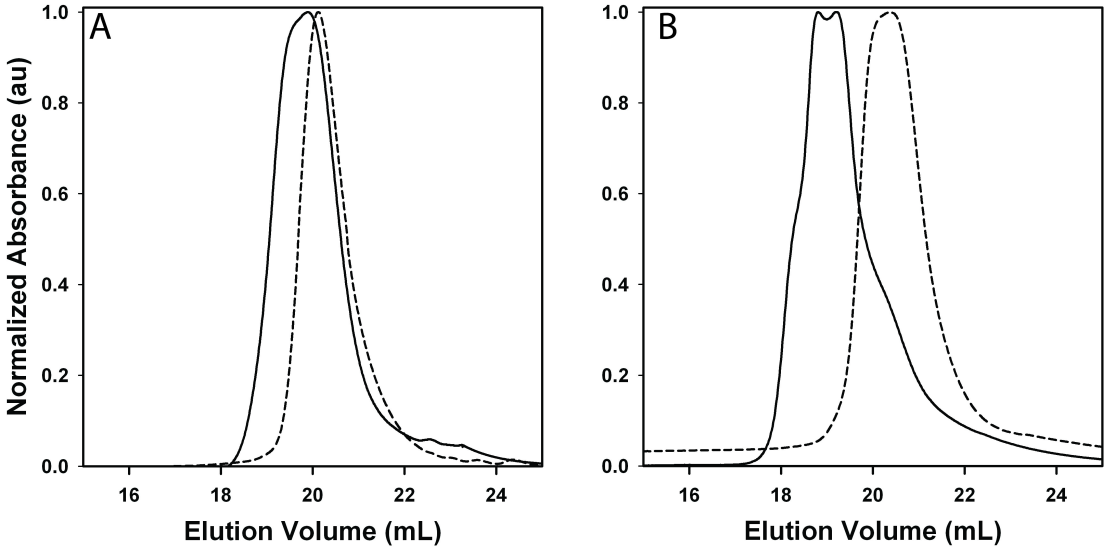

Figure 4.5 (A) Gel permeation chromatogram of p3HT (dashed line) and p3HT-b-Py initiated by $Ni(dppp)Cl_2$ ([**3**] = [**4**] = 0.25 M, [Ni] = 6.3 mM). (B) Gel permeation chromatogram of pPy (dashed line) and pPy-b-3HT initiated by $Ni(dppp)Cl_2$ ([**3**] = [**4**] = 0.25 M, [Ni] = 6.3 mM).

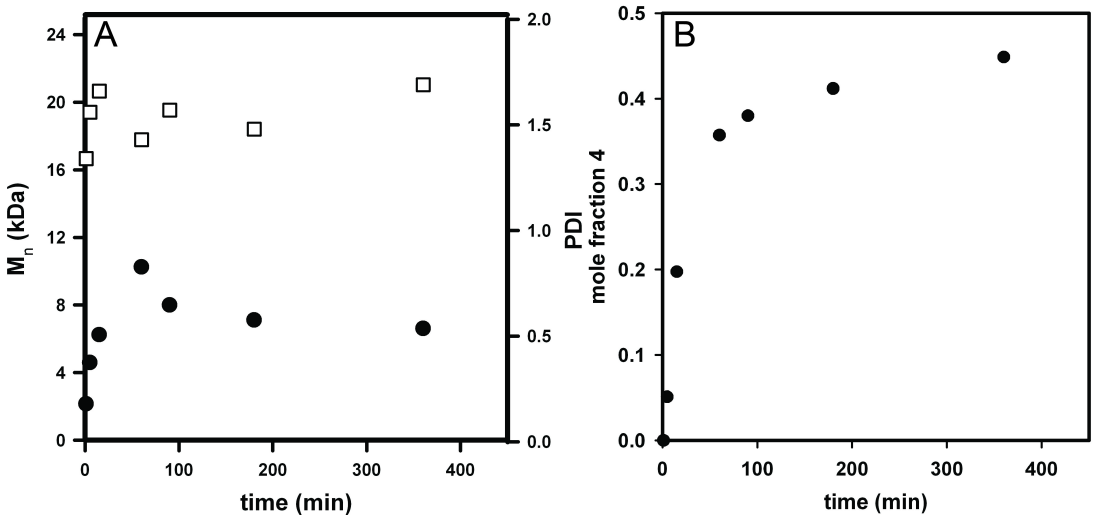

Figure 4.6 (A) Plot of M_n (●) and PDI (□) versus time for the batch copolymerization of **3** and **4** initiated by Ni(dppp)Cl_2 ([**3**]= [**4**] = 0.25 M, [Ni] = 6.3 mM). (B) Plot of the mole fraction of **4** in the copolymer versus time during the batch copolymerization of **3** and **4.**

Copolymerizations of 3-hexylthiophene and 3-octyloxythiophene

We investigated copolymerization of 3-hexylthiophene and 3-octyloxythiophene monomers **3** and **5**. Prior to our investigations, little attention had been focused on the homo or copolymerization behavior and mechanism of 3-alkoxythiophenes, but there were indications that polymerization of these monomers followed a chain-growth mechanism, such as low polymer polydispersity.[19] 3-Alkoxythiophenes exhibit a smaller bandgap, longer absorption wavelength, lower oxidation potential, and higher magnetic spin density compared to 3-alkylthiophenes.[11c, 20] We anticipated that copolymers of **3** and **5** would exhibit new optical and electronic properties, such as tunable bandgaps or broad absorption profiles for increased energy collection in organic photovoltaics.

We began copolymerization studies with block copolymerizations of **3** and **5** with both orders of monomer addition (Scheme 4.4). The precursor to monomer **5** was synthesized via etherification of 3-bromothiophene, followed by bromination and iodination to yield 2-bromo-5-iodo-3-(octyloxy)thiophene (Appendix 3). Monomers **3** and **5** were generated in situ by magnesium-halogen exchange from the corresponding 5-bromo-2-iodothiophene precursor to regioselectively generate the Grignard reagents. Negligible chain-extension was observed in the block copolymerizations (p3HT-*b*-3OOT, p3OOT-*b*-3HT) regardless of the monomer addition order. These data suggests a large

degree of catalyst dissociation and chain-termination during cross-propagation between these two monomers.

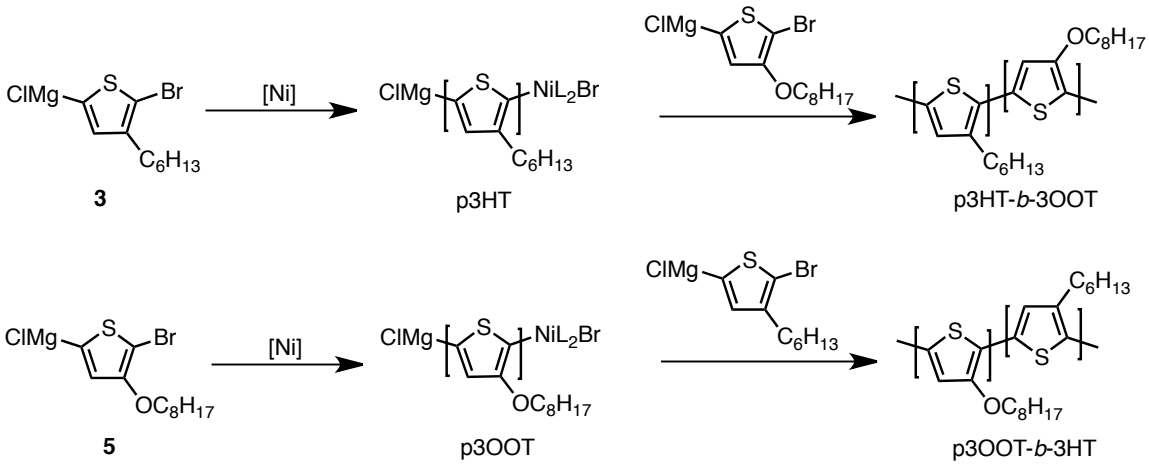

Scheme 4.4 Block copolymerizations of 3-hexylthiophene and 3-octyloxythiophene ([**3**] = [**5**] = 0.1 M, [Ni] = 1.5 mM).

Table 4.2 Summary of block copolymerization data for copolymerization of **3** and **5**

	p3HT		**p3HT-*b*-3OOT**	
[Ni]	**M_n (kDa)**	**PDI**	**M_n (kDa)**	**PDI**
$Ni(dppe)Cl_2$	3.3	1.2	3.5	1.5
$Ni(dppp)Cl_2$	3.5	1.2	4.5	1.5
	p3OOT		**p3OOT-*b*-3HT**	
	M_n (kDa)	**PDI**	**M_n (kDa)**	**PDI**
$Ni(dppe)Cl_2$	1.7	1.2	2.4	1.4
$Ni(dppp)Cl_2$	1.5	1.3	2.1	1.5

The homopolymerization of **5** was investigated to test whether this monomer did undergo a living, chain-growth polymerization mechanism or if its use was leading to a breakdown in controlled polymerization behavior. $Ni(dppp)Cl_2$ was used to initiate the polymerization because previously reported polymerizations of 3-alkoxythiophenes reported high polymer molecular weights and low polydispersities when using this catalyst.[12] The homopolymerization of **5** did not display a linear increase of M_n as a function of conversion (Figure 4.7A) and the end polymer molecular weight was not determined by the monomer to initiator ratio (Figure 4.7B). A living, chain-growth polymerization exhibits both of these characteristics, therefore we determined that Ni-

catalyzed polycondensation of **5** is not a controlled polymerization. Koeckelberghs and coworkers have recently demonstrated that polymerization of 2-bromo-4-[(S)-3,7-dimethyloctyloxy]thienylmagnesium bromide (**5a**) initiated by Ni(dppp)Cl_2 follows a chain-growth mechanism with significant amounts of catalyst dissociation from growing polymer chains.[21] These results are consistent with our observations of uncontrolled polymerization, suggesting that electron-rich monomers form a more labile Ni-polymer π-complex.

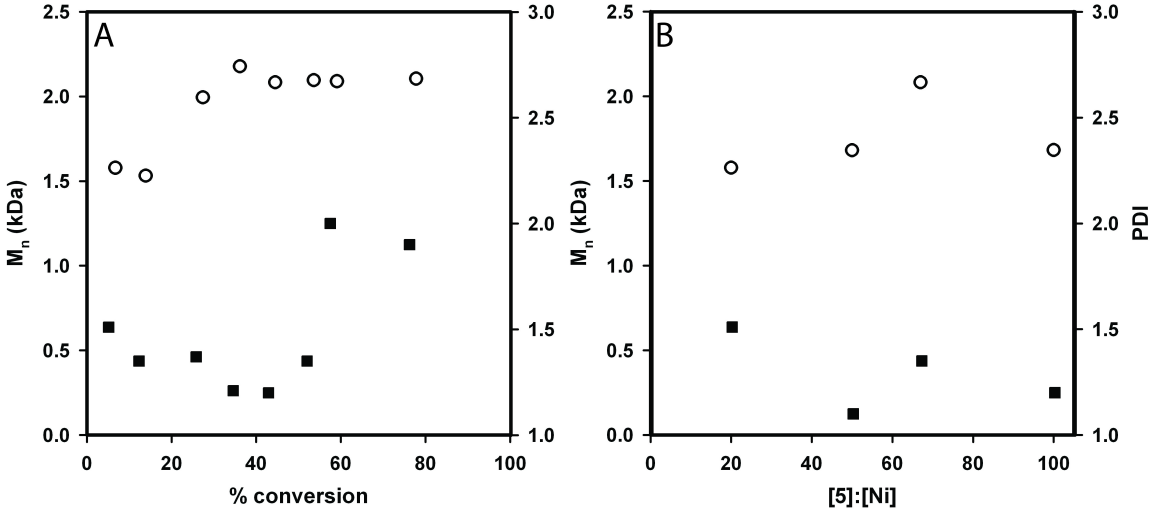

Figure 4.7 (A) Plot of M_n (○) and PDI (■) versus conversion for the Ni(dppp)Cl_2 initiated polymerization of **5** ([**5**] = 0.10 M, [Ni] = 1.5 mM). (B) Plot of M_n (○) and PDI (■) versus monomer to initiator ratio for the Ni(dppp)Cl_2 initiated polymerization of **5** ([**5**] = 0.10 M).

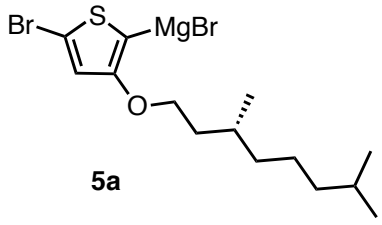

5a

Polymerizations of 4-octylthiazole

To date, Ni-catalyzed controlled polycondensations have been limited to the polymerization of electron-rich monomers for the synthesis of p-type π-conjugated polymers. Thiazoles were targeted as potential monomers for the chain-growth polymerization because they are electron-accepting relative to thiophene.[22] We hypothesized that gradient copolymers incorporating both thiophene and thiazole

monomers would exhibit tunable charge-separation and conduction properties. Synthetic modification of electronic properties could lead to more efficient charge collection in polymer photovoltaics. To expand the substrate scope for chain-growth polymerizations we investigated the polymerization behavior of 3-octylthiazole monomers **6a** and **6b** (Scheme 4.5).

We examined the polymerization behavior of **6a** and **6b** using a series of Ni initiators (Scheme 4.5). Steric stabilization has been shown to be critical for chain-growth polymerization, therefore we tested both monomer regioisomers separately.[23] Initial investigations utilized Ni dichloride initiators, which yielded polymers of lower molecular weight than the 10 kDa theoretically expected from the monomer to initiator ratio (Table 4.3). Ni-aryl halide initiators were also tested as steric stabilization during initiation has also been shown to be critical for successful chain-growth polymerization.[24] ^{1}H NMR spectroscopic analysis of the polymers initiated by the Ni-aryl halide complexes showed negligible incorporation of the aryl ligand into the polymers, indicating that Ni had dissociated from initially formed oligomers to begin new polymer chains. In a controlled polymerization, aryl groups present on the initiator are maintained as polymer end groups. None of the Ni initiators tested yielded high-molecular weight polymer with polydispersity lower than 1.5 for either thiazole monomer. From this data we concluded that the polymerizations were not controlled under these conditions.

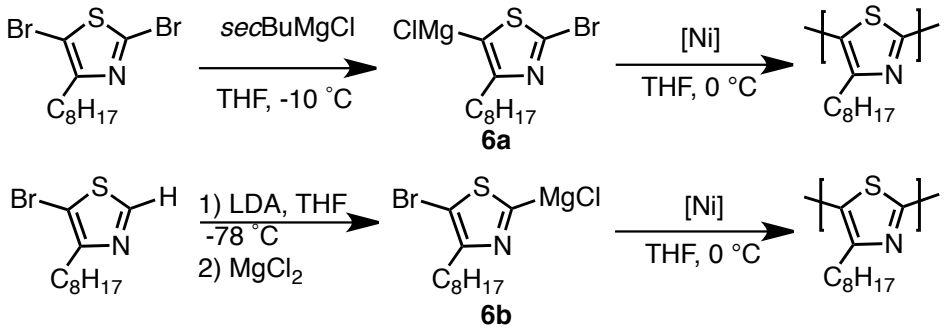

Scheme 4.5 Generation and polymerization of 4-octylthiazole monomers**. [6]** = 0.1 M, [Ni] = 1 mM

Table 4.3 Summary of 4-octylthiazole polymerizations

Monomer	[Ni]	M_n (kDa)	PDI	% Conversion
6a	Ni(dppp)Cl_2	2.5	1.8	71
	Ni(dppe)Cl_2	2.8	1.6	65
	Ni(depe)Cl_2	3.2	1.9	63
	Ni(dppe)(*o*-anisyl)Br	2.5	2.2	65
	Ni(dppe)(Ph)Br	5.6	2.2	77
6b	Ni(dppp)Cl_2	2.7	1.7	59
	Ni(dppe)Cl_2	2.1	1.6	63
	Ni(dppe)(*o*-anisyl)Br	2.2	1.5	65

Polymerization of 2,5-dihexylbenzene

Polymerization of 2,5-dihexylbenzene monomer **7** (Scheme 4.6) was attempted to broaden the scope of the Ni-catalyzed chain-growth polycondensation and examine monomer steric effects. Monomer **7** was formed in situ from 1-bromo-2,5-dihexyl-4-iodobenzene via magnesium-iodine exchange. While treatment of **7** with Ni dichloride initiators resulted in monomer consumption, only low molecular weight oligomers were formed in the cross-coupling (Table 4.4). The increased steric bulk of the hexyl side chains of **7** relative to the hexyloxy groups of **1** may lead to decomposition of the Ni-polymer oxidative addition complex or retard Ni^0 reoxidative addition into the polymer, (Scheme 4.1) leading to Ni dissociation from the growing polymer chains and uncontrolled polymerization.

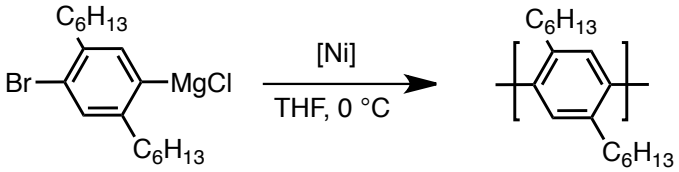

7

Scheme 4.6 Polymerization of 2,5-dihexylbenzene monomer **7** ([**7**] = 0.2 M, [Ni] = 3 mM).

Table 4.4 Summary of polymerization data for 2,5-dihexylbenzene monomer **7**

[Ni]	M_n (kDa)	PDI	% Conversion
Ni(dppp)Cl_2	0.7	1.1	89
Ni(dppe)Cl_2	0.8	1.1	85

Conclusions

In conclusion, we have examined the copolymerization of several monomer pairs and new monomers for living, chain-growth copolymerization behavior. The copolymerizations suffer from dissociation of the Ni catalyst from the initially formed polymer chains during or after cross-propagation of the monomers, leading to uncontrolled polymerization behavior. Despite their apparent similarity to monomers that do undergo controlled polymerization, monomers **5**, **6** and **7** do not undergo living, chain-growth homopolymerization under the conditions examined, possibly due to dissociation of Ni from the polymer during the reaction or a step-growth polymerization mechanism. Development of more electron-rich Ni catalysts that decrease the degree of catalyst dissociation from the growing polymer, such as alkylphosphine, phosphite or N-heterocyclic carbene ligands could overcome these challenges by forming a less labile Ni-polymer π-complex. Additives such as LiCl[25] or acac[26] have been shown to influence the homopolymerization of thiophene and fluorene monomers. Continued investigation into how additives interact with growing polymer chains, especially the proposed Ni^0–polymer intermediate, may decrease catalyst dissociation in copolymerizations. Development of improved initiators or polymerization conditions may lead to the ability to synthesize copolymers with complex sequences, such as gradient copolymers.

References Cited

(1) (a) Kiriy, A.; Senkovskyy, V.; Sommer, M. *Macromol. Rapid Commun.* **2011**, *32*, 1503–1517. (b) Okamoto, K.; Luscombe, C.K. *Polym. Chem.* **2011**, *2*, 2424-2434. (c) Yokozawa, T.; Yokoyama, A. *Chem. Rev.* **2009**, *109*, 5595–5619.

(2) Ouhib, F.; Khoukh, A.; Ledeuil, J.-B.; Martinez, H.; Desbrières, J.; Dagron-Lartigau, C. *Macromolecules* **2008**, *41*, 9736-9743.

(3) (a) Wu, S.; Bu, L.; Huang, L.; Yu, X.; Han, Y.; Geng, Y.; Wang, F. *Polymer*, **2009**, *50*, 6245-6251. (b) Miyakoshi, R.; Yokoyama, A.; Yokozawa, T. *Chem. Lett.* **2008**, *37*, 1022-1023.

(4) Javier, A. E.; Varshney, S. R.; McCullough, R. D. *Macromolecules* **2010**, *43*, 3233-3237.

(5) Yokoyama, A.; Kato, A.; Miyakoshi, R.; Yokozawa, T. *Macromolecules* **2008**, *41*, 7271-7273.

(6) Locke, J.R.; McNeil, A. J. *Macromolecules* **2010**, *43,* 8709-8710.

(7) (a) Benanti, T. L.; Kalaydjian, A.; Venkataraman, D. *Macromolecules* **2008**, *41*, 8312-8315. (b) Ouhib, F.; Dkhissi, A.; Iratçabal, P.; Hiorns, R. C.; Khoukh, A.; Desbrières, J.; Pouchan, C.; Dagron-Lartigau, C. *J. Polym. Sci., Part A: Polym. Chem*. **2008**, *46*, 7505-7516. (c) Li, Y.; Xue, Y.; Xia, H.; Xu, B.; Wen, S.; Tian, W. *J. Polym. Sci., Part A: Polym. Chem*. **2008**, *46*, 3970-3984. (d) Vallat, P.; Lamps, J.-P.; Schosseler, F.; Rawiso, M.; Catala, J.-M. *Macromolecules* **2007**, *40*, 2600-2602. (e) Adachi, I.; Miyakoshi, R.; Yokoyama, A.; Yokozawa, T. *Macromolecules* **2006**, *39*, 7793-7795. (f) Koeckelberghs, G.; Vangheluwe, M.; Van Doorsselaere, K.; Robijns, E.; Persoons, A.; Verbiest, T. *Macromol. Rapid Commun*. **2006**, *27*, 1920-1925. (g) Sheina, E. E.; Khersonsky, S. M.; Jones, E. G.; McCullough, R. D. *Chem. Mater.* **2005**, *17*, 3317-3319.

(8) (a) Ouhib, F.; Dupuis, G.; de Bettignies, R.; Bailly, S.; Khoukh, A.; Martinez, H.; Desbrières, J.; Hiorns, R.C.; Dagron-Lartigau, C. *J. Poly. Sci. Part A: Poly. Chem.* **2012**, *50* , 1953-1966. (b) Woo, C. H.; Holcombe, T. W.; Unruh, D. A.; Sellinger, A.; Fréchet, J. M. J. *Chem. Mater.* **2010**, *22* , 1673 - 1679. (c) Holcombe, T. W.; Woo, C. H.; Kavulak, D. F.; Thompson, B. C.; Fréchet, J. M. J. *J. Am. Chem. Soc.* **2009**, *131*, 14160-14161. (d) Gadisa, A.; Svensson, M.; Andersson, M. R.; Inganas, O. *Appl. Phys. Lett.* **2004**, 84, 1609–1611.

(9) Palermo, E.F; McNeil, A.J. *Manuscript submitted*

(10) Miyakoshi, R.; Shimono, K.; Yokoyama, A.; Yokozawa, T. *J. Am. Chem. Soc.* **2006**, *128*, 16012-16013.

(11) (a) Huang, L.; Wu, S.; Qu, Y.; Geng, Y.; Wang, F. *Macromolecules* **2008**, *41*, 8944-8947. (b) Stefan, M. C.; Javier, A. E.; Osaka, I.; McCullough, R. D. *Macromolecules* **2009**, *42*, 30-32.

(12) Akcelrud, L. *Prog. Polym. Sci*. **2003**, *28*, 875–962.

(13) (a) Shi, L.; Knochel, P.; Mayr, H. *Org. Lett.* **2009**, *11,* 3502–3505. (b) Shi, L.; Chu, Y.; Knochel, P.; Mayr, H. *Angew. Chem., Int. Ed.* **2008**, *47*, 202-204. (c) Krasovskiy, A.; Straub, B. F.; Knochel, P. *Angew.Chem., Int. Ed.* **2006**, *45*, 159-162. (d) Hauk, D.; Lang, S.; Murso, A. *Org. Process Res. Dev.* **2006**, *10*, 733-738. (e) Krasovskiy, A.; Knochel, P. *Angew. Chem., Int. Ed.* **2004**, *43*, 3333-3336. (f) Knochel, P.; Dohle, W.; Gommermann, N.; Kneisel, F. F.; Kopp, F.; Korn, T.; Sapountzis, I.; Vu, V. *Angew. Chem., Int. Ed*. **2003**, *42*, 4302-4320.

(14) Sheina, E.E.; Liu, J.; Iovu, M.C.; Laird, D.W.; McCullough, R.D. *Macromolecules* **2004**, *37*, 3526-3528.

(15) Senkovsky, V.; Khanduyeva, N.; Komber, H.; Oertel, U.; Stamm, M.; Kuckling, D.; Kiriy, A. *J. Am. Chem. Soc.* **2007**, *129,* 6626-6632.

(16) (a) van Herk, A. M.; Droge, T.; *Macromol. Theory Simul.* **1997**, *6*, 1263-1276. (b) Hautus, F. L. M.; German, A. L. *J. Polym. Sci., Polymer Letters* **1985**, *23*, 311-315. (c) Odian, G. Chain Copolymerization. In *Principles of Polymerization*, 4th ed.; John Wiley & Sons: Hoboken, 2004; pp 464-543.

(17) (a) Yokoyama, A.; Miyakoshi, R.; Yokozawa, T. *Macromolecules* **2004**, *37,* 1169-1171. (b) Miyakoshi, R.; Yokoyama, A.; Yokozawa, T. *J. Am. Chem. Soc.* **2005**, *127*, 17542-17547. (c) Sheina, E.

E.; Liu, J.; Iovu, M. C. Laird, D. W.; McCullough, R. D. *Macromolecules* **2004**, *37*, 3526-3528. (d) Iovu, M. C.; Sheina, E. E.; Gil, R. R.; McCullough, R. D. *Macromolecules* **2005**, *38*, 8649-8656.

(18) We were unable to monitor conversion of monomer **4** due to the rapid oxidation of 2-bromo-*N*-hexylpyrrole under ambient conditions.

(19) (a) Koeckelberghs, G.; Vangheluwe, M.; Van Doorsselaere, K.; Robijns, E.; Persoons, A.; Verbiest, T. *Macromol. Rapid Commun.* **2006**, *27*, 1920–1925. (b) Koeckelberghs, G.; Vangheluwe, M.; Samyn, C.; Persoons, A.; Verbiest *T. Macromolecules*, **2005**, *38*, 5554–5559. (c) Sheina, E.E.; Khersonsky, S.M.; Jones E.G.; McCullough, R.D. *Polym. Prepr.* **2003**, *44*, 855-856.

(20) (a) Vandeleene, S.; Jivanescu, M.; Stesmans, A.; Cuppens, J.; Van Bael, J. H.; Yamada, M.; Sato, N.; Verbiest, T.; Koeckelberghs, G. *Macromolecules* **2010**, *43*, 2910-2915. (b) Koeckelberghs, G.; Vangheluwe, M.; Samyn, C.; Persoons, A.; Verbiest, T. *Macromolecules* **2005**, *38*, 5554-5559.

(21) Van den Bergh, K.; De Winter, J.; Gerbaux, P.; Verbiest, T.; Koeckelberghs, G. *Macromol. Chem. Phys.* **2011**, *212*, 328–335.

(22) (a) Yamamoto, T.; Arai, M.; Kokubo, H.; Sasaki, S. *Macromolecules* 2003, *36*, 7986-7993. (b) Nanos, J. I.; Kampf, J. W.; Curtis, M. D. *Chem. Mater.* **1995**, *7*, 2232-2234.

(23) Beryozkina, T.; Senkovskyy, V.; Kaul, E.; Kiriy, A. *Macromolecules* **2008**, *41*, 7817-7823.

(24) Boyd, S.; Jen, A.K.Y.; Luscombe, C.K. *Macromolecules*, **2009**, *42*, 9387-9389.

(25) Wu, S.; Huang, L.; Tian, H.; Geng, Y.; Wang, F.; *Macromolecules*, **2011**, *44,* 7558–7567.

(26) Sui, A.; Shi, X.; Wu, S.; Tian, H.; Geng, Y.; Wang, F. *Macromolecules* [online early access] DOI: 10.1021/ma3009299. Published on line June 22, 2012. http://pubs.acs.org (accessed June 22, 2012)

Chapter 5

Conclusions and Future Work

The discovery of a chain-growth method for preparing π-conjugated polymers has increased interest in their synthesis and application, as well as provided access to new polymers and composite materials.[1] Controlled copolymerization to create π-conjugated copolymers would further increase the ability to synthetically tune the physical, optical, or electronic properties of these useful materials.[2] We are specifically interested in gradient copolymers, wherein the monomer composition varies continuously along the polymer chain. Gradient copolymers are a type of copolymer accessible only through controlled copolymerizations and have been shown to act as phase compatibilizers in immiscible non-conjugated polymer blends.[3] We anticipate that gradient π-conjugated copolymers may solve a long-standing challenge in polymer-based electronics by providing access to stable, nanostructured polymer blends.[4]

We have demonstrated that controlled copolymerizations can used to create conjugated copolymers with sequences determined by the reactivites and concentrations of the comonomers and that copolymer sequence influences the material's properties.[5] Block, random and gradient copolymers of 3-hexylthiophene and 3-(hexyloxy)methylthiophene were prepared via Ni-catalyzed living, chain-growth copolymerization. The copolymer melting transition temperatures were influenced by the copolymer sequence, demonstrating that copolymer crystallinity can be tuned by changing sequence. The ability to tune the crystallinity of π-conjugated polymers could provide a means of adjusting the charge mobility in polymer thin films, enabling device optimization through synthetic modification of the polymeric material. Copolymerizations of 3-alkyl[6] or 3-aryl[7] thiophene monomers exhibit controlled behavior, making a variety of polythiophene copolymers accessible. However, it has proven difficult to develop controlled copolymerizations utilizing monomers with different main-chain aromatic groups even when combining monomers which homopolymerize in a controlled manner.

We undertook studies on the cross-propagation of 3-alkylthiophene and 2,5-dialkoxybenzene monomers in Ni-catalyzed Kumada cross-coupling copolymerizations. While these monomers undergo controlled homopolymerizations, a significant amount of catalyst dissociation from the polymer occurs during copolymerizations, leading to mixtures of copolymer sequences. We found that electron-rich Ni initiators displayed less catalyst dissociation during copolymerizations. The most significant result from our model studies found that catalyst dissociation from the polymer does not directly result from the different π-binding abilities of the 3-alkylthiophene and 2,5-dialkoxybenzene monomer units but may be due to Ni "ring-walking" preventing fast oxidative addition into reactive chain ends.[8]

We sought to increase the substrate scope of controlled polymerization for π-conjugated (co)polymers. Expanding this method was problematic due to cross-propagation-promoted catalyst dissociation leading to uncontrolled polymerization behavior. Combining monomers that participate in living, chain-growth homopolymerizations rarely results in a controlled copolymerizaton. New monomer design is also challenging because small changes in Ni-polymer interactions strongly influence polymerization behavior.[9] A better understanding of structure-property relationships in controlled cross-coupling (co)polymerizations would greatly increase the applicability of this method for design of new materials.

There are significant challenges remaining in the design of controlled copolymerizations for π-conjugated polymers of block, random, or gradient sequence. Understanding and overcoming the causes of catalyst dissociation from the polymer chain is necessary to increase the types of copolymers that can be accessed. To this end, catalysts that display negligible chain-transfer during cross-propagation must be developed. Increasing electron density at the Ni center with strongly electron donating diimine, phosphite or N-heterocyclic carbene ligands should decrease dissociation of the Ni-polymer complex during cross-propagation and increase the rate of oxidative addition into the polymer-Br bond.[10] Alternatively, utilizing a softer Pd complex as the polymerization initiator should increase the duration of the metal-polymer intermediate through increased π-bond affinity. A recent report from our lab identified a Pd-N-heterocyclic carbene complex that promoted controlled Kumada coupling polymerization

of 3-hexylthiophene and 2,5-bishexyloxybenzene monomers.[11] When this Pd complex was utilized for block copolymerization both orders of monomer addition led to efficient cross-propagation and yielded block copolymers. Current investigations in our laboratory are focusing on structurally modifying this complex for increased ability to efficiently copolymerize 3-hexylthiophene and 2,5-bishexyloxybenzene monomers. Future optimization of the electronic and steric properties of Pd-N-heterocyclic carbene initiators for controlled polycondensations should focus on preventing catalyst dissociation from the growing polymer during copolymerizations.

The causes of the breakdown of the controlled polymerization mechanism during copolymerization are still largely unknown. We have shown that the π-binding abilities of monomers in the polymer chain likely do not prevent reoxidative addition of Ni^0 into the polymer chain end. An alternative explanation lies in the recent observation of Ni "ring-walking" during the polymerization.[8] This proposed mechanism posits a long-lived association between the Ni^0 and the polymer chain after reductive elimination that can lead to ligand exchange at the metal center, leading to dissociation of the catalyst from the polymer. Why Ni-ring-walking leads to significant amounts of catalyst dissociation during copolymerizations while there is negligible decomposition during homopolymerizations remains an unanswered question. Also unanswered is the nature of the ligands at the metal center that are initially exchanged for the polymer. Studies on whether external aromatics can intercept the Ni-polymer complex and lead to dissociation could answer these questions. Yokozawa and coworkers conducted the homopolymerization of 3-hexylthiophene Grignard monomer initiated with $Ni(dppp)Cl_2$ in the presence of 4-trifluoromethylbromobenzene and did not observe any consumption of the external aryl halide, suggesting that the Ni catalyst does not dissociate from the propagating polymer chain during polymerization.[12] Kiriy and coworkers conducted polymerizations of 3-hexylthiophene Grignard monomer initiated by $Ni(PPh_3)_2(Ph)Br$ in the presence of 2-bromotoluene as well as a 2-tolyl/Br terminated oligothiophene and only observed polymers with Ph/H endgroups.[13] These results confirm that the Ni catalyst remains associated with propagating polymer throughout homopolymerization. Similar studies conducted on copolymerizations would provide evidence for catalyst dissociation promoted by cross-propagation.

A potential avenue of improvement in controlled cross-coupling copolymerizations lies in the use of additives that promote living polymerization. A recent report by Wang and coworkers implies that acetoacetate plays a role in preventing catalyst dissociation from the polymer during the Ni-catalyzed polycondensation for polyfluorene.[14] This result suggests that continued exploration in the use additives to the cross-coupling polymerizations may give rise to more robust homo and copolymerizations.

Once the complexities facing controlled copolymerization are surmounted it will be possible to synthesize a range of new, well-defined materials that will have a significant impact on future applications of π-conjugated polymers. A particularly interesting application would be utilizing controlled copolymerization in the synthesis of gradient copolymers of monomers with different electronic properties, such as an electron donor and acceptor. A gradient donor-acceptor material may display interesting photophysical properties and create interesting nanoscale morphologies. Donor-acceptor gradient conjugated copolymers may find use in applications where charge separation or recombination is critical to device performance, such as polymer photovoltaics or light emitting diodes.

References Cited

(1) (a) Kiriy, A.; Senkovskyy, V.; Sommer, M. *Macromol. Rapid Commun.* **2011**, *32*, 1503–1517. (b) Okamoto, K.; Luscombe, C.K. *Polym. Chem.* **2011**, *2*, 2424-2434. (c) Yokozawa, T.; Yokoyama, A. *Chem. Rev.* **2009**, *109*, 5595–5619. (c) Osaka, I.; McCullough, R. D. *Acc. Chem. Res.* 2008, *41*, 1202-1214.

(2) (a) Facchetti, A. *Chem. Mater.* **2011**, *23*, 733–758. (b) Bilby, D.; Kim, B.G.; Kim, J. *Pure Appl. Chem.* **2011**, *83*, 127-139. (c) Liang, Y.; Yu, L. *Polymer Reviews* **2010**, *50*, 454–473. (d) Roncali, J. *Chem. Rev.* **1997**, *97*, 173−205.

(3) (a) Tao, Y.; Kim, J.; Torkelson, J. M. *Polymer* **2006**, *47*, 6773-6781. Kim, J.; Gray, M. K.; Zhou, H.; Nguyen, S.T.; Torkelson, J. M. *Macromolecules* **2005**, *38*, 1037-1040. (b) Aksimentiev, A.; Hoylst, R. *J. Chem. Phys*. **1999**, *111*, 2329-2339.

(4) (a) Wu, F.I.; Dodda, R.; Reddy D. S.; Shu C.F. *J. Mater. Chem.* **2002**, *12*, 2893–2897. (b) Giovanella, U.; Pasini, M.; Destri, S.; Porzio, W.; Botta, C. *Synth.Met.* **2008**, *158*, 113–119.

(5) Locke, J.R.; McNeil, A. J. *Macromolecules* **2010**, *43,* 8709-8710.

(6) (a) Benanti, T. L.; Kalaydjian, A.; Venkataraman, D. *Macromolecules* **2008**, *41*, 8312-8315. (b) Ouhib, F.; Dkhissi, A.; Iratçabal, P.; Hiorns, R. C.; Khoukh, A.; Desbrières, J.; Pouchan, C.; Dagron-Lartigau, C. *J.*

Polym. Sci., Part A: Polym. Chem. **2008**, *46*, 7505-7516. (c) Li, Y.; Xue, Y.; Xia, H.; Xu, B.; Wen, S.; Tian, W. *J. Polym. Sci., Part A: Polym. Chem*. **2008**, *46*, 3970-3984. (d) Vallat, P.; Lamps, J.-P.; Schosseler, F.; Rawiso, M.; Catala, J.-M. *Macromolecules* **2007**, *40*, 2600-2602. (e) Adachi, I.; Miyakoshi, R.; Yokoyama, A.; Yokozawa, T. *Macromolecules* **2006**, *39*, 7793-7795. (f) Koeckelberghs, G.; Vangheluwe, M.; Van Doorsselaere, K.; Robijns, E.; Persoons, A.; Verbiest, T. *Macromol. Rapid Commun*. **2006**, *27*, 1920-1925. (g) Sheina, E. E.; Khersonsky, S. M.; Jones, E. G.; McCullough, R. D. *Chem. Mater.* **2005**, *17*, 3317-3319.

(7) (a) Ouhib, F.; Dupuis, G.; de Bettignies, R.; Bailly, S.; Khoukh, A.; Martinez, H.; Desbrières, J.; Hiorns, R.C.; Dagron-Lartigau, C. *J. Poly. Sci. Part A: Poly. Chem.* **2012**, *50* , 1953-1966. (b) Woo, C. H.; Holcombe, T. W.; Unruh, D. A.; Sellinger, A.; Fréchet, J. M. J. *Chem. Mater.* **2010**, *22* , 1673 - 1679. (c) Holcombe, T. W.; Woo, C. H.; Kavulak, D. F.; Thompson, B. C.; Fréchet, J. M. J. *J. Am. Chem. Soc*. **2009**, *131*, 14160-14161. (d) Gadisa, A.; Svensson, M.; Andersson, M. R.; Inganas, O. *Appl. Phys. Lett.* **2004**, 84, 1609–1611.

(8) Tkachov, R.; Senkovskyy, V.; Komber, H.; Sommer, J.-U.; Kiriy, A. *J. Am. Chem. Soc.* **2010**, *132*, 7803-7810.

(9) Vandeleene, S.; Jivanescu, M.; Stesmans, A.; Cuppens, J.; Van Bael, J. H.; Yamada, M.; Sato, N.; Verbiest, T.; Koeckelberghs, G. *Macromolecules* **2010**, *43*, 2910-2915.

(10) Lee, S. R.; Bryan, Z. J.; Wagner, A. M.; McNeil, A. J. *Chem. Sci.* **2012**, *3*, 1562-1566.

(11) Bryan, Z.J.; Smith, M.L.; McNeil, A.J. *Macromol. Rapid Commun.* **2012**, *33*, 842-847.

(12) Miyakoshi, R.; Yokoyama, A.; Yokozawa, T.; *J. Polym. Sci. Part A: Polymer Chemistry* **2008,** *46,* 753-765.

(13) Beryozkina, T.; Senkovskyy, V.; Kaul, E.; Kiriy A. *Macromolecules* **2008**, *41*. 7817–7823.

(14) Sui, A.; Shi, X.; Wu, S.; Tian, H.; Geng, Y.; Wang, F. *Macromolecules* [online early access] DOI: 10.1021/ma3009299. Published on line June 22, 2012. http://pubs.acs.org (accessed June 22, 2012)

Appendix 1
Supporting Information for
Chapter 2
Syntheses of π-Conjugated Gradient Copolymers of Thiophene

Contents

Materials

Flash chromatography was performed on SiliCycle silica gel (40-63 μm) and thin layer chromatography was performed on Merck TLC plates pre-coated with silica gel 60 F254. *i*-PrMgCl (2 M in THF) was purchased in 100 mL quantities from Aldrich, $Ni(PPh_3)_2Cl_2$, Ni(dppp)Cl_2, and Ni(dppe)Cl_2 were purchased from Strem. N-bromosuccinimide (NBS) was purchased from Aldrich, recrystallized from boiling water and dried over P_2O_5. All reagent grade materials and solvents were purchased from Aldrich, Acros, EMD, or Fisher and used without further purification unless otherwise noted. THF was dried and deoxygenated using an Innovative Technology (IT) solvent purification system composed of activated alumina, copper catalyst, and molecular sieves. All glassware was oven-dried at 120 ^oC for at least 1 h before use.

II. General Experimental

NMR Spectroscopy: ^1H, ^{31}P and ^{13}C NMR spectra for all compounds were acquired in $CDCl_3$ or CD_2Cl_2 as noted on a Varian MR400 or a Varian Inova 400 Spectrometer operating at 400, 162 and 100 MHz, respectively. For ^1H, ^{31}P and ^{13}C NMR spectra the chemical shift data are reported in units of δ (ppm) relative to tetramethylsilane (TMS). ^1H and ^{13}C NMR spectra are referenced to residual solvent. ^{31}P NMR spectra are referenced to external H_3PO_4. Multiplicities are reported as follows: singlet (s), doublet (d), doublet of doublets (dd), multiplet (m), triplet (t) and broad resonance (br). All NMR spectra were recorded at rt.

Mass Spectrometry: HRMS data were obtained on a Micromass AutoSpec Ultima

Magnetic Sector mass spectrometer.

Gel-Permeation Chromatography: Polymer molecular weights were determined by comparison with polystyrene standards (Varian, EasiCal PS-2 MW 580-377,400) on a Waters 1515 HPLC instrument equipped with Waters Styragel® (7.8 x 300 mm) THF HR 0.5, THF HR 1, and THF HR 4 type columns in sequence and analyzed with Waters 2487 dual absorbance detector (254 nm). Samples were dissolved in THF (with mild heating) and passed through a 0.2 μm PTFE filter prior to analysis.

UV-vis Spectroscopy: UV-vis spectra were acquired using a Perkin Elmer Lambda 850 UV-vis Spectrometer. Solution samples were prepared at 1 x 10^{-4} M in $CHCl_3$. Thin-films were spin-cast on glass slides from ~1 mg/mL solutions in chlorobenzene.

Gas Chromatography: Gas chromatography was carried out using a Shimadzu GC 2010 containing a Shimadzu SHRX5 (crossbound 5% diphenyl – 95% dimethyl polysiloxane; 15 m, 0.25 mm ID, 0.25 μm df) column.

Fluorescence Spectroscopy: Fluorescence spectra were recorded on a Fluoromax-2 fluorimeter. Solution samples were prepared at 1 x 10^{-4} M in $CHCl_3$.

Differential Scanning Calorimetry: DSC was performed on a TA Instruments DSC Q10. Samples were placed in aluminum hermetic pans and sealed using a TA Instruments crimper. Samples were heated and cooled from 0-250 ˚C before scanning to erase thermal history. The temperature range was 0-250 ˚C with a heating rate of 10 ˚C/min.

III. Synthetic Procedures

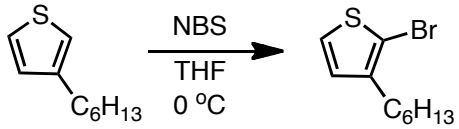

S1

2-bromo-3-hexylthiophene (S1): An oven-dried 100 mL Schlenk flask equipped with a stir bar and septum was cooled under a positive flow of N_2, then 3-hexylthiophene (5.00 g, 0.0297 mol, 1.00 equiv) and THF (50 mL) were added. The flask was then placed in an ice-water bath and cooled for 5 min, after which NBS (5.82 g, 0.0327 mol, 1.10 equiv) was added under positive N_2. After 1 h the reaction was quenched with 10% aq Na_2CO_3 (30 mL) and extracted with hexanes (3 x 25 mL). The combined organics were washed with brine (1 x 20 mL), dried over decolorizing carbon and $MgSO_4$, filtered and concentrated in vacuo. The resulting yellow oil was chromatographed through silica gel using hexanes as eluent then purified via distillation (65 ˚C, 0.020 torr) to yield 2-bromo-3-hexylthiophene (**S1**) (6.21 g, 85% yield) as a clear oil. HRMS (EI): Calcd. for C10H15BrS [M+] 246.0078; found, 246.0081.

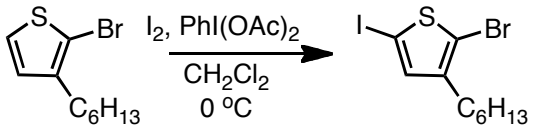

S1 **S2**

2-bromo-3-hexyl-5-iodothiophene (S2): An oven-dried 50 mL Schlenk flask equipped with a stir bar and septum was cooled under a positive flow of N_2. **S1** (2.59 g, 0.0105 mol, 1.00 equiv) and CH_2Cl_2 (28 mL) were added to the flask and the flask was cooled in an ice-water bath. I_2 (1.46 g, 0.00576 mol, 0.550 equiv) and $PhI(OAc)_2$ (1.86 g, 0.00578 mol, 0.550 equiv) were added under positive N_2. The reaction was stirred at 0 ˚C for 2.5 h after which it was quenched with saturated aq Na_2SO_3 (~30 mL) and extracted with CH_2Cl_2 (2 x 25 mL). The combined organics were then washed with brine (1 x 20 mL), dried over decolorizing carbon and $MgSO_4$, filtered and concentrated in vacuo. The resulting yellow oil was chromatographed through silica using hexanes as eluent and then purified via distillation (100 ˚C, 0.050 torr) to yield 2-bromo-3-hexyl-5-iodothiophene (**S2**) (2.40 g, 61% yield) as a clear oil. HRMS (EI): Calcd. for C10H14BrIS [M+] 371.9044; found, 371.9046.

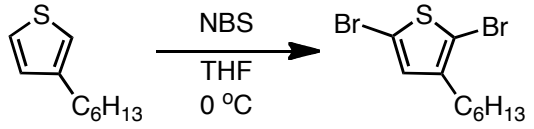

S3

2,5-dibromo-3-hexylthiophene (S3): An oven-dried 100 mL flask was equipped with a stir bar and placed in an ice bath. Sequentially, 3-hexylthiophene (5.00 g, 0.0297 mol, 1.00 equiv), THF (60 mL) and NBS (13.2 g, 0.0743 mol, 2.50 equiv) were added to the flask. The flask was then stirred under N_2. After 2 h the reaction was quenched with aq saturated Na_2CO_3 (25 mL). The aqueous mixture was extracted with hexanes (3 x 25 mL) and the combined organic layers were washed with H_2O (2 x 25 mL) and brine (1 x 25 mL), dried over $MgSO_4$, filtered, and concentrated in vacuo. The resulting oil was purified by distillation (85 ˚C, 0.03 torr) followed by filtration through silica gel using hexanes as the eluent to give **S3** as a clear oil (7.90 g, 82% yield). HRMS (EI): Calcd. for $C_{10}H_{14}Br_2S$ [M+] 323.9183; found, 323.9176.

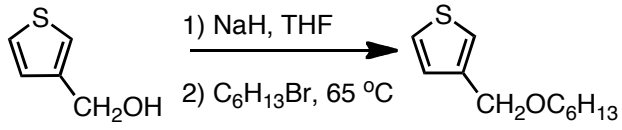

S4

3-(hexyloxy)methylthiophene (S4): An oven-dried 100 mL Schlenk flask equipped with a stir bar and septum was cooled under a positive flow of N_2. NaH (2.22 g, 60% in mineral oil, 0.0555 mol, 1.26 equiv) was added and suspended in THF (85 mL). Thiophene-3-methanol (5.00 g, 0.0439 mol, 1.00 equiv) was added dropwise over 30 min. The reaction was stirred an additional 30 min then 1-bromohexane (9.13 g, 0.0550

mol, 1.26 equiv) was added. The mixture was then refluxed overnight. The reaction was then cooled to rt, quenched with H_2O and extracted with ether (3 x 30 mL). The combined organics were washed with brine (20 mL), dried over $MgSO_4$, filtered and concentrated in vacuo. The resulting oil was chromatographed on silica gel using 1:9 EtOAc:hexanes as eluent. The resulting oil was purified via distillation (85 ˚C, 30 torr) to yield 3-(hexyloxy)methylthiophene (**S4**) (5.86 g, 69% yield). HRMS (EI): Calcd. for C11H18OS [M+] 198.1080; found, 198.1078.

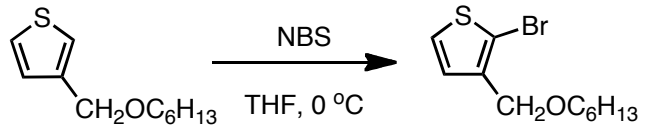

S4 **S5**

2-bromo-3-(hexyloxy)methylthiophene (S5): An oven-dried 100 mL Schlenk flask equipped with a stir bar and septum was cooled under a positive flow of N_2. **S4** (5.86 g, 0.0295 mol, 1.00 equiv) was added to the flask and dissolved in THF (60 mL). The flask was cooled to 0 ˚C in an ice-water bath and NBS (5.49 g, 0.0310 mol, 1.05 equiv) was added. The reaction was stirred for 2 h, then quenched with 10% aq Na_2CO_3 (30 mL) and extracted with hexanes (3 x 30 mL). The combined organics were washed with brine (20 mL), dried over decolorizing carbon and $MgSO_4$, filtered and concentrated in vacuo. The resulting yellow oil was chromatographed through silica gel, eluting with hexanes and distilled (100 ˚C, 0.030 torr) to yield **S5** (6.50 g, 80% yield) as a clear oil. HRMS (EI): Calcd. for C11H17OSBr [M+] 276.0183; found, 276.0190.

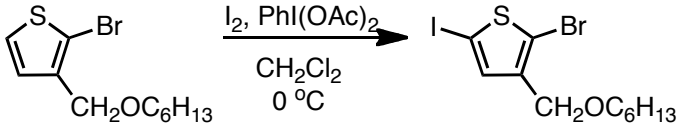

S5 **S6**

2-bromo-3-((hexyloxy)methyl)-5-iodothiophene (S6): An oven-dried 100 mL Schlenk flask equipped with a stir bar and septum was cooled under a positive flow of N_2. **S5** (6.32 g, 0.0229 mol, 1.00 equiv) was added to the flask, dissolved in CH_2Cl_2 (46 mL) and the flask cooled to 0 ˚C in an ice-water bath. I_2 (3.76 g, 0.0148 mol, 0.650 equiv) and $PhI(OAc)_2$ (4.55 g, 0.0137 mol, 0.600 equiv) were added under positive N_2 and the reaction maintained at 0 ˚C for 6 h. The reaction was quenched with saturated aq Na_2SO_3 (30 mL) and extracted with CH_2Cl_2 (2 x 25 mL). The combined organics were washed with brine (1 x 20 mL), dried over decolorizing carbon and $MgSO_4$, filtered and concentrated in vacuo. The resulting yellow oil was chromatographed through silica eluting with hexanes and distilled (105 ˚C, 0.030 torr) to yield **S6** (7.92 g, 86% yield) as a clear oil. HRMS (EI): Calcd. for C11H16OSBrI [M+] 401.9150; found, 401.9162.

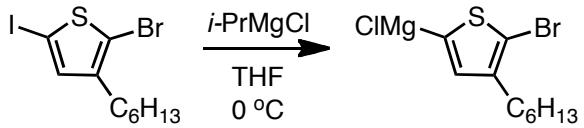

S2 **1**

1: S2 (0.205 g, 0.550 mmol, 1.10 equiv) was dissolved in THF (1.8 mL) in a 25 mL Schlenk tube equipped with a stir bar and septum. The tube was sealed and cooled to 0 ˚C. *i*-PrMgCl (0.250 mL, 0.500 mmol, 1.00 equiv) was added under N_2 and the reaction stirred at 0 °C for 30 min.

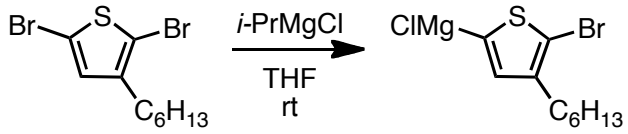

S3 **1**

1: S3 (0.179 g, 0.550 mmol, 1.10 equiv) was dissolved in THF (1.8 mL) in a 25 mL Schlenk tube equipped with a stir bar and septum. The tube was sealed and cooled to 0 ˚C. *i*-PrMgCl (0.250 mL, 0.500 mmol, 1.00 equiv) was added under N_2 and the reaction stirred at rt for 30 min.

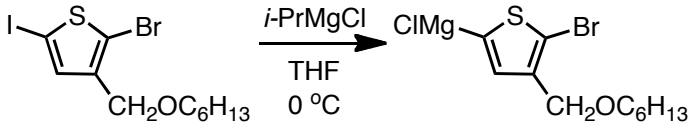

S6 **2**

2: S6 (0.221 g, 0.550 mmol, 1.10 equiv) was dissolved in THF (1.8 mL) in a 25 mL Schlenk tube equipped with a stir bar and septum. The tube was sealed and cooled to 0 ˚C. *i*-PrMgCl (0.250 mL, 0.500 mmol, 1.00 equiv) was added under N_2 and the reaction stirred at 0 ˚C for 30 min.

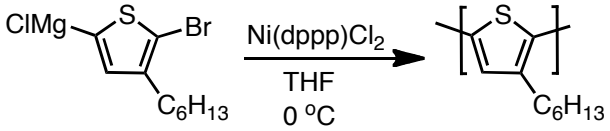

1 **p3HT**

---

p3HT: An oven-dried 50 mL Schlenk flask equipped with a stir bar and three-way adapter with septum was evacuated and cooled under vacuum. Once cool, the flask was filled with N_2 and re-evacuated: this process was repeated twice and the flask filled with N_2. THF (5 mL) was added to the flask and cooled to 0 ˚C. **1** (2.05 mL, 0.500 mmol 1.00 equiv) (see pg 62) was added by syringe and the solution stirred for 1 min. Then catalyst solution (0.50 mL, 0.012 mmol, 0.024 equiv) (see pg 64) was added to the reaction and the reaction maintained at 0 ˚C for 5 h. The reaction was quenched with 5 M HCl (10 mL), extracted with $CHCl_3$ (3 x 10 mL) and the solvent removed in vacuo. The resultant

purple solid was then taken up in a minimum amount of $CHCl_3$ and precipitated into MeOH. The precipitate was collected after centrifugation and dried under vacuum (0.065 g, 78% yield) M_n = 18.5 kDa, PDI = 1.1.

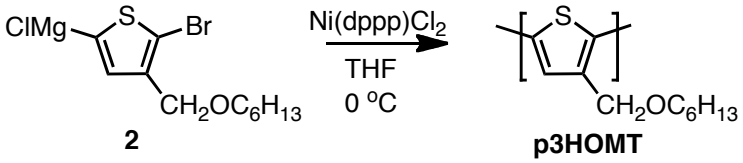

2 **p3HOMT**

p3HOMT: An oven-dried 50 mL Schlenk flask equipped with a stir bar and three-way adapter with septum was evacuated and cooled under vacuum. Once cool, the flask was filled with N_2 and re-evacuated: this process was repeated twice and the flask filled with N_2. THF (5 mL) was added to the flask and cooled to 0 ˚C. **2** (2.05 mL, 0.500 mmol 1.00 equiv) (see pg 62) was added by syringe and the solution stirred for 1 min. Then catalyst solution (0.50 mL, 0.012 mmol, 0.024 equiv) (see pg 64) was added to the reaction and the reaction maintained at 0 ˚C for 5 h. The reaction was quenched with 5 M HCl (10 mL), extracted with $CHCl_3$ (3 x 10 mL) and the solvent removed in vacuo. The resultant red solid was then taken up in a minimum amount of $CHCl_3$ and precipitated into MeOH. The precipitate was collected via centrifugation and dried under vacuum (0.071 g, 72% yield) M_n = 16.5 kDa, PDI = 1.1.

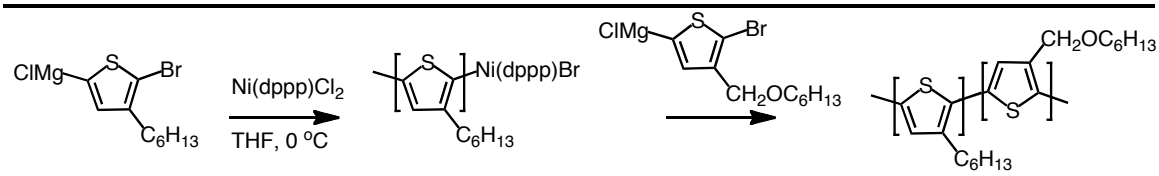

Block Copolymer: An oven-dried 50 mL Schlenk flask equipped with a stir bar and three-way adapter with septum was evacuated and cooled under vacuum. Once cool, the flask was filled with N_2 and re-evacuated: this process was repeated twice and the flask filled with N_2. THF (5 mL) was added to the flask and cooled to 0 ˚C. **1** (2.05 mL, 0.500 mmol 1.00 equiv) (see pg 62) was added by syringe and the solution stirred for 1 min. Then catalyst solution (0.50 mL, 0.012 mmol, 0.024 equiv) (see pg 64) was added to the reaction and the reaction maintained at 0 ˚C for 2 h. An aliquot (~0.250 mL) was removed via syringe and quenched in 5 M HCl (1 mL). The aliquot was then extracted with $CHCl_3$ (2 mL), the solvent removed in vacuo prepared for GPC analysis (M_n = 10.5 kDa, PDI = 1.1). **2** (2.05 mL, 0.500 mmol 1.00 equiv) was added and the reaction stirred at 0 ˚C for an additional 3 h. The reaction was quenched with 5 M HCl (10 mL), extracted with $CHCl_3$ (3 x 10 mL) and the solvent removed in vacuo. The resultant purple solid was then taken up in a minimum amount of $CHCl_3$ and precipitated into MeOH. The precipitate was collected via centrifugation and dried under vacuum (0.145 g, 72% yield) M_n = 22.1 kDa, PDI = 1.1.

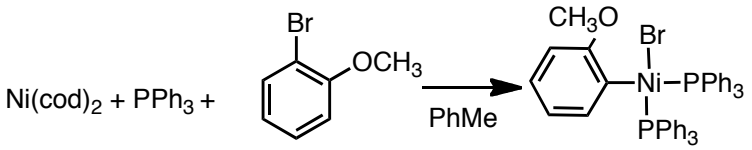

S7

(*o*-anisyl)bis(triphenylphosphino)nickel bromide (S7): In the glovebox, $Ni(cod)_2$ (0.413 g, 1.50 mmol, 1.00 equiv) and PPh_3 (0.787 g, 3.00 mmol, 2.00 equiv) were dissolved in PhMe (7.5 mL) in an oven-dried 50 mL flask equipped with a stir bar. *o*-bromoanisole (0.206 mL, 1.65 mmol, 1.10 equiv) was added and the reaction stirred for 45 min at rt. Hexanes (12 mL) was added and the resultant yellow precipitate was collected via filtration and washed with hexanes (~15 mL) to yield **S7** as a yellow powder (0.723 g, 63% yield).

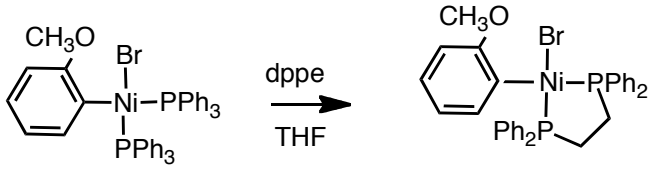

S7 **S8**

(*o*-anisyl)(1,2-bis(diphenylphosphino)ethane)nickel bromide (S8): In the glovebox, **S7** (0.723 g, 0.939 mmol, 1.00 equiv) was dissolved in THF (20 mL) in a 25 mL oven-dried flask equipped with a stir bar. Then dppe (0.412 g, 1.03 mmol, 1.10 equiv) was added and the reaction stirred for 1 h at rt. The reaction volume was reduced to ~5 mL in vacuo, then hexanes (15 mL) was added and the resultant precipitate isolated via filtration. The yellow powder was then washed with Et_2O (5 mL), hexanes (2 x 5 mL) and MeOH (2 mL), then dried in vacuo to yield **S8** (0.403 g, 59% yield).

Representative Procedure for Preparing Catalyst Solution

All actions were performed in a glovebox under N_2 atmosphere. A 4 mL vial was equipped with a stir bar. Sequentially, $Ni(dppp)Cl_2$ (13 mg, 0.024 mmol, 1.00 equiv), THF (0.8 mL), and **1** (0.20 mL, 0.25 M, 2.5 equiv) were added to the flask. The reaction mixture was stirred for 15 min until homogeneous.

NMR Spectra

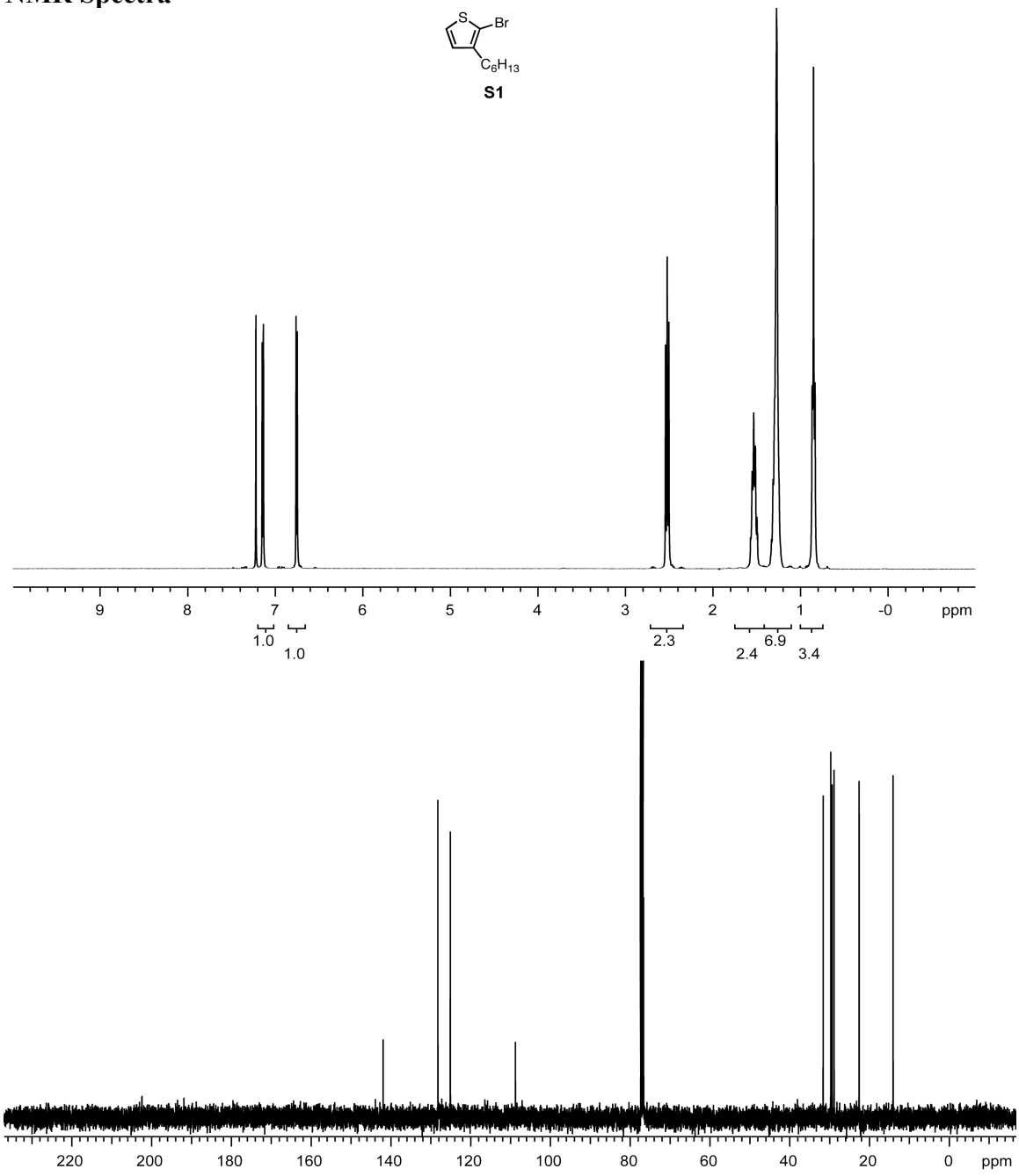

Figure S1. ^{1}H and ^{13}C NMR spectra for **S1**
^{1}H NMR (400 MHz, $CDCl_3$) δ 7.18 (d, J = 5.4 Hz, 1H), 6.79 (d, J = 5.7 Hz, 1H), 2.56 (t, J = 7.8 Hz, 2H), 1.53 (m, 2H), 1.30 (br, 6H), 0.89 (t, J = 6.6 Hz, 3H). ^{13}C NMR (100 MHz, $CDCl_3$) δ 141.95, 128.22. 125.10, 108.76, 31.60, 29.68, 29.37, 28.87, 22.58, 14.07.

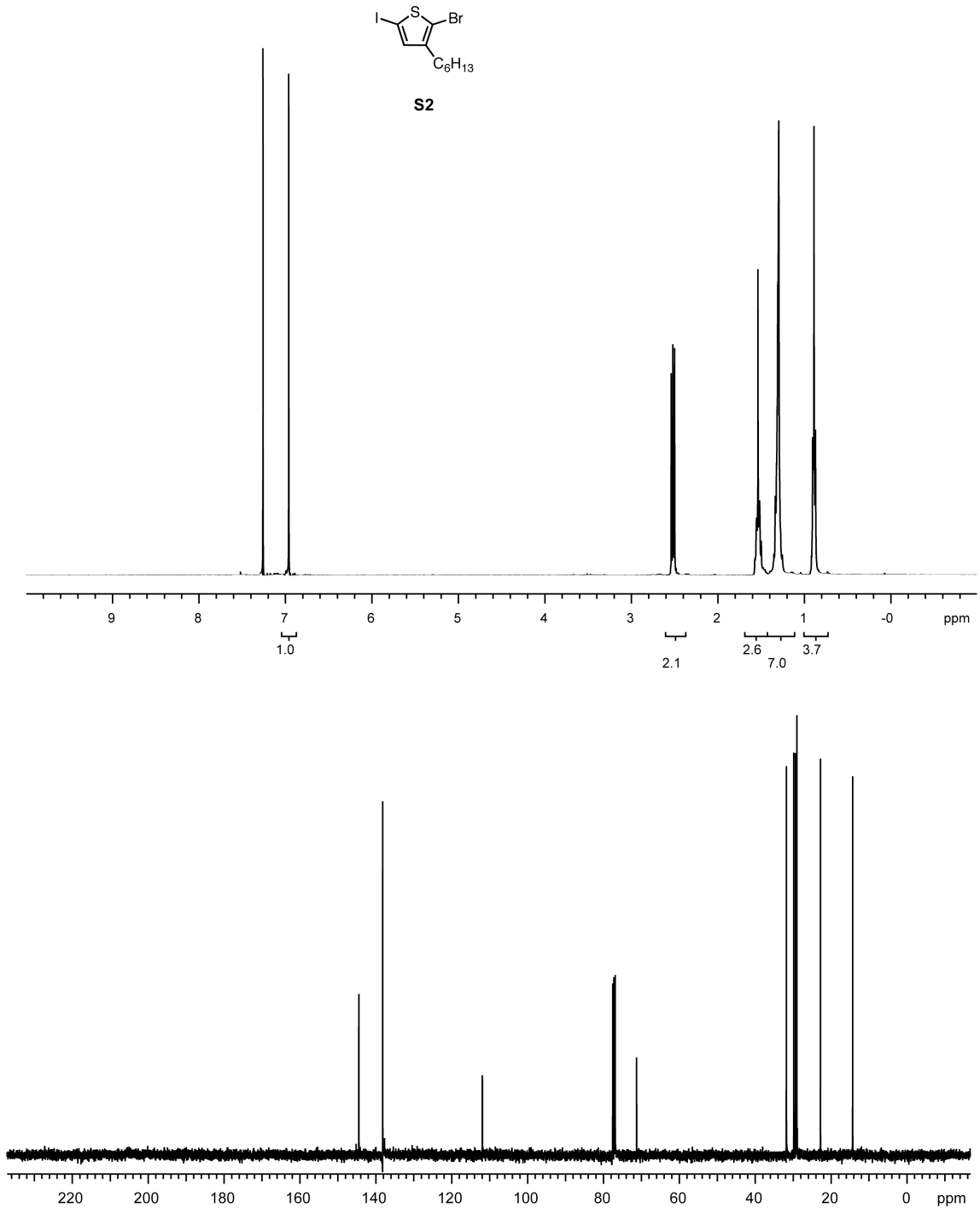

Figure S2. ^{1}H and ^{13}C NMR spectra for **S2**
^{1}H NMR (400 MHz, $CDCl_3$) δ 6.96 (s, 1H), 2.52 (t, J = 7.6 Hz, 2H), 1.52 (m, 2H), 1.28 (m, 6H), 0.87 (t, J = 7.2 Hz, 3H). ^{13}C NMR (100 MHz, $CDCl_3$) δ 144.91, 137.92, 111.53, 71.08, 31.50, 29.61, 29.18, 28.80, 22.56, 14.08.

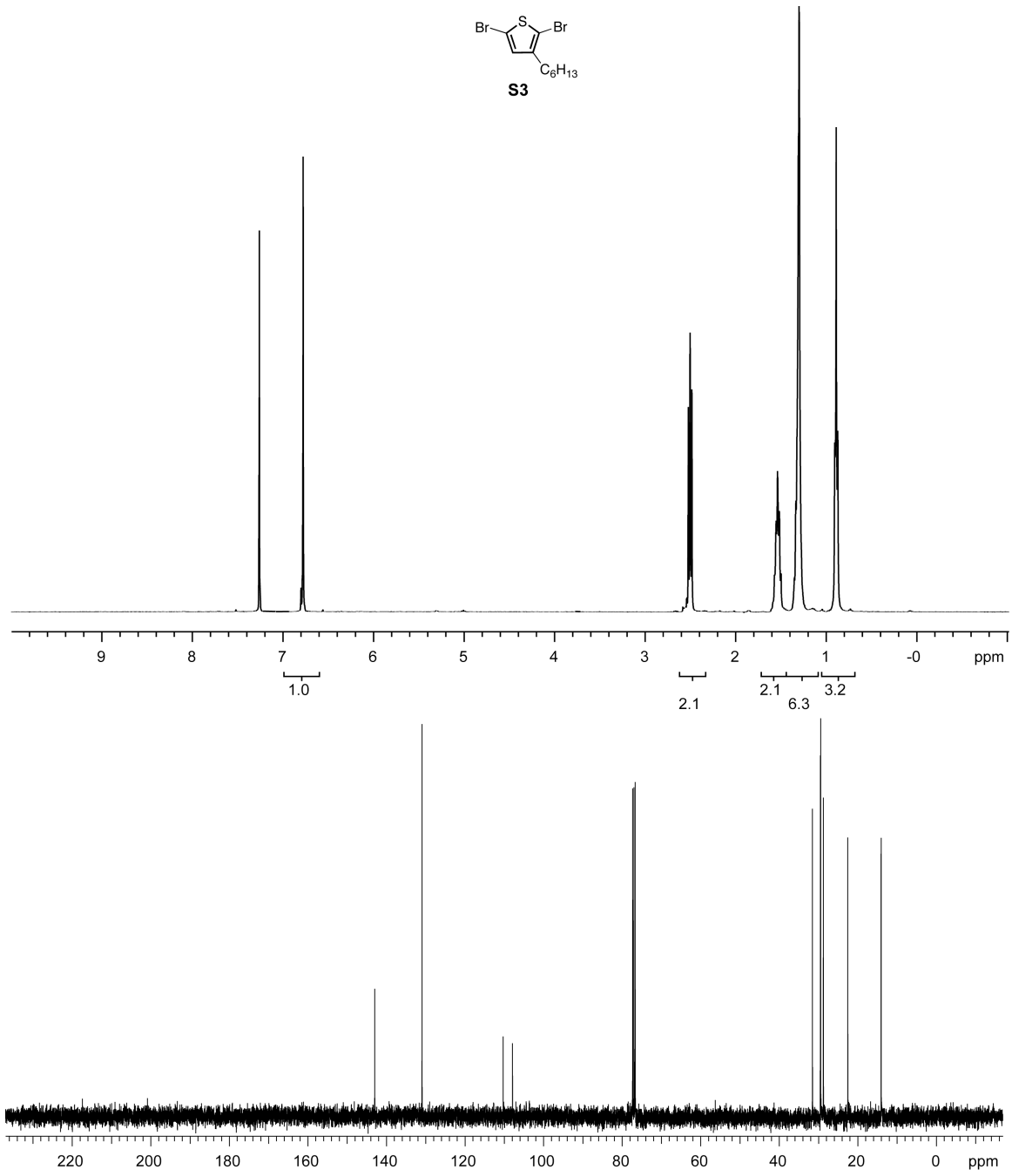

Figure S3. ^{1}H and ^{13}C NMR spectra for **S3**
^{1}H NMR (400 MHz, $CDCl_3$) δ 6.78 (s, 1H), 2.50 (t, J = 7.2 Hz, 2H), 1.53 (m, 2H), 1.30 (br m, 6H), 0.89 (t, J = 6.8 Hz, 3H). ^{13}C NMR (100 MHz, $CDCl_3$) δ 142.97, 130.94, 110.27, 107.90, 31.55, 29.53, 29.46, 28.76, 22.55, 14.06.

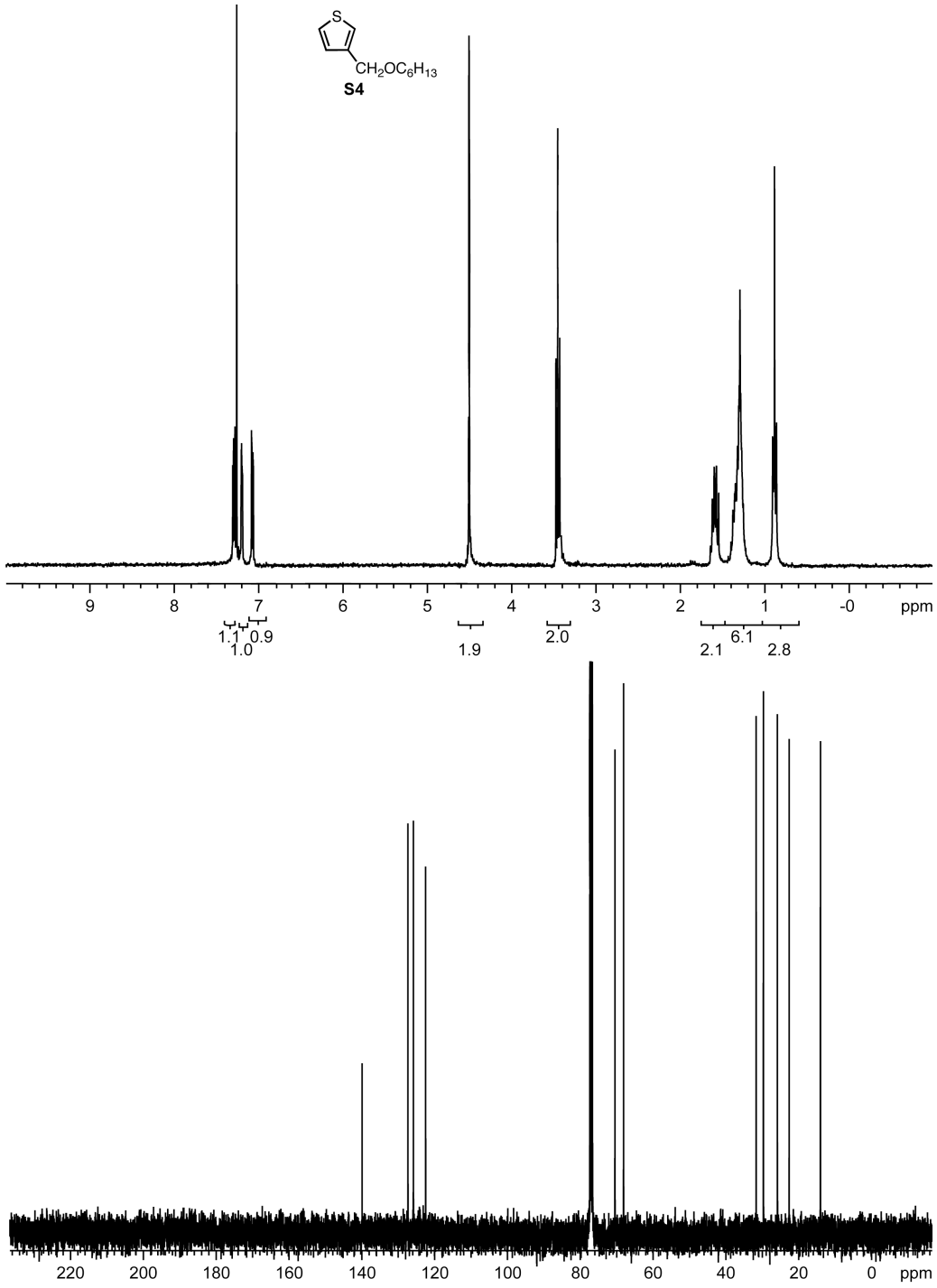

Figure S4. ^{1}H and ^{13}C NMR spectra for **S4**
^{1}H NMR (400 MHz, $CDCl_3$) δ 7.29 (dd, *J* = 3.1 Hz, 5.1 Hz, 1H), 7.19 (m, 1H), 7.07 (d, *J* = 5.1 Hz, 1H), 4.51 (s, 2H), 3.45 (t, *J* = 6.6 Hz, 2H), 1.59 (m, 2H), 1.34 (br m, 6H), 0.88 (t, *J* = 6.8 Hz, 3H). ^{13}C NMR (100 MHz, $CDCl_3$) δ 139.89, 127.31, 125.82, 122.46, 70.46, 68.10, 31.68, 29.70, 25.85, 22.61, 14.03.

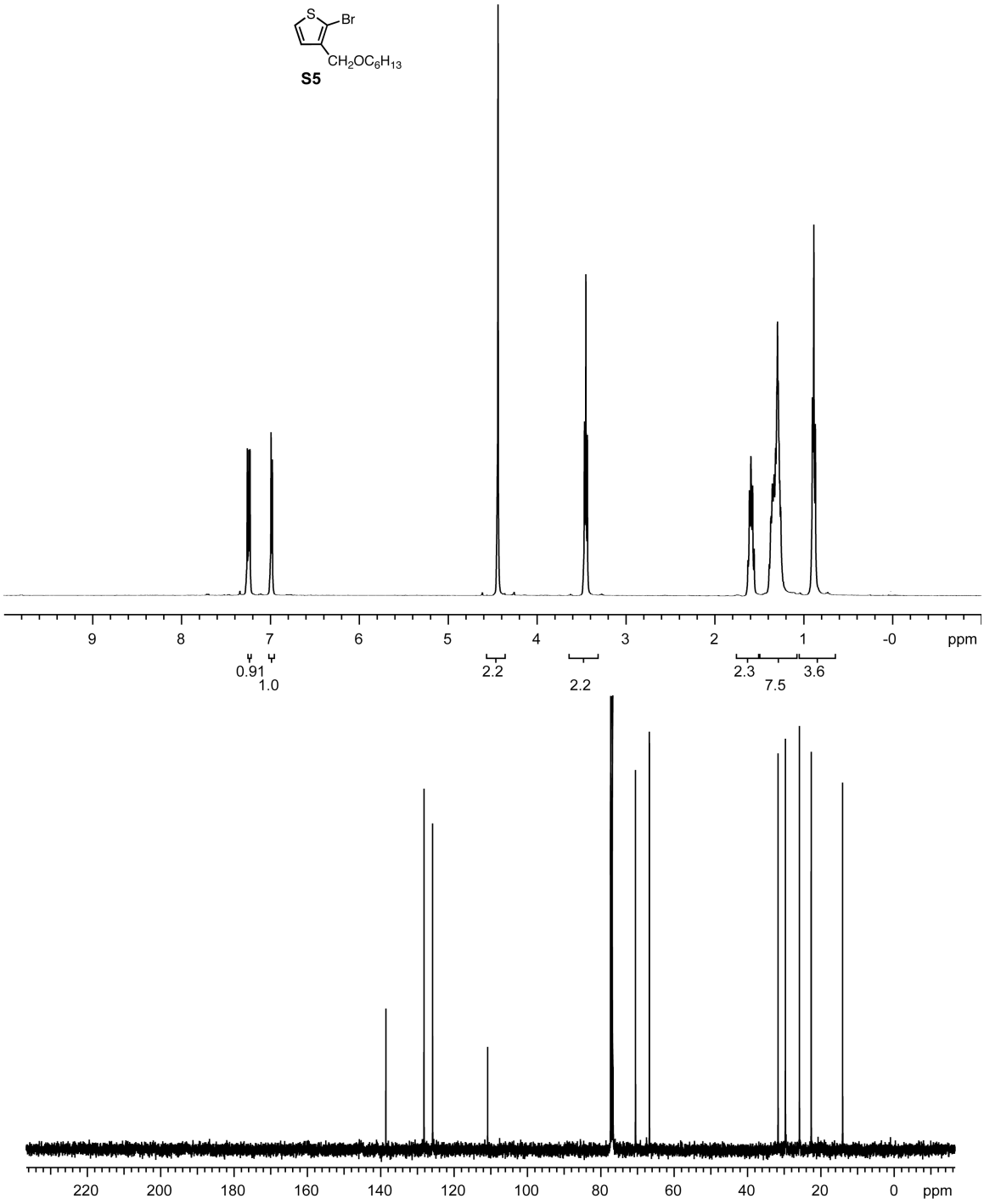

Figure S5. ^{1}H and ^{13}C NMR spectra for **S5**
^{1}H NMR (400 MHz, $CDCl_3$) δ 7.25 (d, J = 5.6 Hz, 1H), 6.99 (d, J = 5.6 Hz, 1H), 4.44 (s, 2H), 3.45 (t, J = 6.8 Hz, 2H), 1.58 (m, 2H), 1.29 (br, 6H), 0.89 (t, J = 4.8 Hz, 3H). ^{13}C NMR (100 MHz, $CDCl_3$) δ 138.58, 128.19, 125.85, 110.85, 70.53, 66.74, 31.65, 29.65, 25.82, 22.62, 14.05.

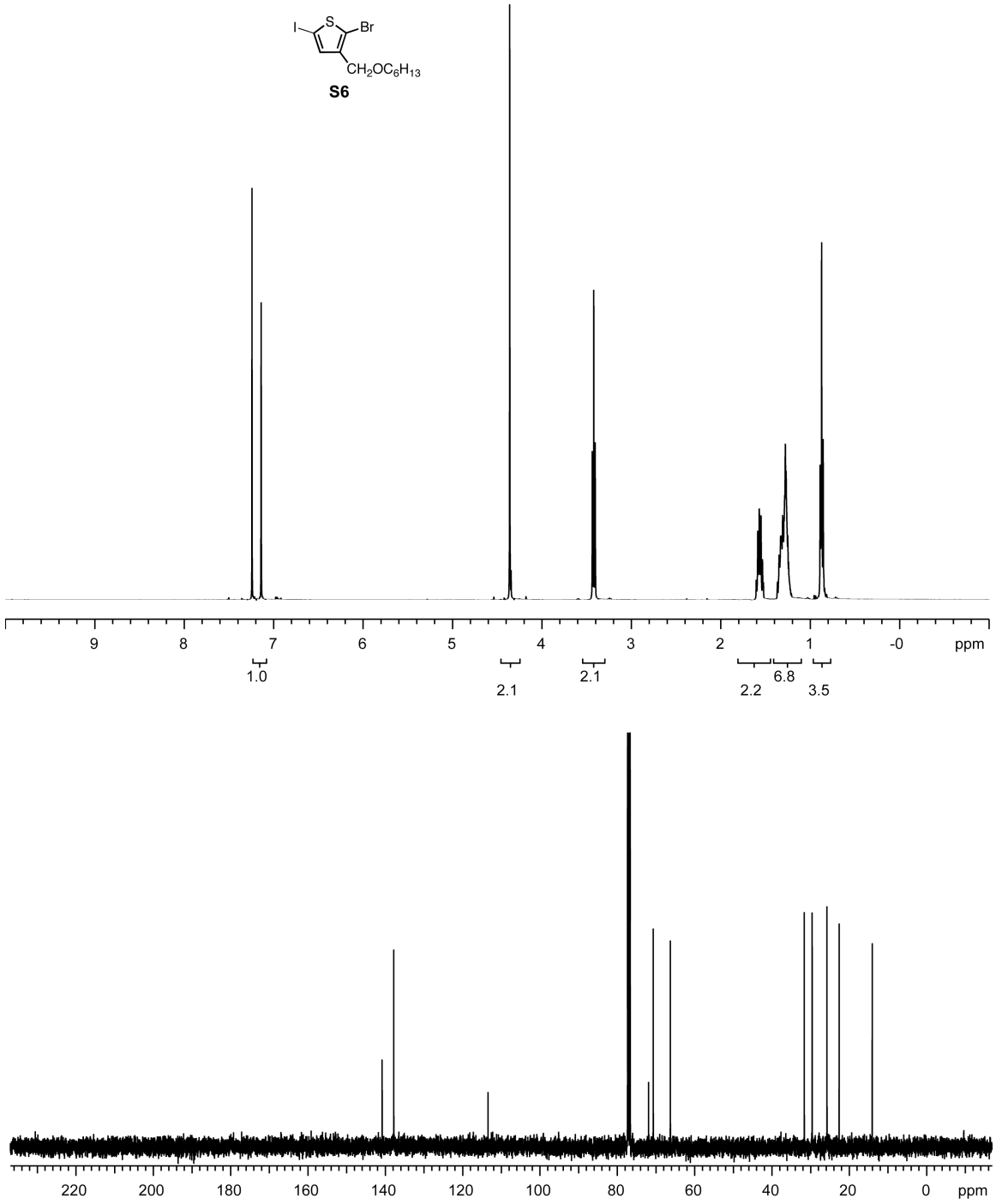

Figure S6. ^{1}H and ^{13}C NMR spectra for **S6**
^{1}H NMR (400 MHz, $CDCl_3$) δ 7.15 (s, 1H), 4.37 (s, 2H), 3.44 (t, J = 6.6 Hz, 2H), 1.59 (m, 2H), 1.34 (br m, 6H), 0.89 (t, J = 6.9 Hz, 3H). ^{13}C NMR (100 MHz, $CDCl_3$) δ 140.81, 137.81, 113.43, 71.89, 70.69, 66.26, 31.63, 29.59, 25.77, 22.61, 14.05.

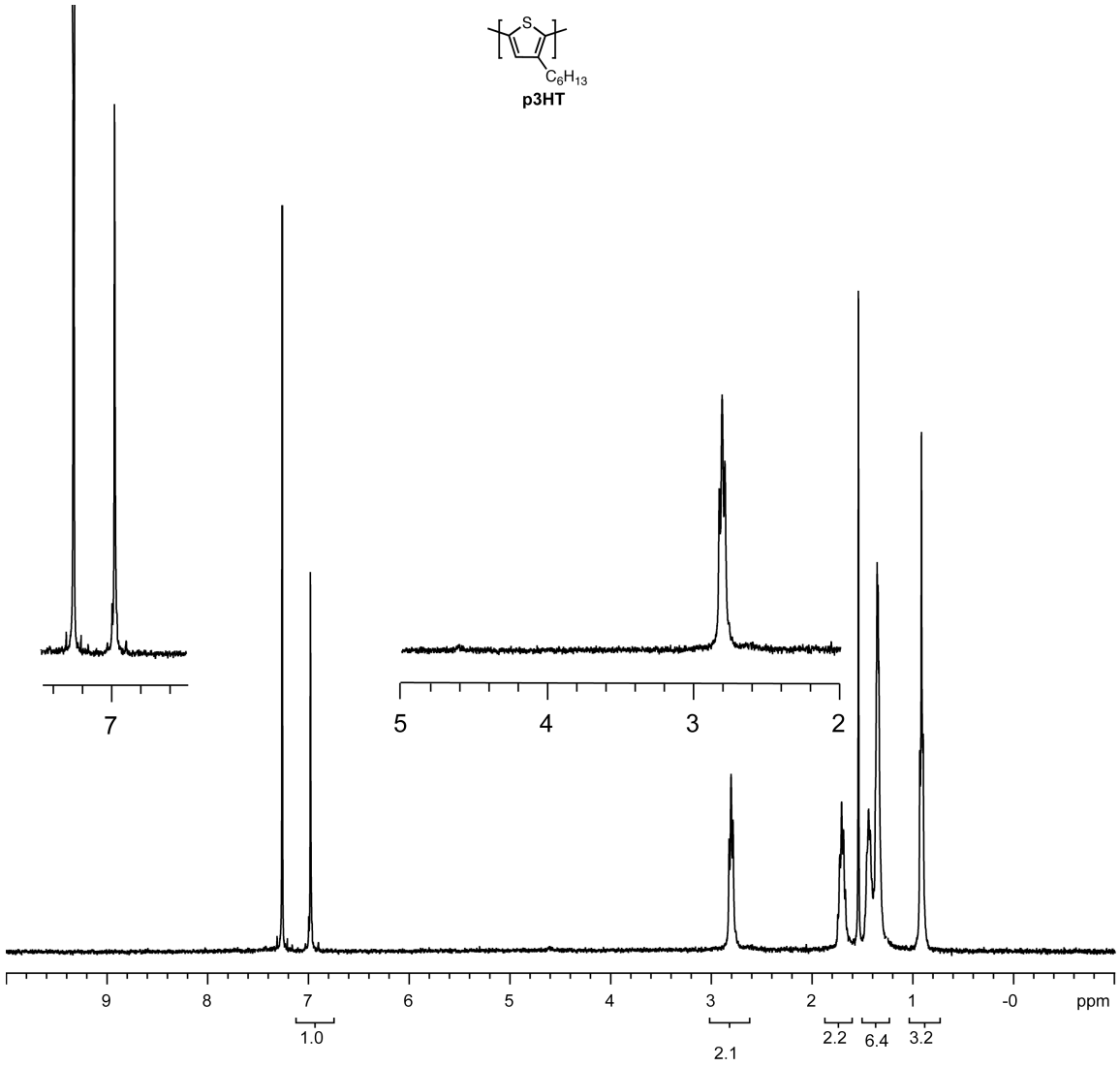

Figure S7. ^{1}H NMR spectrum for **p3HT**
^{1}H NMR (400 MHz, $CDCl_3$) δ 6.98 (s, 1H), 2.80 (t, J = 8 Hz, 2H), 1.71 (m, 2H), 1.4-1.3 (br m, 6H), 0.91 (t, J = 6.8 Hz, 3H).

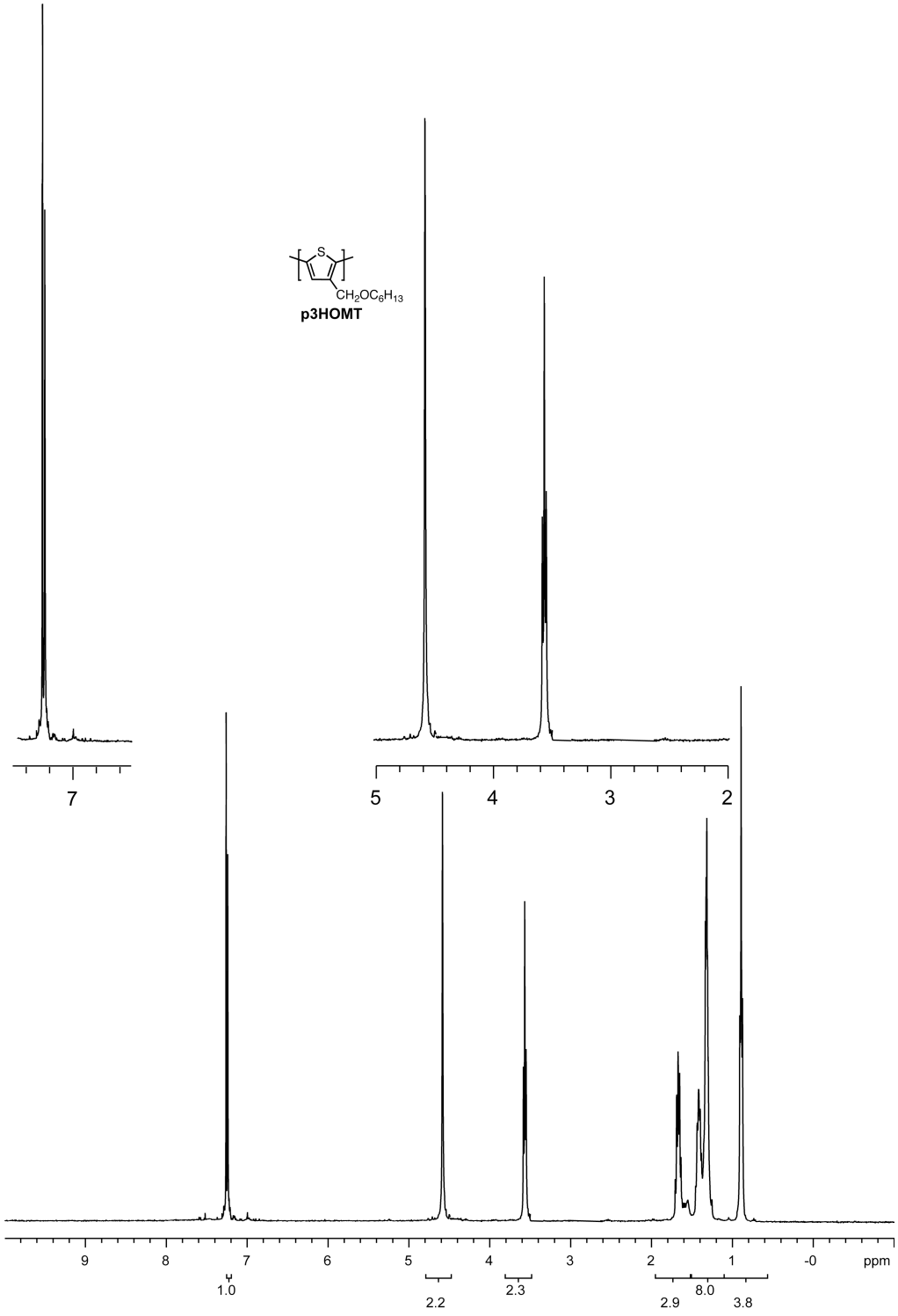

Figure S8. ^{1}H NMR spectrum for **p3HOMT**
^{1}H NMR (400 MHz, $CDCl_3$) δ 7.20 (s, 1H), 4.54 (s, 2H), 3.53 (t, J = 6.4 Hz, 2H), 1.65 (m, 2H), 1.4-1.3 (br m, 6H), 0.85 (t, J = 7.2 Hz, 3H).

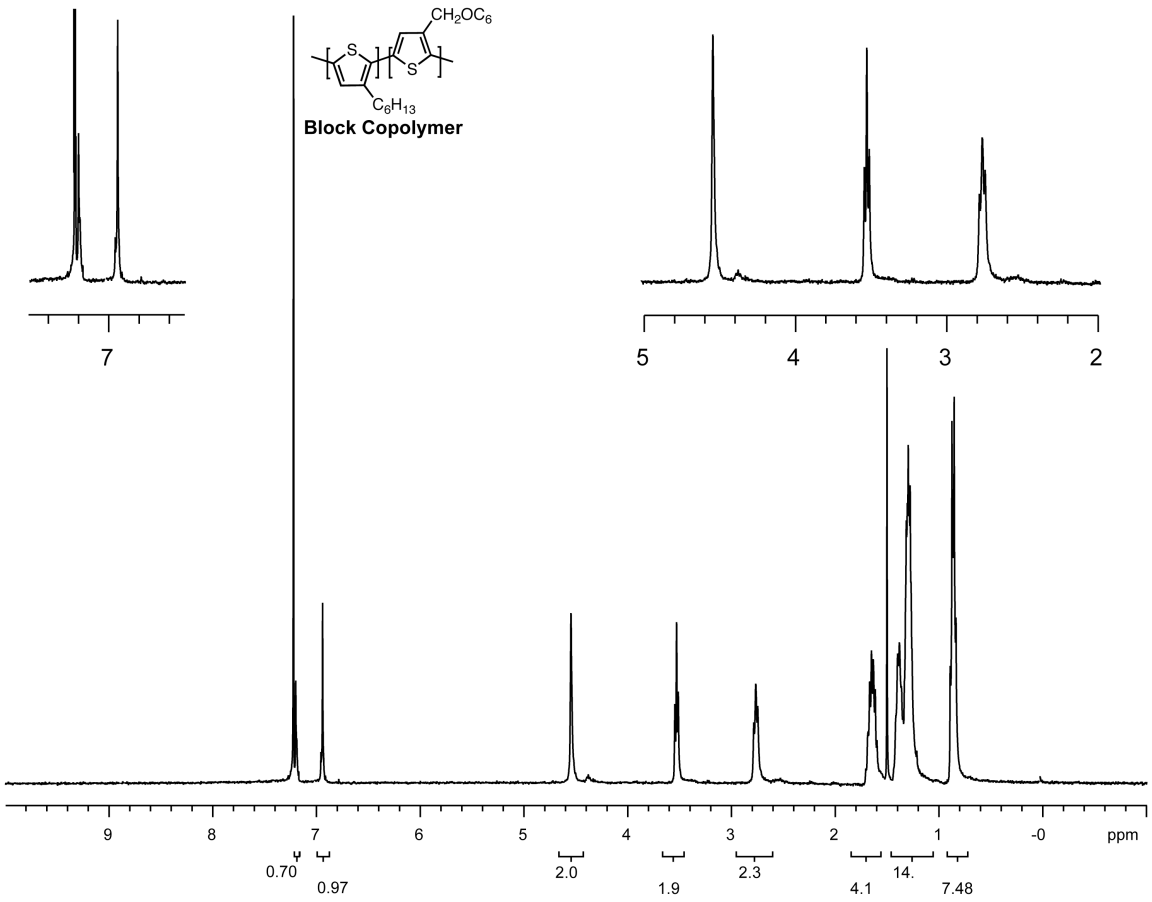

Figure S9. ^{1}H NMR spectrum for block copolymer
^{1}H NMR (400 MHz, $CDCl_3$) δ 7.20 (s, 1H), 6.90 (s, 1H), 4.54 (s, 2H), 3.53 (t, J = 6.4 Hz, 2H), 2.79 (m, 2H), 1.65 (m, 4H), 1.4-1.3 (br m, 12H), 0.85 (t, J = 7.2 Hz, 6H).

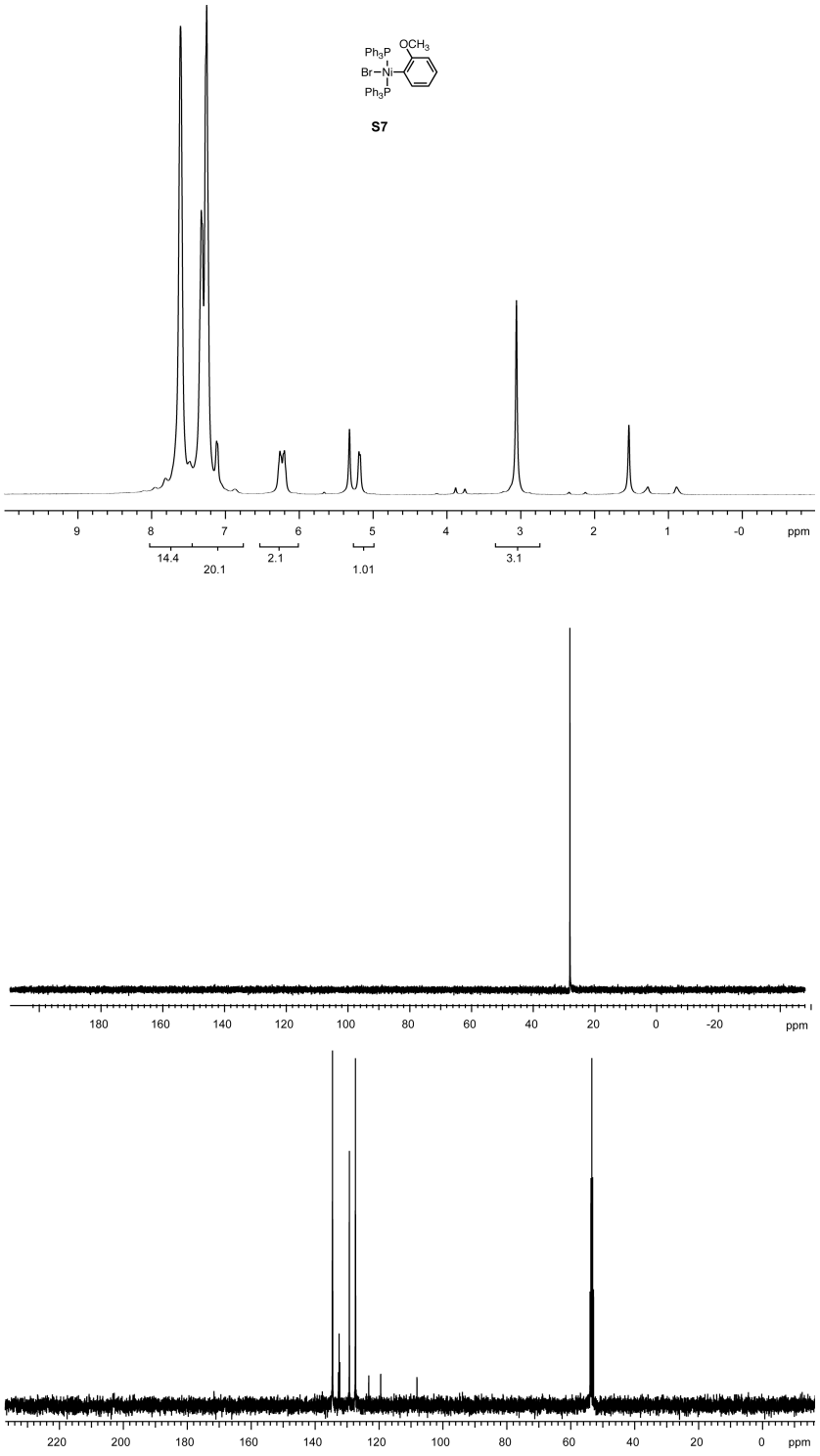

Figure S10. ^{1}H, ^{31}P and ^{13}C NMR spectra for **S7**
^{1}H NMR (400 MHz, CD_2Cl_2) δ 7.61 (br, 12 H), 7.31 (br m, 19 H), 6.24 (m, 2H), 5.19 (br, 1H), 3.06 (br, 3H). ^{31}P NMR (162 MHz, CD_2Cl_2) δ 22.42 (s). ^{13}C NMR (100 MHz, CD_2Cl_2) δ 134.60, 134.54, 134.49, 132.70, 132.48, 132.27, 129.26, 127.40, 127.13, 127.31, 123.20, 119.46, 108.11.

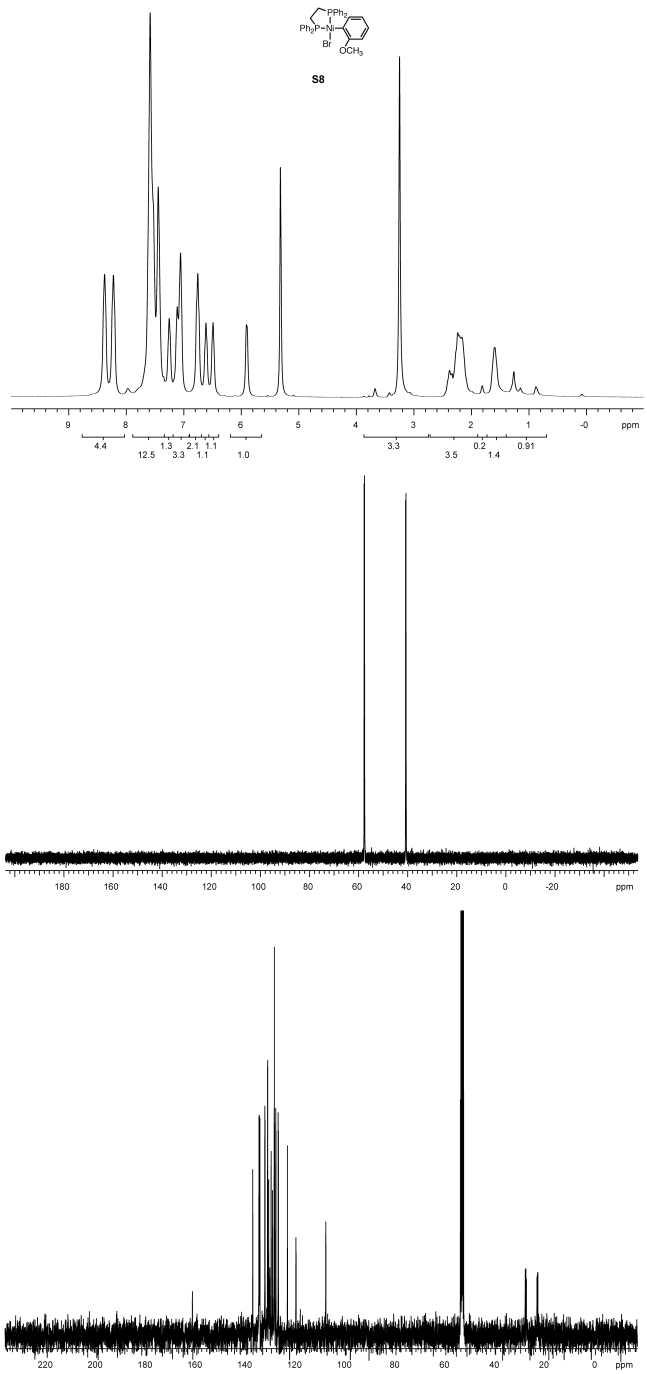

Figure S11. ^{1}H, ^{31}P and ^{13}C NMR spectra for **S8**
^{1}H NMR (400 MHz, CD_2Cl_2) δ 8.38 (s, 1H), 8.22 (s, 2H), 7.58 (br m, 12H), 7.25 (s, 1H), 7.11 (m, 3H), 6.76 (br, 2H), 6.61 (br, 1H), 6.49 (br, 1H), 5.91 (br, 1H) 3.25 (br 3H), 2.24 (br m, 4H). ^{31}P NMR (162 MHz, CD_2Cl_2) δ 57.64 (d, J = 27.3 Hz), 40.75 (d, J = 27.3 Hz). ^{13}C NMR (100 MHz, CD_2Cl_2) δ 161.7, 137.51, 135.03, 134.91, 134.74, 134.63, 132.67, 132.57, 131.58, 131.50, 131.11, 130.13, 129.56, 128.92, 128.82, 128.73, 128.28, 128.18, 127.30, 127.20, 123.57, 120.18, 108.17, 28.12 (dd, J = 26.4, 20.7 Hz), 23.2 (dd, J = 12.5, 11.7 Hz).

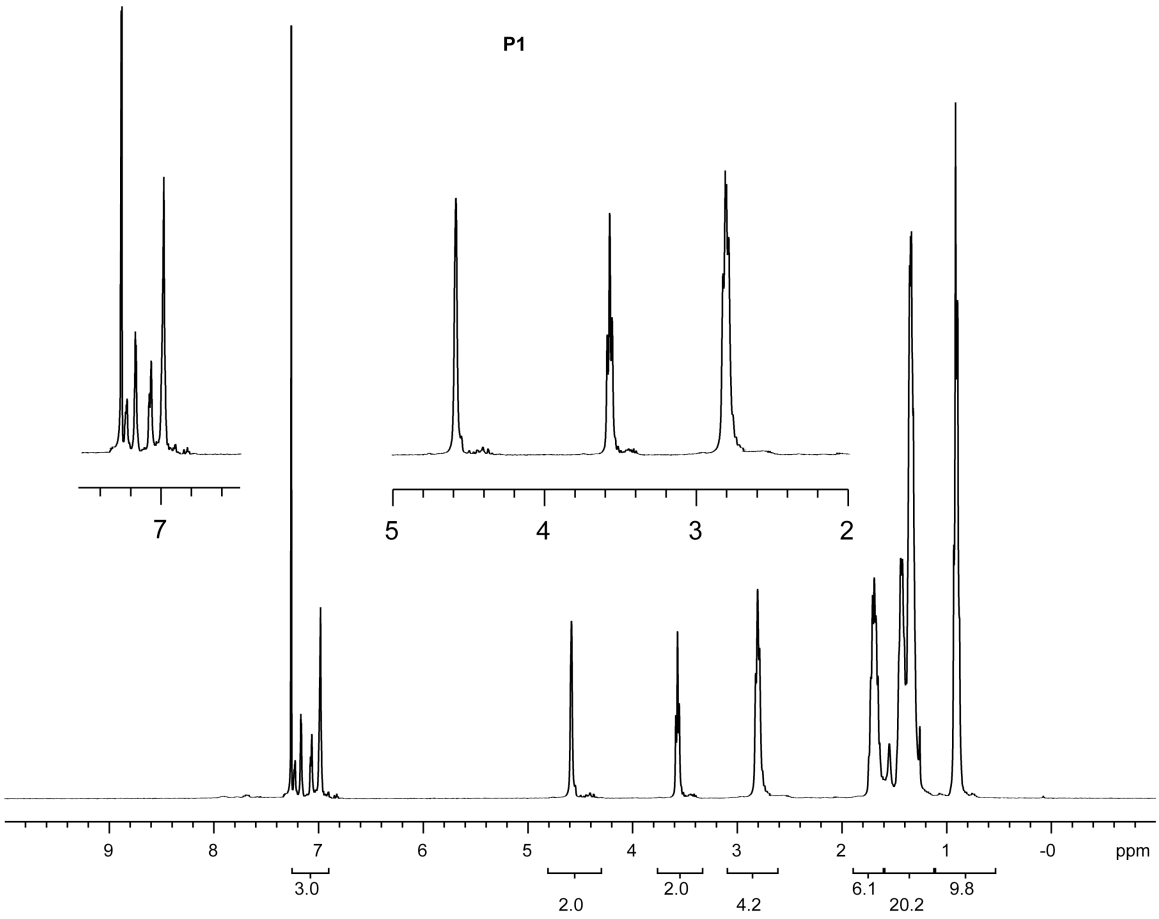

Figure S12. ^{1}H NMR spectrum for **P1**
^{1}H NMR (400 MHz, $CDCl_3$) δ 7.2-6.9 (m, 3H), 4.57 (s, 2H), 3.55 (t, J = 6.4 Hz, 2H), 2.79 (br m, 4H), 1.65 (m, 6H), 1.4-1.3 (br, 18H), 0.90 (br, 9H).

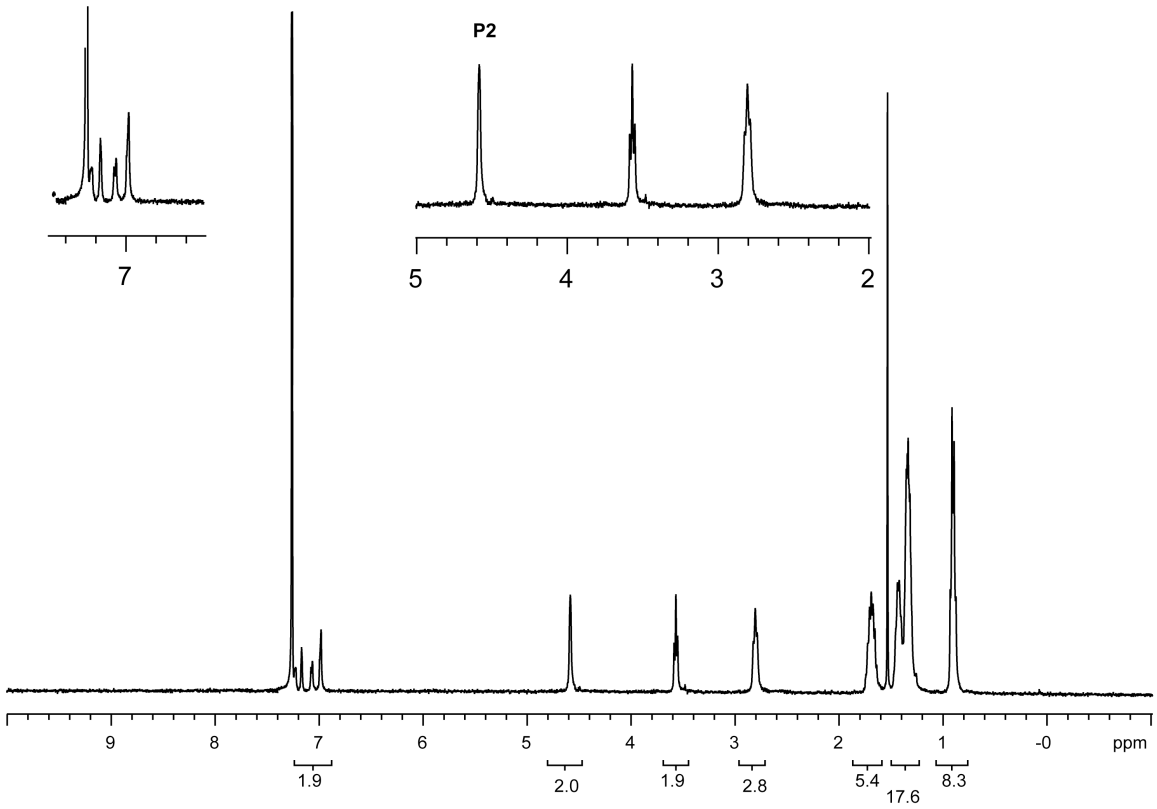

Figure S13. ^{1}H NMR spectrum for **P2**

^{1}H NMR (400 MHz, $CDCl_3$) δ 7.2-6.9 (m, 2H), 4.56 (s, 2H), 3.55 (t, J = 6.8 Hz, 2H), 2.79 (br m, 3H), 1.65 (m, 5H), 1.4-1.3 (br, 18H), 0.90 (br, 9H).

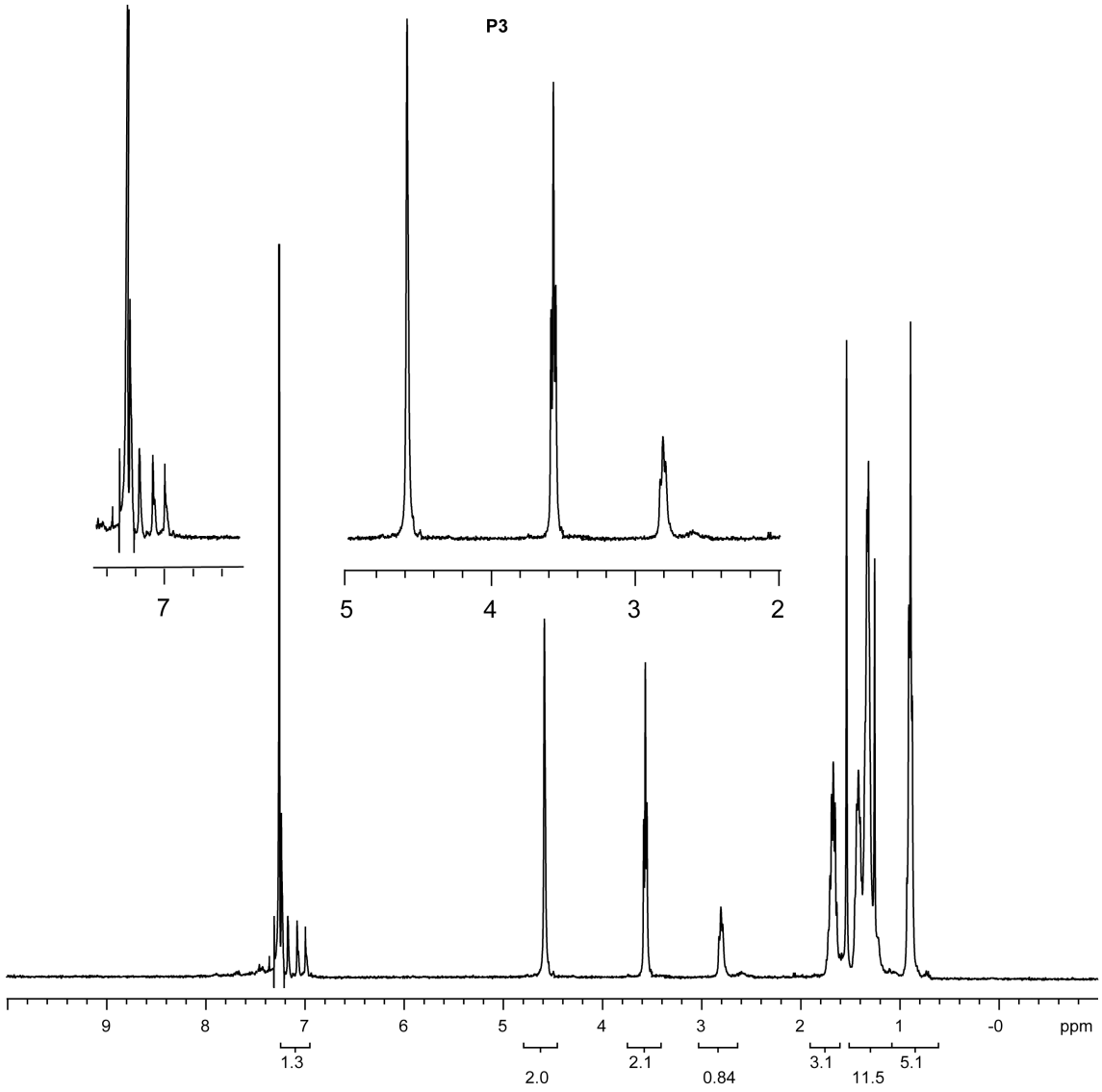

Figure S14. ^{1}H NMR spectrum for **P3**
^{1}H NMR (400 MHz, $CDCl_3$) δ 7.2-6.9 (m, 1.5H), 4.56 (s, 2H), 3.55 (t, J = 6.8 Hz, 2H), 2.79 (br m, 1H), 1.65 (m, 3H), 1.4-1.3 (br, 9H), 0.90 (br, 5H).

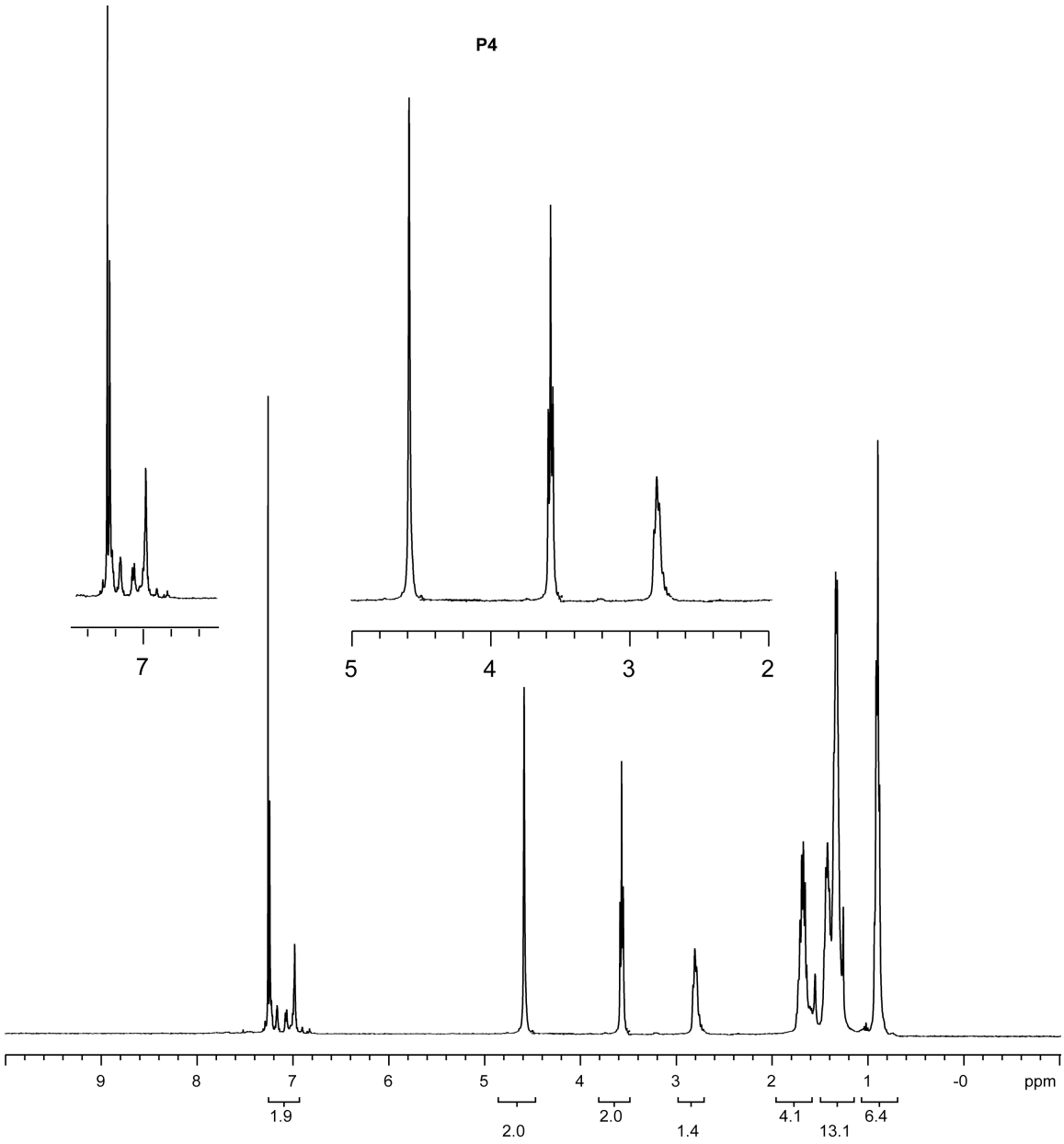

Figure S15. ^{1}H NMR spectrum for **P4**
^{1}H NMR (400 MHz, $CDCl_3$) δ 7.2-6.9 (m, 1.9H), 4.56 (s, 2H), 3.55 (t, *J* = 6.8 Hz, 2H), 2.79 (br m, 1.5H), 1.65 (m, 4H), 1.4-1.3 (br, 16H), 0.90 (br, 6H).

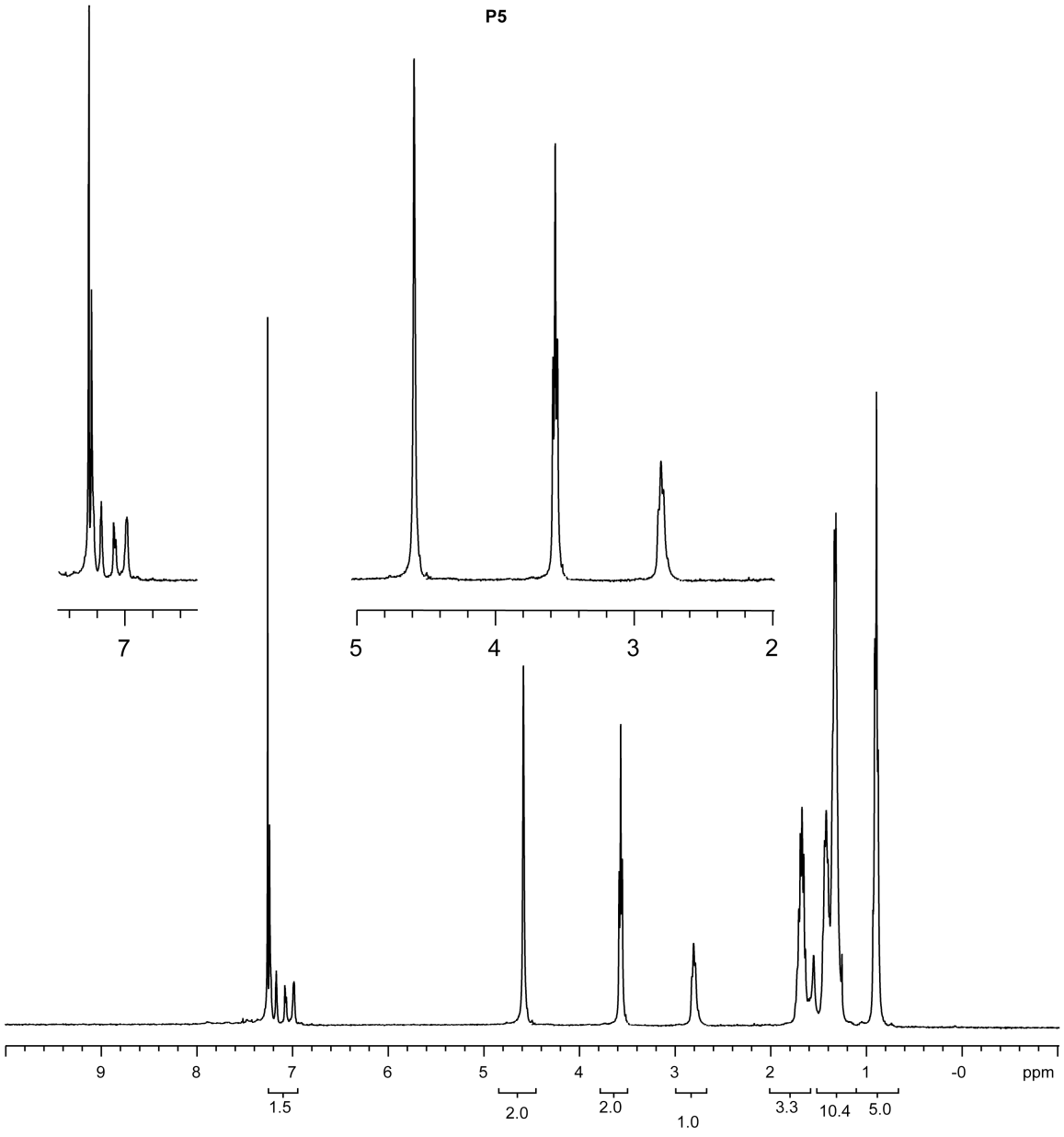

Figure S16. ^{1}H NMR spectrum for **P5**
^{1}H NMR (400 MHz, $CDCl_3$) δ 7.2-6.9 (m, 1.5 H), 4.56 (s, 2H), 3.55 (t, *J* = 6.8 Hz, 2H), 2.79 (br m, 1H), 1.65 (m, 3H), 1.4-1.3 (br, 9H), 0.90 (br, 5H).

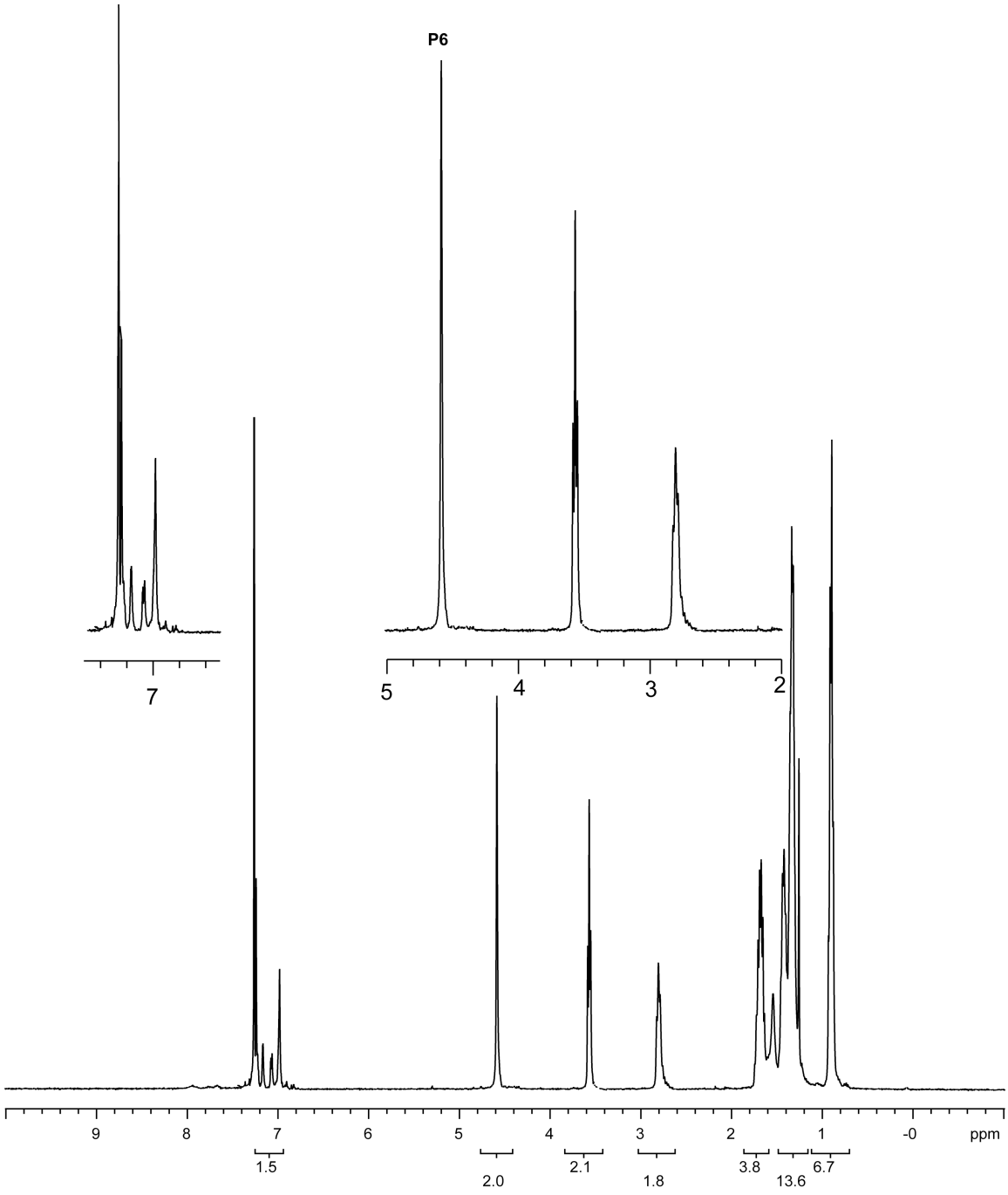

Figure S17. ^{1}H NMR spectrum for **P6**

^{1}H NMR (400 MHz, $CDCl_3$) δ 7.2-6.9 (m, 2H), 4.56 (s, 2H), 3.55 (t, J = 6.8 Hz, 2H), 2.79 (br m, 1.8H), 1.65 (m, 4H), 1.4-1.3 (br, 16H), 0.90 (br, 6H).

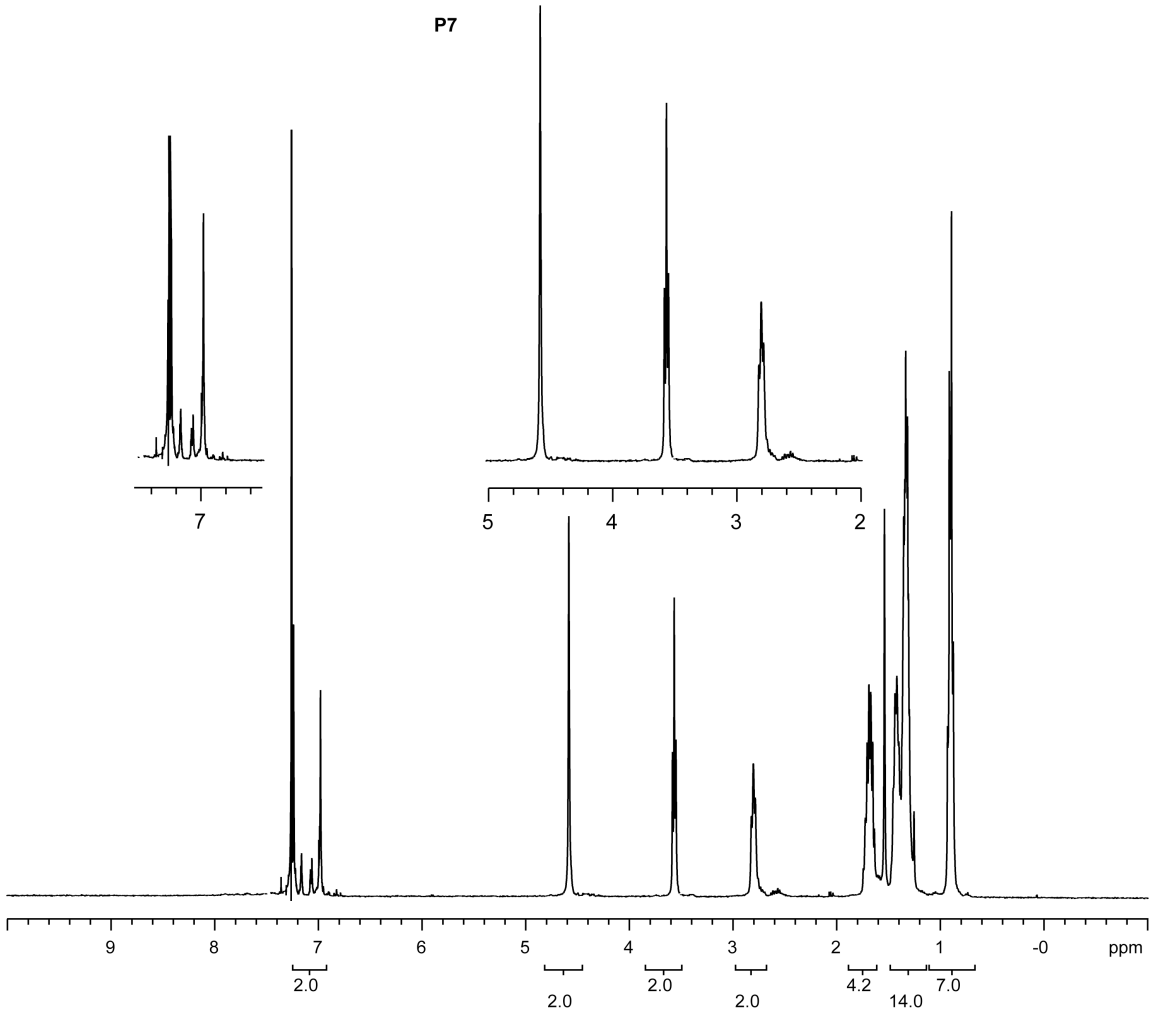

Figure S18. ^{1}H NMR spectrum for **P7**
^{1}H NMR (400 MHz, $CDCl_3$) δ 7.2-6.9 (m, 2H), 4.56 (s, 2H), 3.55 (t, J = 6.8 Hz, 2H), 2.79 (br, 2H), 1.65 (m, 4H), 1.4-1.3 (br, 16H), 0.90 (br, 6H).

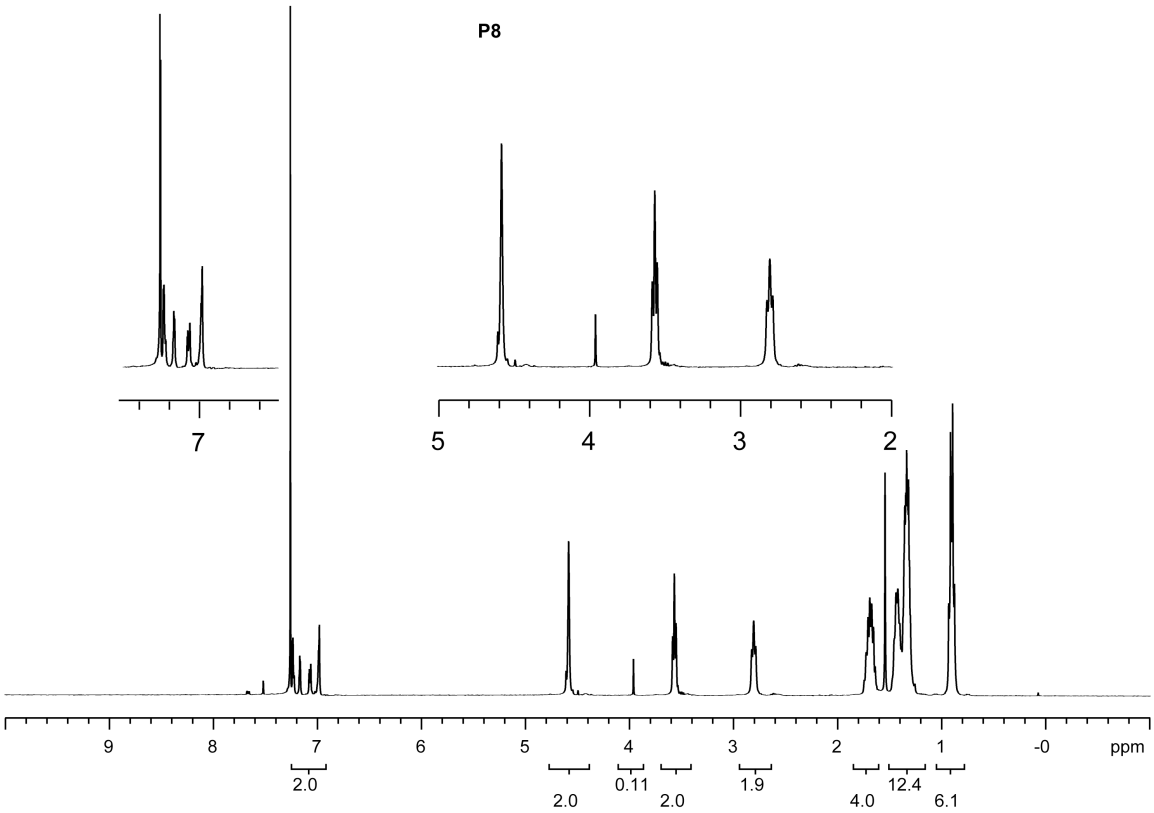

Figure S19. ^{1}H NMR spectrum for **P8**
^{1}H NMR (400 MHz, $CDCl_3$) δ 7.2-6.9 (m, 2H), 4.56 (s, 2H), 3.96 (s, 0.2H), 3.55 (t, J = 6.8 Hz, 2H), 2.79 (br m, 2H), 1.65 (m, 4H), 1.4-1.3 (br, 16H), 0.90 (br, 6H).

V. Calibration Curves

Solutions containing a constant concentration of docosane (0.010 M) and varying concentrations of **S1** and **S5** were prepared in $CHCl_3$. Each was analyzed by GC and the response factor **F** calculated by fitting the data to the following equation:

$$\frac{\text{analyte area}}{\text{[analyte]}} = \mathbf{F}\,\frac{\text{docosane area}}{\text{[docosane]}}$$

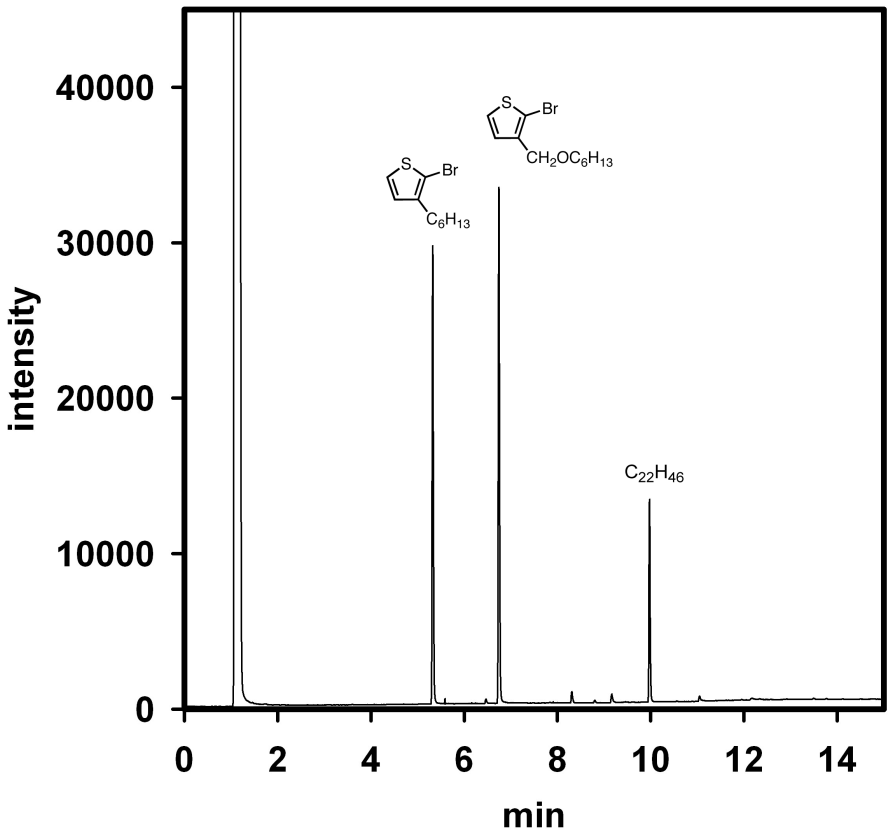

Figure S20. Representative GC chromatogram of quenched polymerization aliquot.

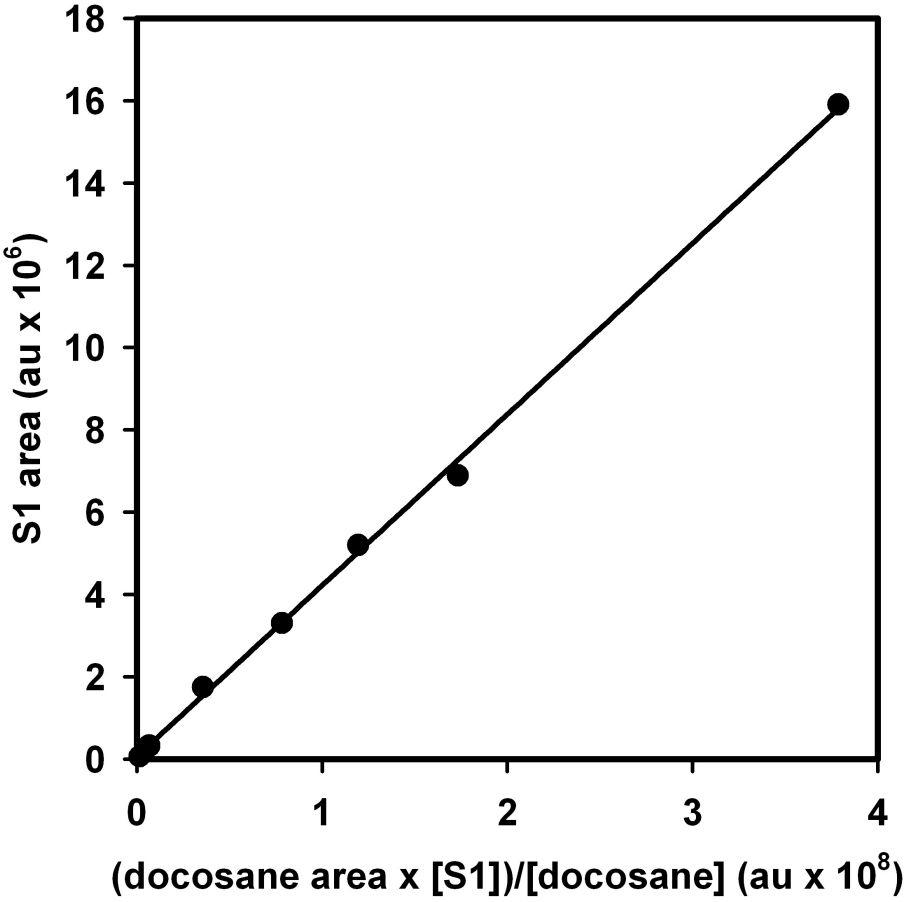

Figure S21. Plot of **S1** area versus (docosane area x [**S1**]) / [docosane] fitted to y = *m*x + *b* where *m* = 0.041 ± 0.006 and *b* = -6.08 ± 0.23 x 10^4.

Table S1. Data for the plot in Figure S21.

[S1] (M)	Area **S1** (au x 10^6)	area docosane (au x 10^7)	(docosane area x **[S1]**) / [docosane] (au x 10^8)
0.20	15.9	1.89	3.79
0.10	6.89	1.73	1.73
0.075	5.20	1.59	1.19
0.050	3.35	1.57	0.784
0.025	1.75	1.42	0.357

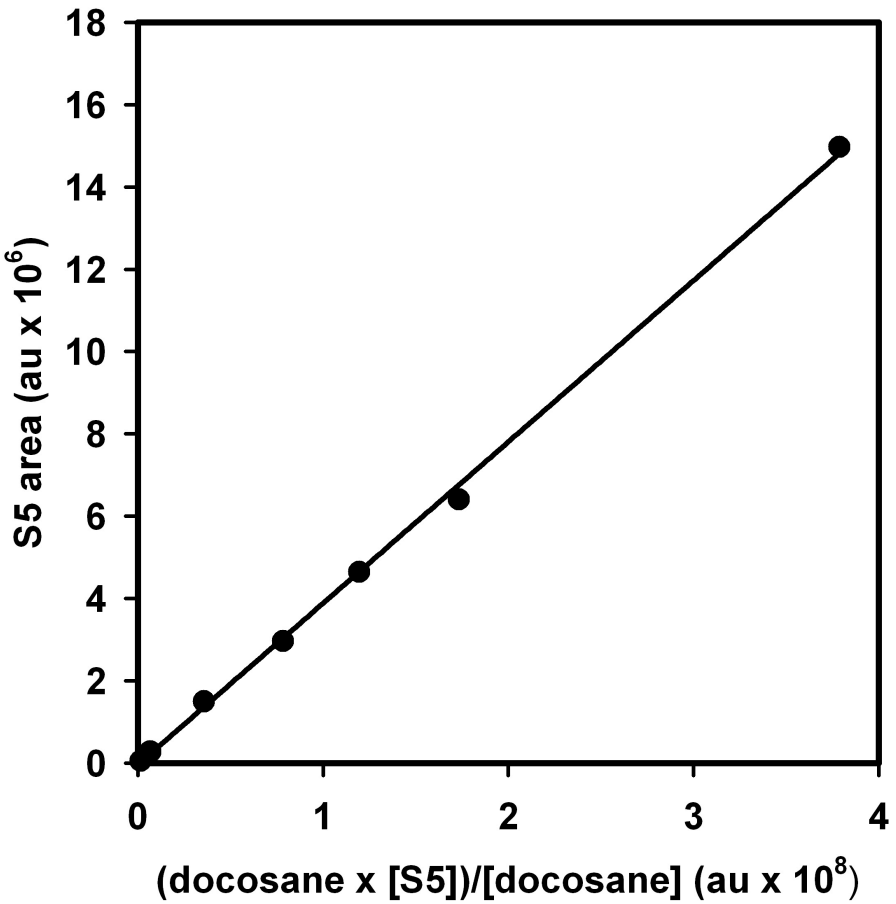

Figure S22. Plot of **S5** area versus (docosane area x [**S5**]) / [docosane] fitted to y = *m*x + *b* where *m* = 0.039 ± 0.004 and *b* = -3.51 ± 0.15 x 10^4.

Table S2. Data for the plot in Figure S22.

[S5] (M)	Area **S5** (au x 10^6)	area docosane (au x 10^7)	(docosane area x **[S4]**) / [docosane] (au x 10^8)
0.20	18.9	1.89	3.79
0.10	1.73	1.73	1.73
0.075	4.65	1.59	1.19
0.050	2.96	1.57	0.784
0.025	1.50	1.42	0.357
0.0050	0.283	1.33	0.0669

VI. M_n and PDI versus Conversion

General procedure for obtaining plots of M_n and PDI versus conversion:
A 50 mL Schlenk flask equipped with a stir bar and three-way adapter equipped with a septum was evacuated and cooled under vacuum. Once cool, the flask was filled with N_2 and re-evacuated: this process was repeated twice and the flask was filled with N_2. THF (10 mL) was added to the flask and cooled to 0 ˚C. **1**, **2** (see pg 62) and a $C_{22}H_{46}$ solution (0.5 mL, 0.2 M in THF) were added by syringe and the solution stirred for 1 min. A ~0.2 mL aliquot was withdrawn via syringe and quenched with 5 MHCl (~ 1 mL). Then the catalyst solution (see pg 64) was added to the reaction. Aliquots (~0.2 mL) were taken from the reaction via syringe and quenched with 5 M HCl (~ 1 mL). Each aliquot was then extracted with $CHCl_3$ (2 mL) and the solvent removed in vacuo. The samples were dissolved in THF (~1 mL). The samples were then divided and analyzed by GC and GPC.

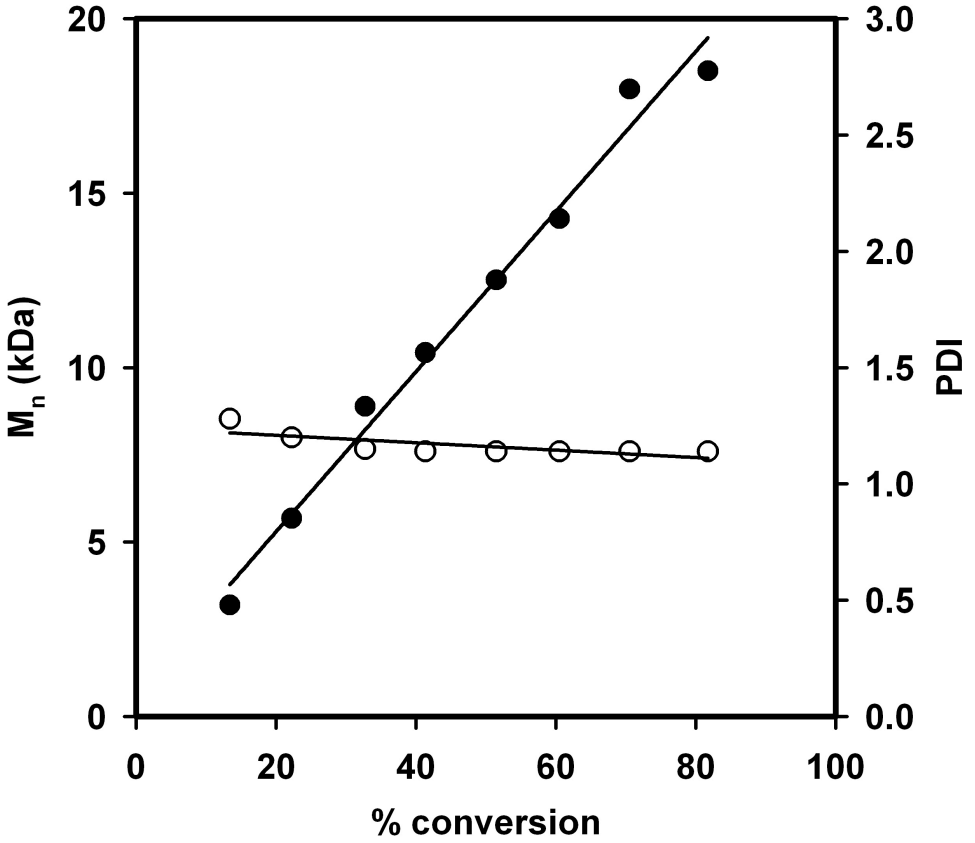

Figure S23. Plot of M_n (●) and PDI (○) versus conversion for Ni(dppp)Cl_2-catalyzed copolymerization of **1** and **2** at 0 ˚C ([**1**] = [**2**] = 0.04 M; [Ni(dppp)Cl_2] = 0.002 M).

Table S3. Data for plot in Figure S23.

Percent Conversion	M_n (kDa)	PDI
13.4	3.2	1.3
22.3	5.7	1.2
32.8	8.9	1.2
41.4	10.4	1.1
51.5	12.5	1.1
60.5	14.3	1.1
70.6	18.0	1.1
81.8	18.5	1.1

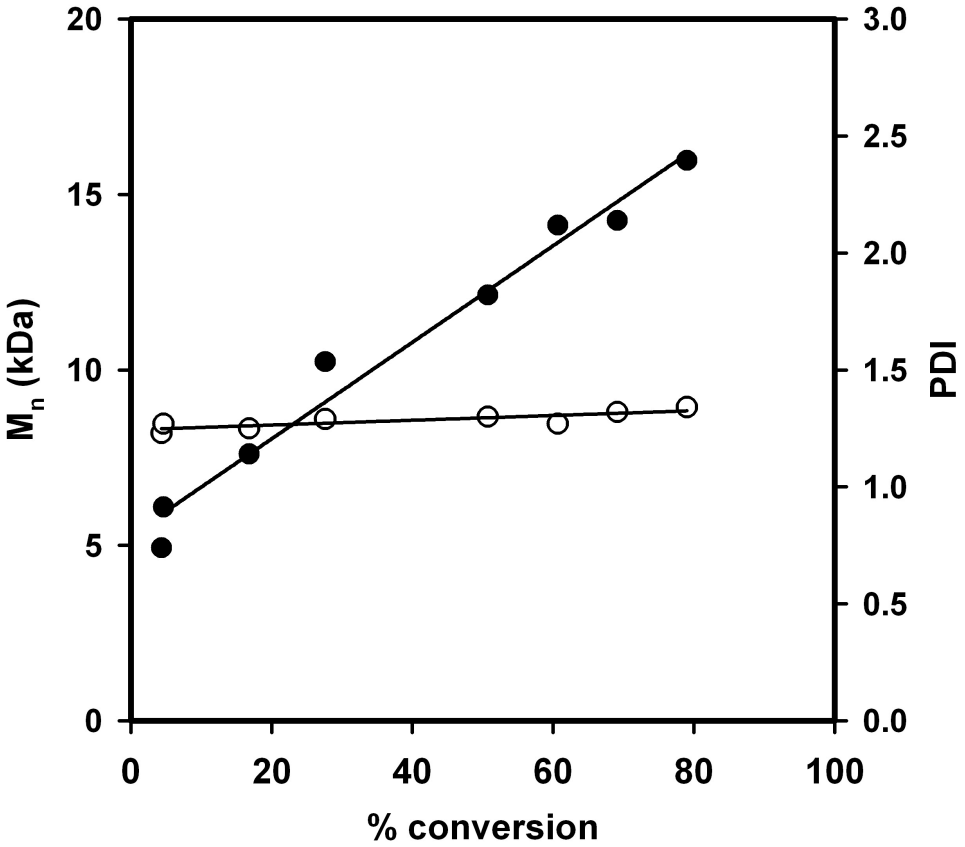

Figure S24. Plot of M_n (●) and PDI (○) versus conversion for Ni(dppe)Cl_2-catalyzed copolymerization of **1** and **2** at 0 ˚C ([**1**] = [**2**] = 0.04 M; [Ni(dppe)Cl_2] = 0.002 M).

Table S4. Data for plot in Figure S24.

Percent Conversion	M_n (kDa)	PDI
4.37	4.9	1.2
4.68	6.1	1.3
16.8	7.6	1.3
27.6	10.2	1.3
50.7	12.1	1.3
60.7	14.1	1.3
69.1	14.2	1.3
79.0	16.0	1.3

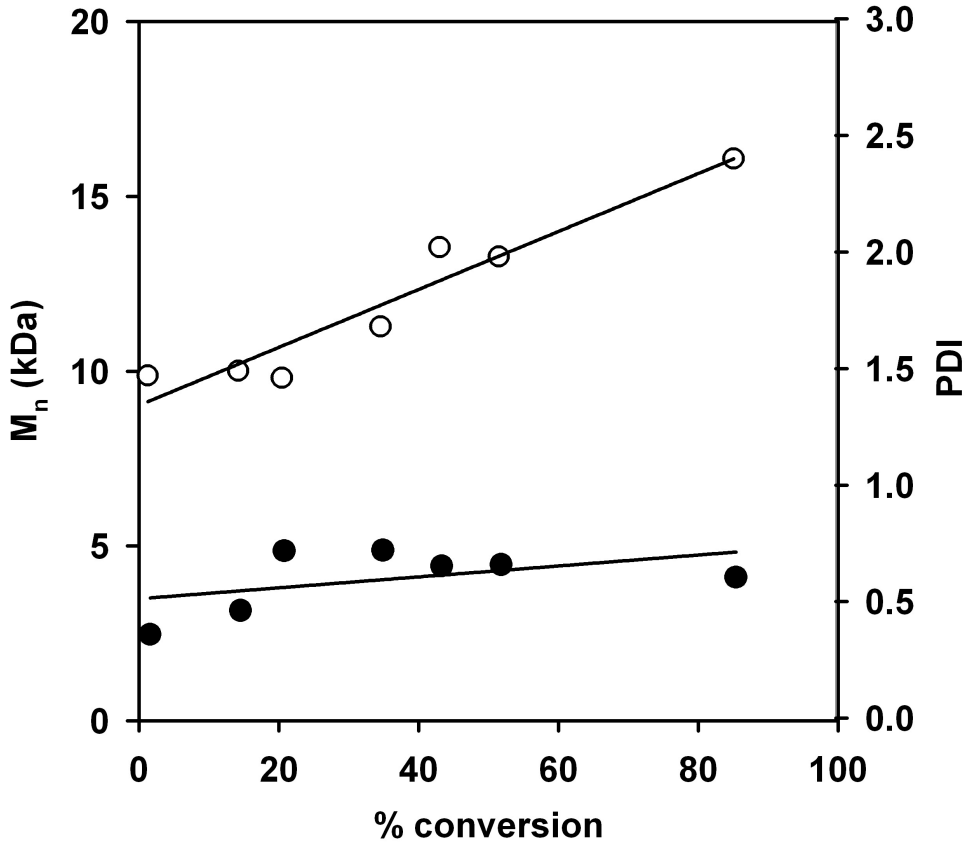

Figure S25. Plot of M_n (●) and PDI (○) versus conversion for Ni(dppf)Cl_2-catalyzed copolymerization of **1** and **2** at 0 ˚C ([**1**] = [**2**] = 0.04 M; [Ni(dppf)Cl_2] = 0.002 M).

Table S5. Data for plot in Figure S25.

Percent Conversion	M_n (kDa)	PDI
1.68	2.5	1.5
14.5	3.2	1.5
20.8	4.9	1.5
34.9	4.9	1.7
43.3	4.4	2 .0
51.8	4.5	2 .0
85.4	4.1	2.4

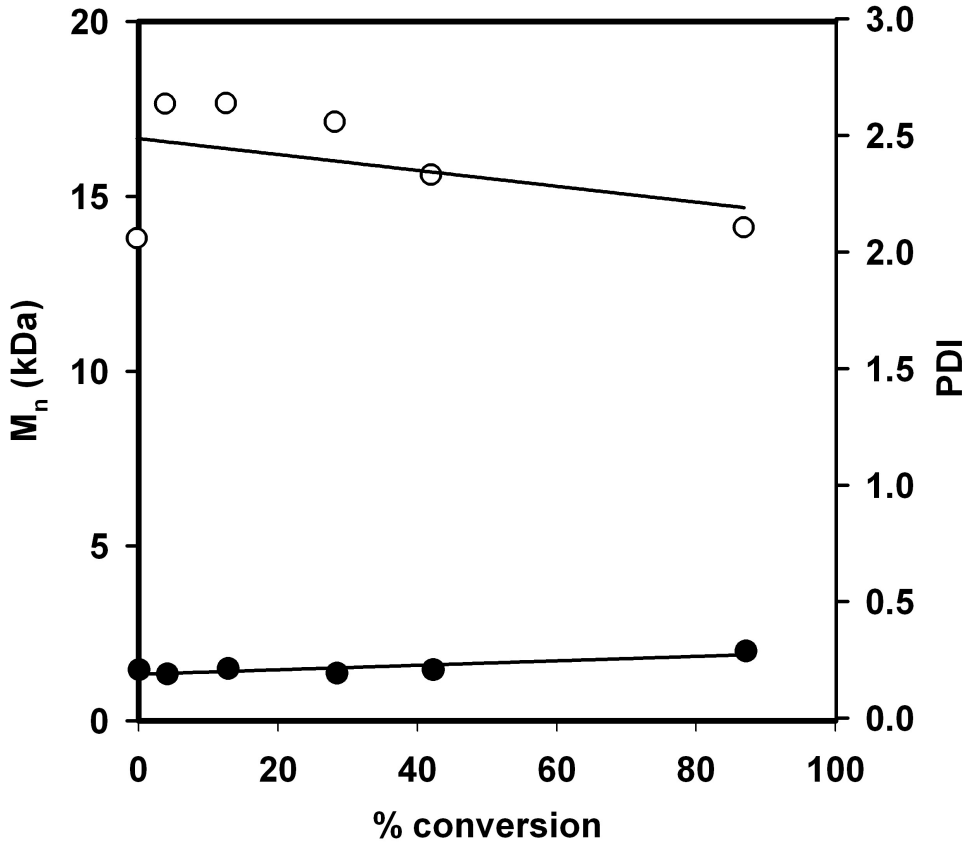

Figure S26. Plot of M_n (●) and PDI (○) versus conversion for $Ni(PPh_3)_2Cl_2$-catalyzed copolymerization of **1** and **2** at 0 ˚C ([**1**] = [**2**] = 0.04 M; $[Ni(PPh_3)_2Cl_2]$ = 0.002 M).

Table S6. Data for plot in Figure S26.

Percent Conversion	M_n (kDa)	PDI
1.21	1.5	2.1
4.15	1.3	2.6
12.9	1.5	2.6
28.5	1.4	2.6
42.3	1.5	2.3
87.2	2.0	2.1

VII. Batch Copolymerizations

General procedure for conducting batch copolymerizations:
An oven-dried 50 mL Schlenk flask equipped with a stir bar and three-way adapter equipped with a septum was evacuated and cooled under vacuum. Once cool, the flask was filled with N_2 and re-evacuated: this process was repeated twice and the flask filled with N_2. THF (10 mL) was added to the flask and cooled to 0 ˚C. **1**, **2** (see pg 62) of varying ratios ($[\mathbf{1} + \mathbf{2}]_{total}$ = 1 mmol) and $C_{22}H_{46}$ solution (0.5 mL, 0.2 M in THF) were added by syringe and the solution stirred for 1 min. An aliquot (~ 0.2 mL) was withdrawn via syringe and quenched with 5 M HCl (~ 1 mL). Then catalyst solution (see pg 64) was added to the reaction. Aliquots (~0.2 mL) were taken from the reaction via syringe and quenched with 5M HCl (~ 1 mL). Each aliquot was then extracted with $CHCl_3$ and the solvent removed in vacuo. The samples were then dissolved in THF (~1 mL). The samples were then divided and analyzed by GC and GPC.

*Procedure for calculating the cumulative mole fraction of **1** in the copolymer*
The cumulative mole fraction of **1** in the copolymer at a given time was determined from the following equation where $[\mathbf{1}]_o$ is the concentration of **1** before addition of the catalyst solution,$[\mathbf{1}]_t$ is the concentration of **1** in the feed at time t, $[\mathbf{1} + \mathbf{2}]_o$ is the total concentration of **1** and **2** in the feed before addition of the catalyst solution, and $[\mathbf{1} + \mathbf{2}]_t$ is the total concentration of **1** and **2** at time t.

$$\frac{[\mathbf{1}]_o - [\mathbf{1}]_t}{[\mathbf{1} + \mathbf{2}]_o - [\mathbf{1} + \mathbf{2}]_t}$$

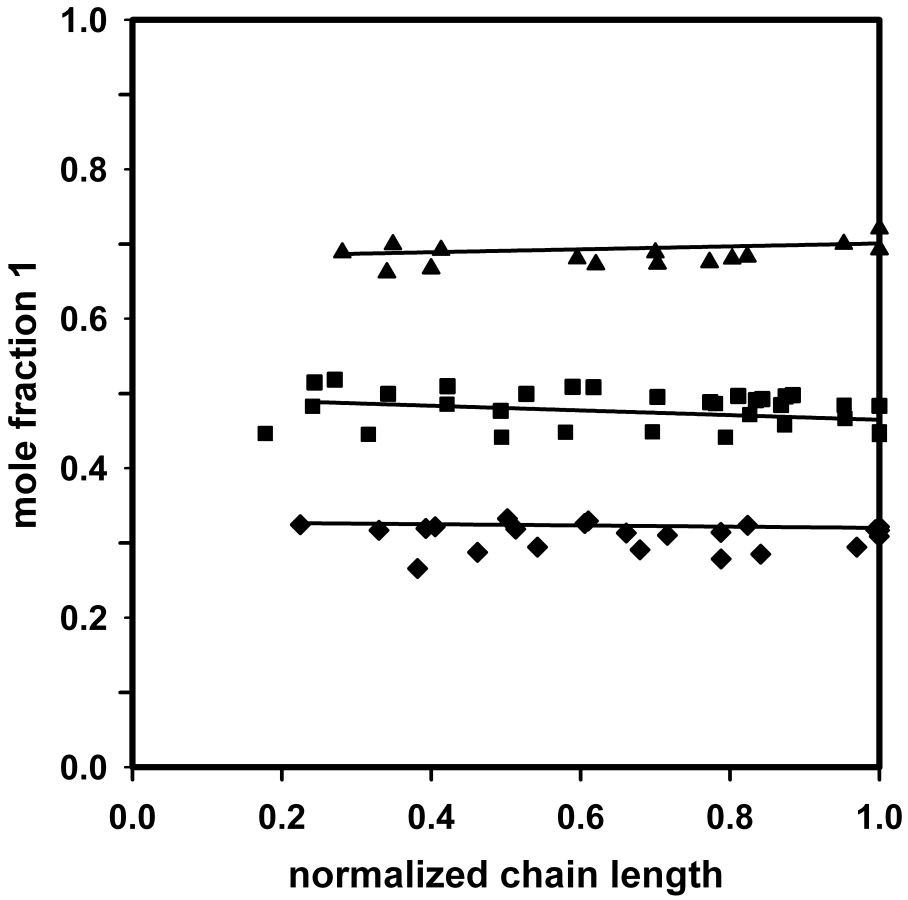

Figure S27. Plot of the cumulative mole fraction of **1** in the copolymer versus the normalized chain length from the batch copolymerizations. ([**1**]:[**2**]; **P1** = 67:33 (▲); **P2** = 50:50 (■); **P3** = 33:67 (♦))

Table S7. Data used for plot in Figure S27.

P1

Polymerization Run	Normalized chain length	Cumulative mole fraction **1**
1	0.413	0.692
1	0.595	0.681
1	0.7	0.689
1	0.803	0.680
1	0.952	0.699
1	1	0.721
2	0.341	0.662
2	0.399	0.667
2	0.620	0.672
2	0.703	0.674
2	0.773	0.676
2	0.823	0.683
2	1	0.693

P2

Polymerization Run	Normalized chain length	Cumulative mole fraction **1**
1	0.178	0.446
1	0.316	0.445
1	0.494	0.442
1	0.579	0.448
1	0.696	0.449
1	0.794	0.442
1	0.954	0.466
1	1	0.449
2	0.241	0.483
2	0.421	0.486
2	0.781	0.486
2	0.826	0.472
2	0.873	0.457
2	1	0.445
3	0.244	0.515
3	0.422	0.509
3	0.527	0.499
3	0.589	0.509
3	0.773	0.488
3	0.811	0.497
3	0.884	0.498
4	0.271	0.518
4	0.342	0.499
4	0.493	0.476
4	0.617	0.508
4	0.703	0.495
4	0.868	0.485
4	1	0.483

P3

Polymerization Run	Normalized chain length	Cumulative mole fraction **1**
1	0.462	0.287
1	0.542	0.294
1	0.679	0.291
1	0.789	0.279
1	0.841	0.285
1	1	0.309
2	0.225	0.325
2	0.405	0.321
2	0.502	0.332
2	0.611	0.329
2	0.661	0.313
2	0.824	0.323
2	1	0.322
3	0.331	0.317
3	0.393	0.319
3	0.513	0.319
3	0.606	0.326

3	0.716	0.311
3	0.788	0.314
3	1	0.317

VIII. Reactivity Ratios

General procedure for determining reactivity ratios

A 10 mL conical flask equipped with a stir bar and septum was evacuated and cooled under vacuum. Once cool, the flask was filled with N_2 and re-evacuated: this process was repeated twice and the flask filled with N_2. THF (2 mL) and $C_{22}H_{46}$ solution (0.1 mL, 0.2 M in THF) were added to the flask and cooled to 0 ˚C. **1** and **2** (see pg 62) were added in varying ratios (total volume added was 1 mL) by syringe and the solution stirred for 1 min. An aliquot (~0.05 mL) was withdrawn via syringe and quenched with MeOH (~0.05 mL) in a GC vial. Then catalyst solution (0.2 mL) (see pg 64) was added to the reaction. Aliquots (~0.05 mL) were taken from the reaction via syringe and quenched as above. Each aliquot was then diluted with $CHCl_3$ to a volume of 1 mL and used in GC analysis. The data were converted to concentrations using the appropriate calibration curves.

From these data the relative rate of monomer conversion was calculated for the first ~10% conversion and fit to the copolymerization equation (Eq S1) where $d[M_1]/d[M_2]$ is ratio of conversion of **1** and **2**, respectively; $[M_1]$ and $[M_2]$ are the initial concentrations of **1** and **2**, respectively, by least-squares regression in SigmaPlot 10.

$$\frac{d[M_1]}{d[M_2]} = \frac{[M_1]}{[M_2]} \frac{k_{11}/k_{12}[M_1] + [M_2]}{[M_1] + k_{22}/k_{21}[M_2]} \quad \text{(S1)}$$

Table S8. Data used to calculate reactivity ratios

$[M_1]_o$ (M)	$[M_2]_o$ (M)	$\Delta[M_1]/\Delta[M_2]$
0.33	0.35	0.79
0.081	0.91	0.089
0.029	0.98	0.0096
0.28	0.31	0.89
0.17	0.56	0.26
0.32	0.89	0.48
0.21	0.78	0.24
0.46	0.77	0.80
0.49	0.67	0.79
0.28	0.31	0.89
0.43	0.15	2.5
0.094	0.53	0.19
0.2	0.47	0.53
0.32	0.44	1.0
0.41	0.34	1.1
0.47	0.28	1.9
0.57	0.16	3.7

IX. Semi-batch Copolymerizations

Procedure for Conducting Semi-batch Copolymerizations:
A 50 mL Schlenk flask equipped with a stir bar and three-way adapter equipped with a septum was evacuated and cooled under vacuum. Once cool, the flask was filled with N_2 and re-evacuated: this process was repeated twice and the flask filled with N_2. THF (10 mL) was added to the flask and cooled to 0 ˚C. **2** (see pg 62) and $C_{22}H_{46}$ solution (0.5 mL, 0.2 M) were added by syringe and the solution stirred for 1 min. **1** (from **S3**, see pg 62) was taken up into a syringe, the needle was inserted through the three-way adapter and the syringe placed in a syringe pump set to a rate of addition but not activated. Then catalyst solution* (see pg 64) was added to the reaction and the syringe pump activated. Aliquots (~0.2 mL) were taken from the reaction via syringe and quenched with 5 M HCl (~1 mL). Each aliquot was then extracted with $CHCl_3$ (2 mL) and the solvent removed in vacuo. Half of each sample was reserved for ^{1}H NMR analysis and the other half was dissolved in THF (~1 mL) and passed through a 0.2 μm PTFE filter for GPC analysis. The samples used for ^{1}H NMR were taken up in a minimum amount of $CHCl_3$ and precipitated in MeOH. The precipitate was then collected, dried under vacuum and taken up in $CDCl_3$ for ^{1}H NMR analysis to determine the mole fraction of **1** in the copolymer.

* For **P8**, **S8** (0.018g, 0.025 mmol, 0.025 equiv) was dissolved in 1.00 mL THF and added to the polymerization as a solution.

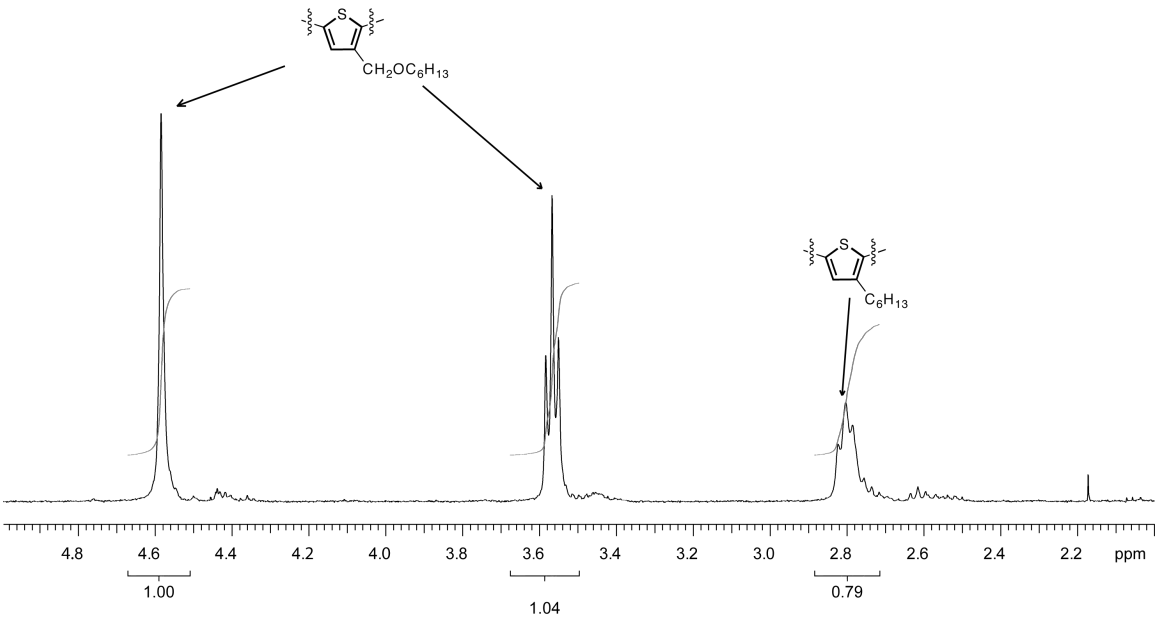

Figure S28. Representative ^{1}H NMR spectrum used to calculate relative mole fractions from a copolymer aliquot.

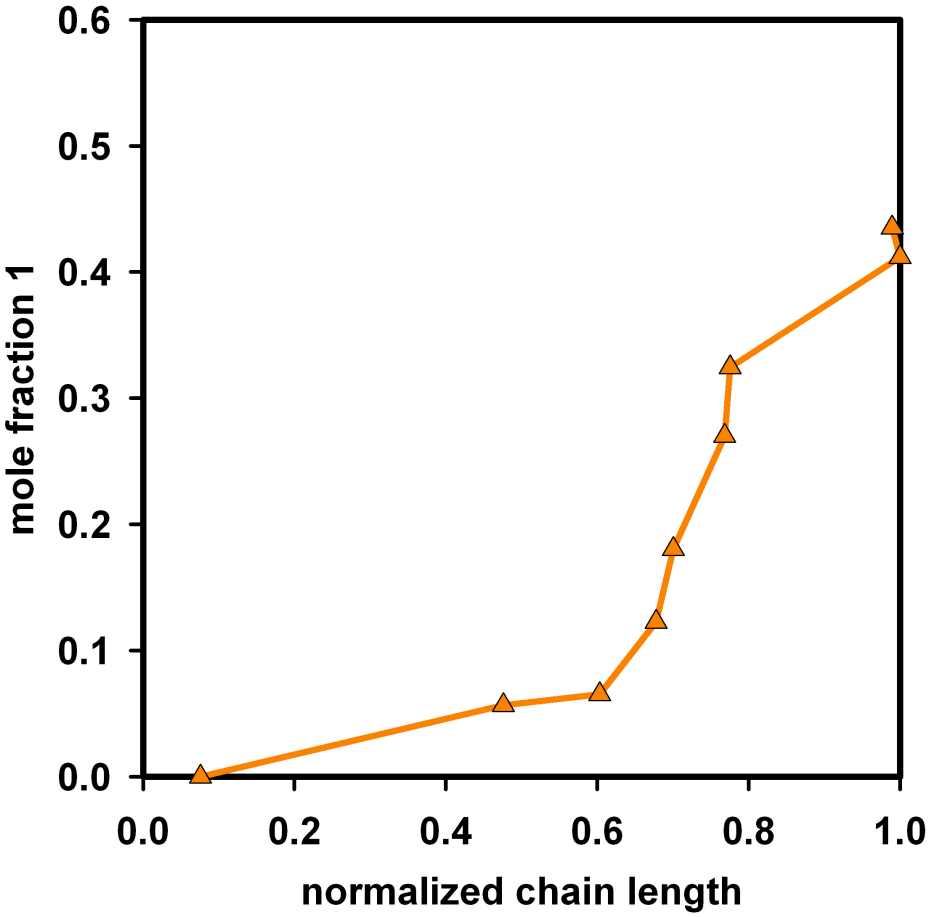

Figure S29. Plot of the cumulative mole fraction of **1** in the copolymer (**P4**) versus the normalized chain length from the semi-batch copolymerization where d[**1**]/dt = 0.12 mmol/min.

Table S9. Data used for the plot in Figure S29.

normalized chain length	mole fraction **1**
0.076	0
0.48	0.057
0.60	0.065
0.68	0.12
0.70	0.18
0.77	0.27
0.78	0.32
0.99	0.41
1	0.43

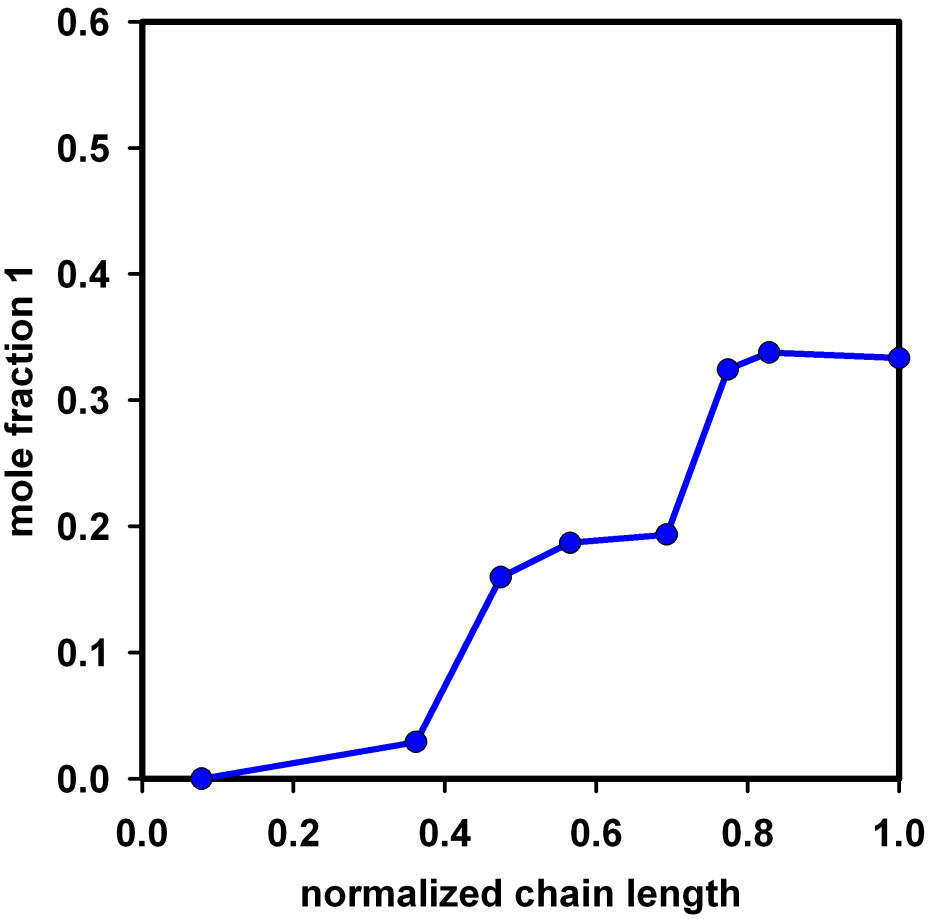

Figure S30. Plot of the cumulative mole of **1** in the copolymer (**P5**) versus the normalized chain length from the semi-batch copolymerization where d[**1**]/dt = 0.20 mmol/min.

Table S10. Data used for the plot in Figure S30.

normalized chain length	mole fraction **1**
0.079	0
0.36	0.029
0.47	0.16
0.56	0.19
0.69	0.19
0.77	0.32
0.83	0.34
1	0.33

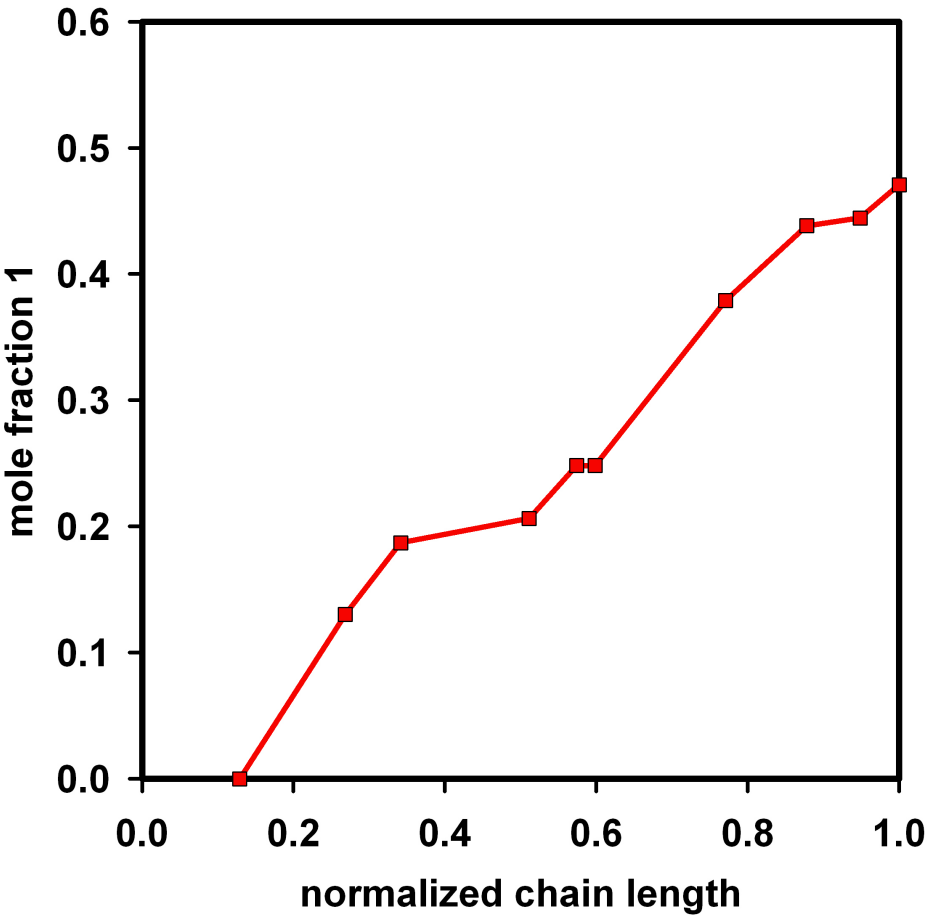

Figure S31. Plot of the cumulative mole fraction of **1** in the copolymer (**P6**) versus the normalized chain length from the semi-batch copolymerization where d[**1**]/dt = 0.28 mmol/min.

Table S11. Data used for the plot in Figure S31.

normalized chain length	mole fraction **1**
0.13	0
0.27	0.13
0.34	0.19
0.51	0.21
0.57	0.25
0.60	0.25
0.77	0.37
0.88	0.43
0.95	0.44
1	0.47

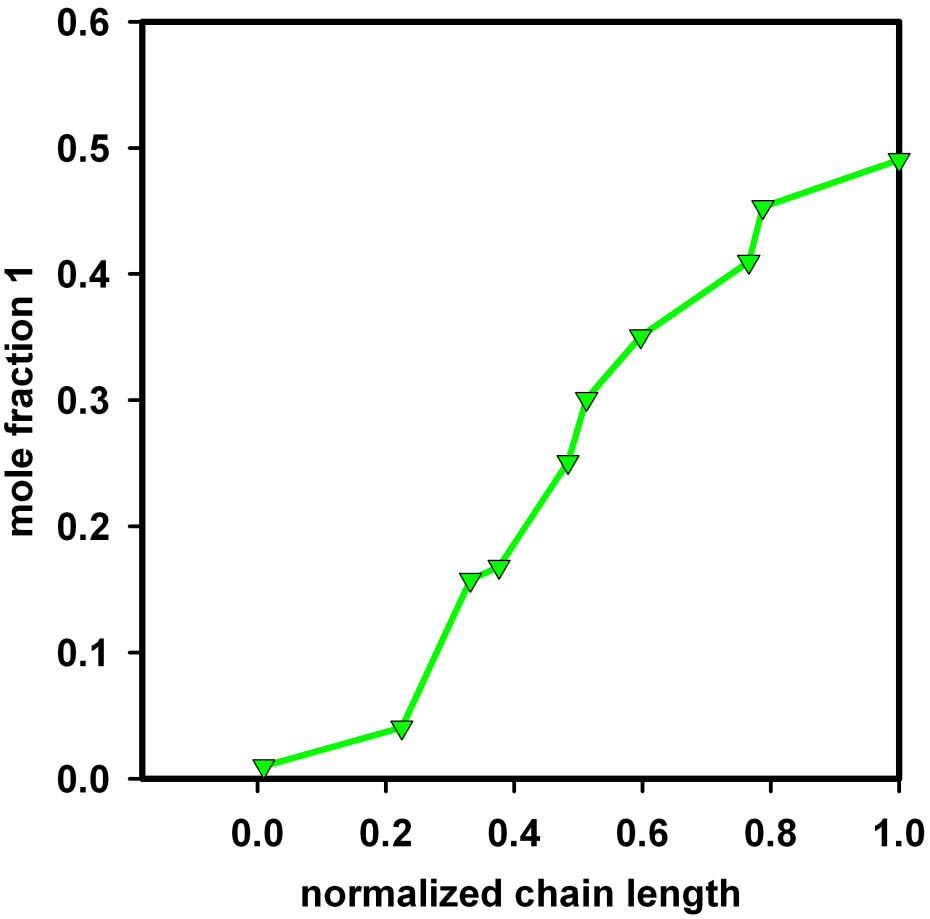

Figure S32. Plot of the cumulative mole fraction of **1** in the copolymer (**P7**) versus the normalized chain length from the semi-batch copolymerization where d[**1**]/dt = 0.40 mmol/min.

Table S12. Data used for the plot in Figure S32.

normalized chain length	mole fraction **1**
0.23	0.041
0.33	0.16
0.38	0.17
0.48	0.25
0.51	0.30
0.60	0.35
0.77	0.41
0.79	0.45
1	0.49

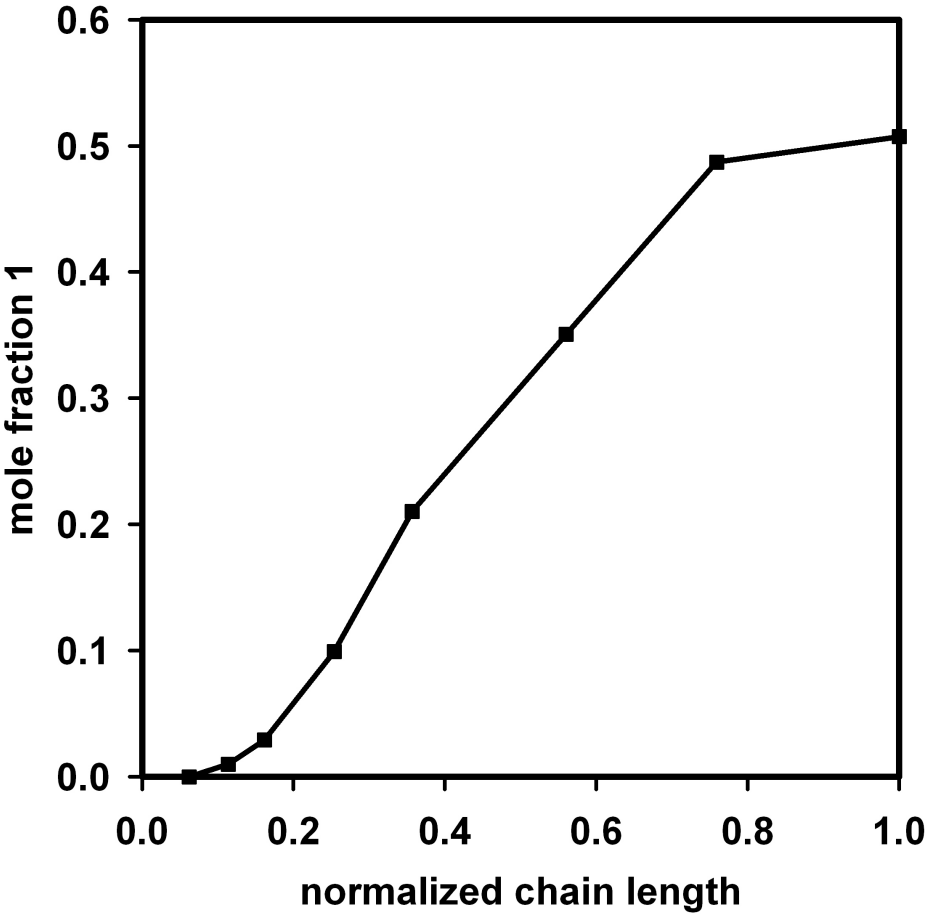

Figure S33. Plot of the cumulative mole fraction of **1** in the copolymer (**P8**) versus the normalized chain length from the semi-batch copolymerization where d[**1**]/dt = 0.48 mmol/min.

Table S13. Data used for the plot in Figure S33.

normalized chain length	mole fraction **1**
0.06	0
0.11	0.0010
0.16	0.029
0.25	0.099
0.36	0.21
0.56	0.35
0.76	0.49
1	0.51

X. UV-vis and fluorescence spectroscopy

Solution absorbance and emission spectra:

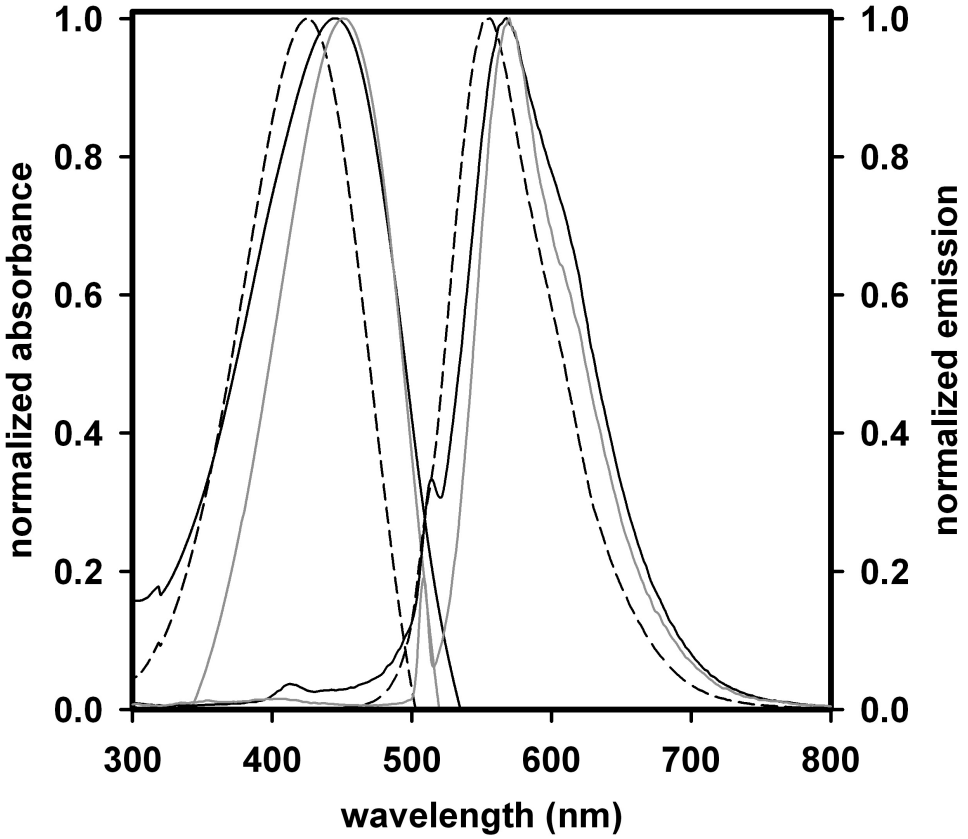

Figure S34. Absorption and emission spectra of p3HT (━), p3HOMT (┈) and block copolymer (━).

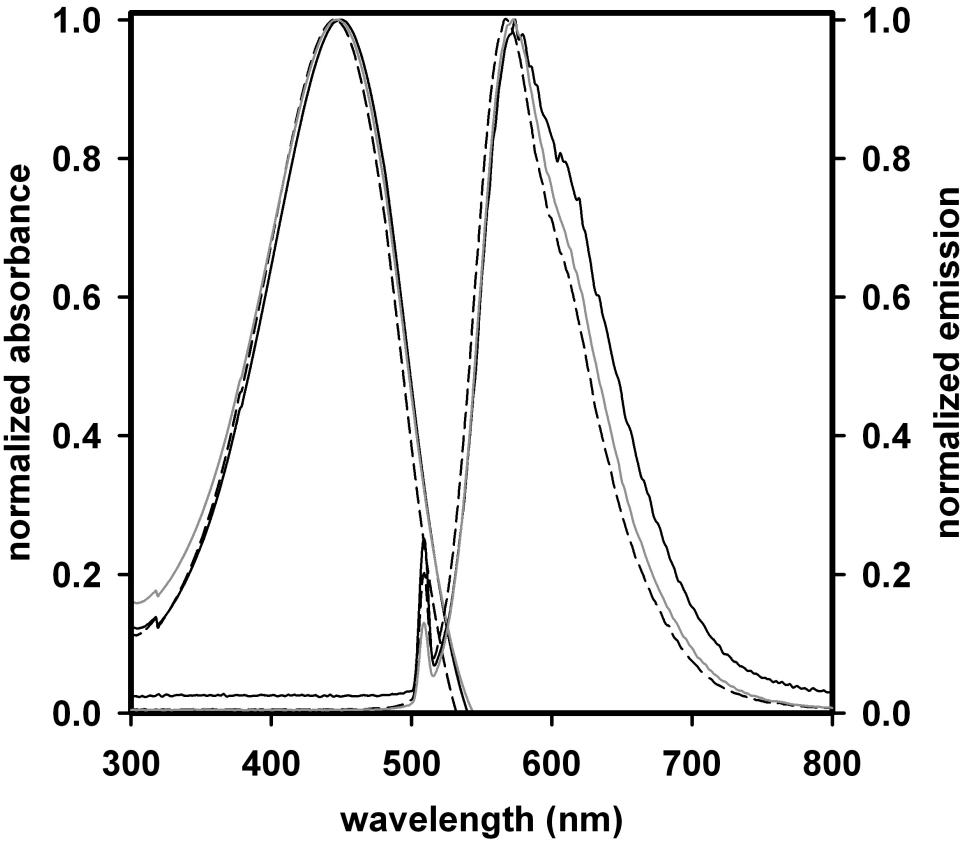

Figure S35. Absorption and emission spectra of **P1** (▬), **P2** (┈┈) and **P3** (▬) .

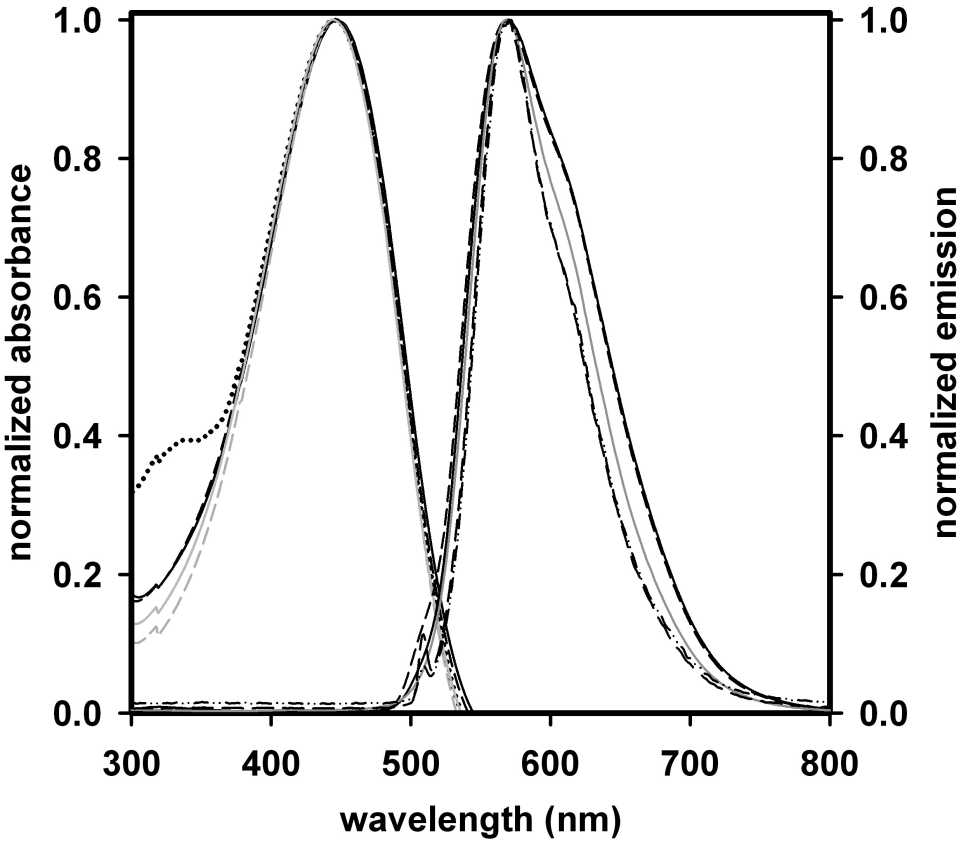

Figure S36. Absorption and emission spectra of **P4** (—), **P5** (- - -), **P6** (····), **P7** (—) and **P8** (- - -).

Thin-film absorbance spectra:

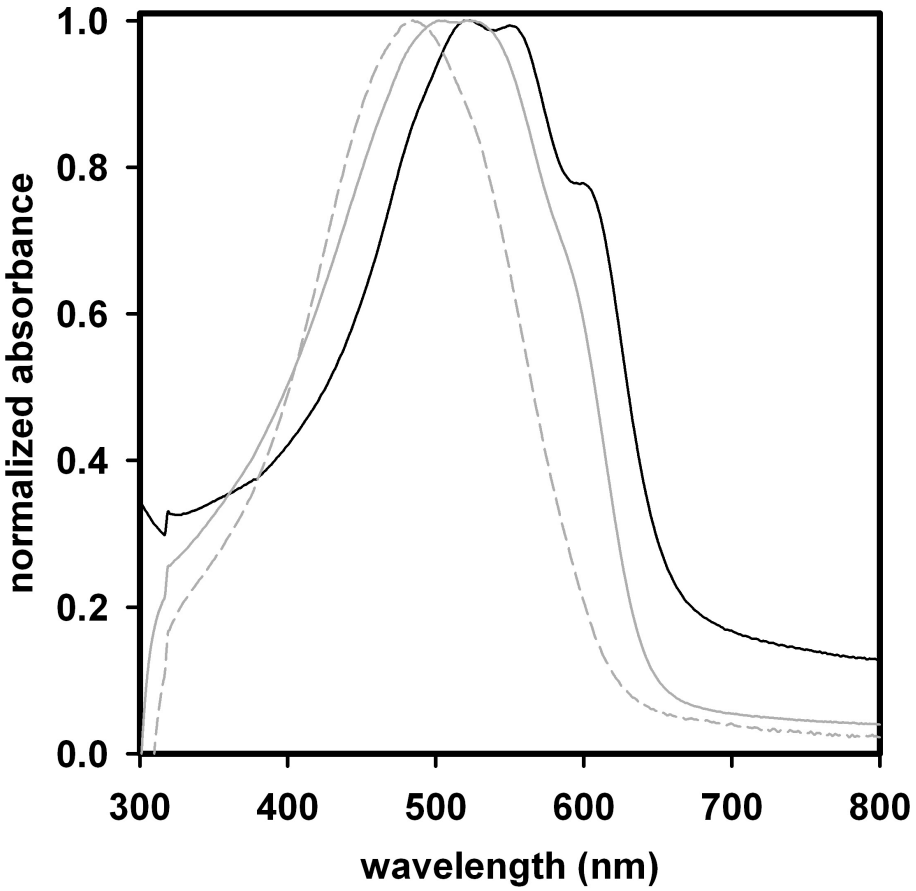

Figure S37. Absorption spectra of thin films of p3HT (━), p3HOMT (┈), and block copolymer (━).

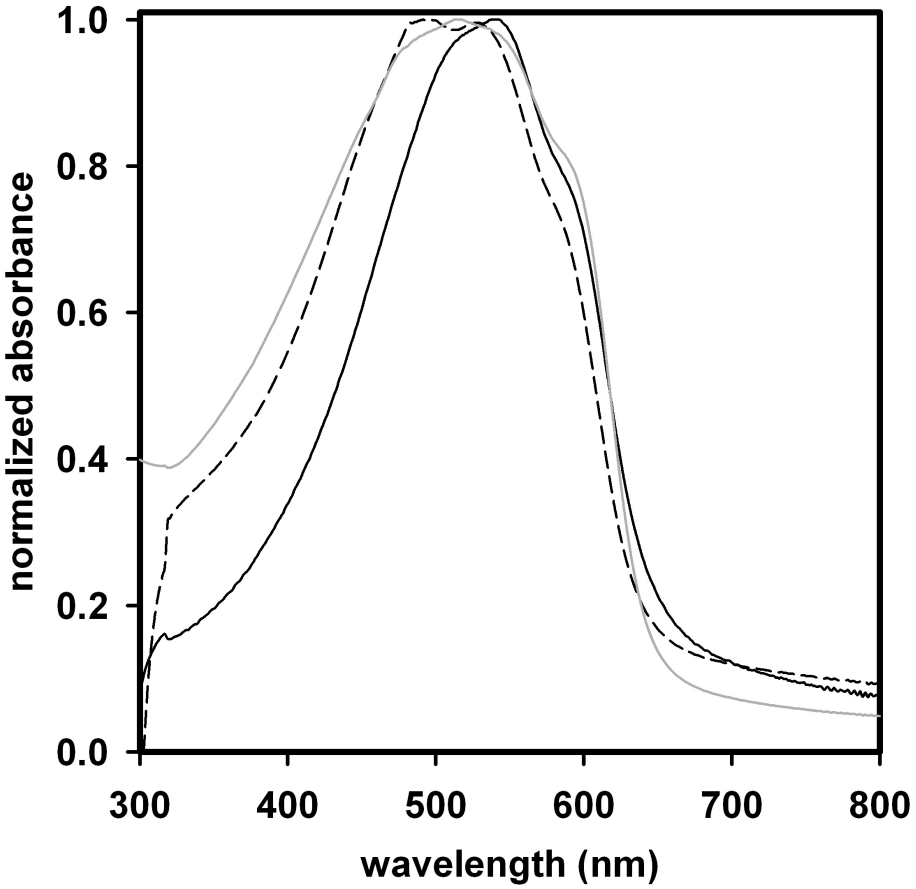

Figure S38. Absorption spectra of thin films of **P1** (▬), **P2** (····) and **P3** (▬).

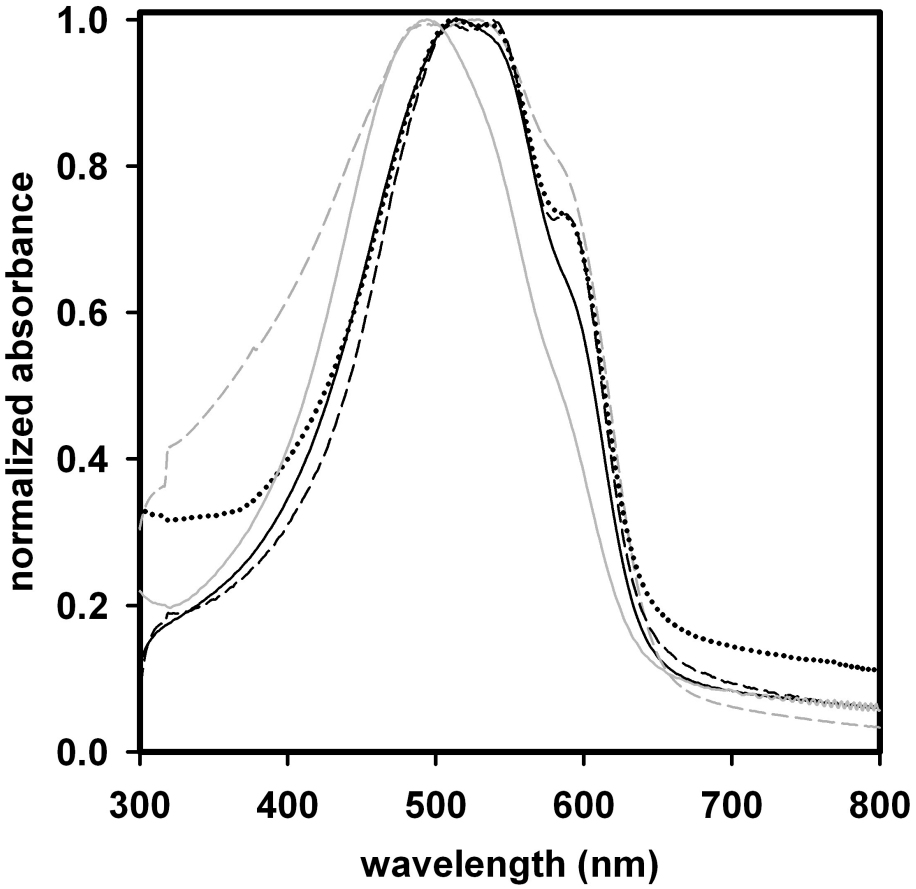

Figure S39. Absorption spectra of thin films of **P4** (▬), **P5** (▬▬), **P6** (····), **P7** (▬) and **P8** (▬▬).

XI. Differential Scanning Calorimetry

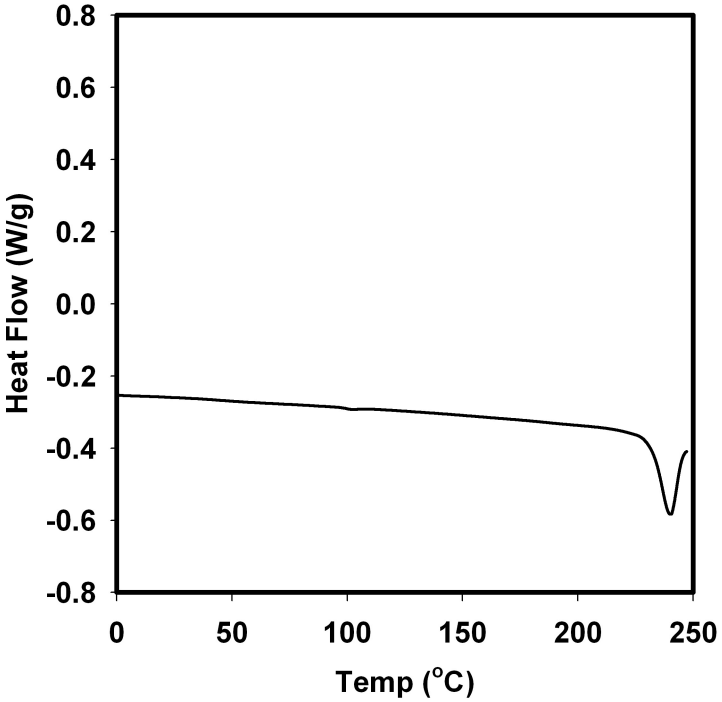

Figure S40. DSC heating curve for p3HT.

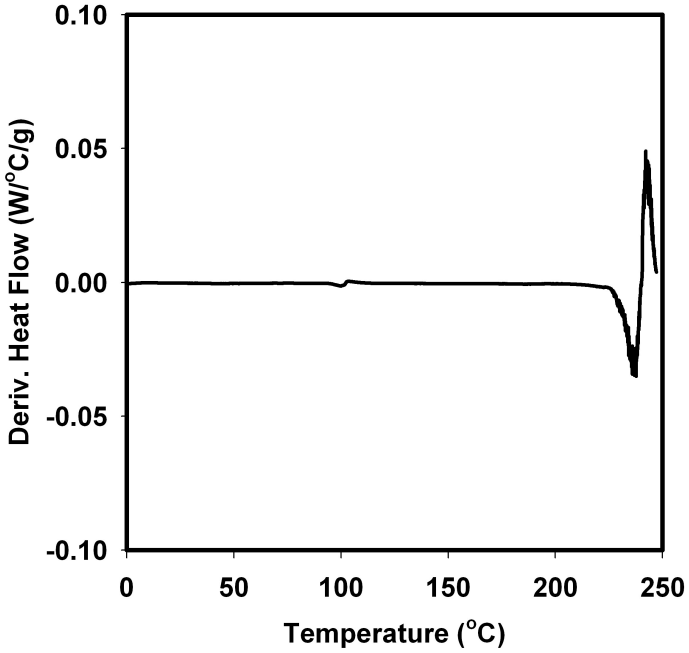

Figure S41. Derivative of the DSC heating curve for p3HT.

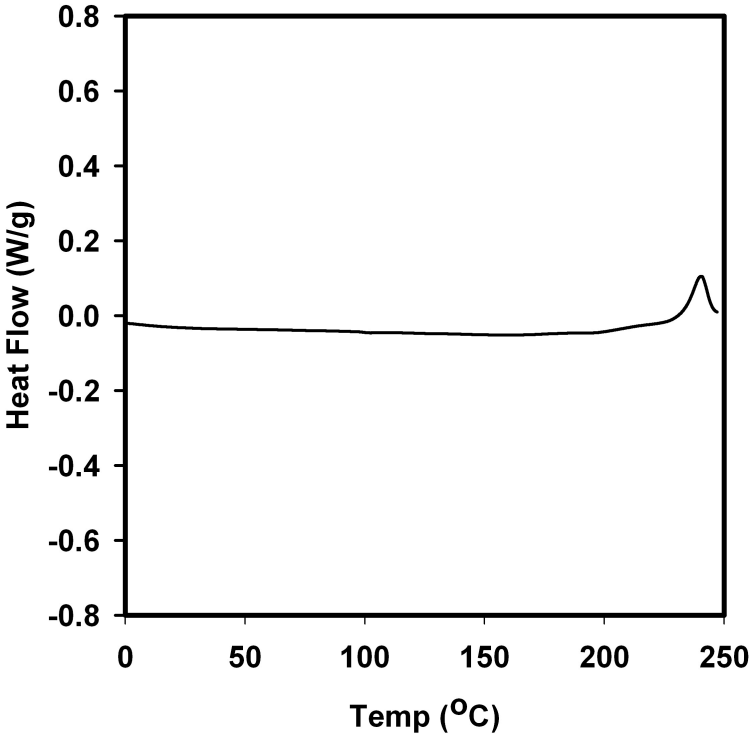

Figure S42. DSC heating curve for p3HOMT.

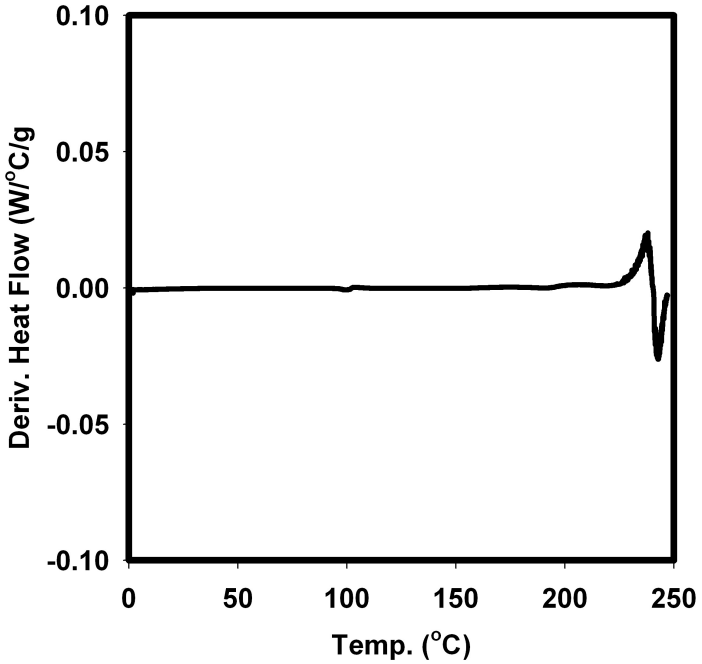

Figure S43. Derivative of the DSC heating curve for p3HOMT.

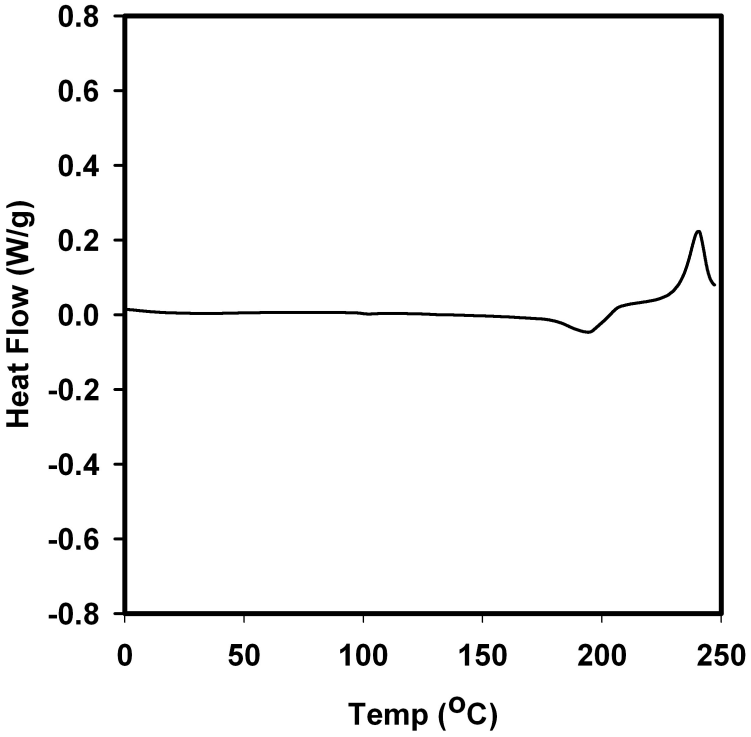

Figure S44. DSC heating curve for **P1**.

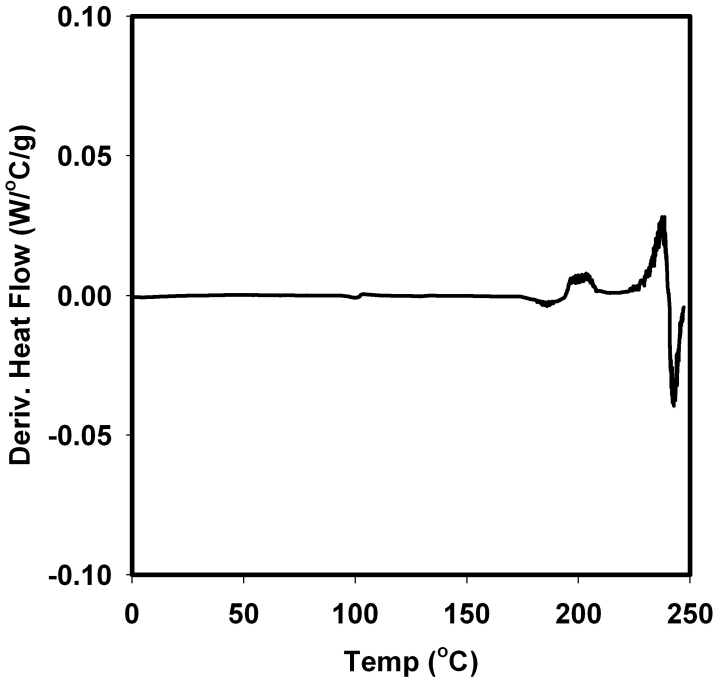

Figure S45. Derivative of the DSC heating curve for **P1**.

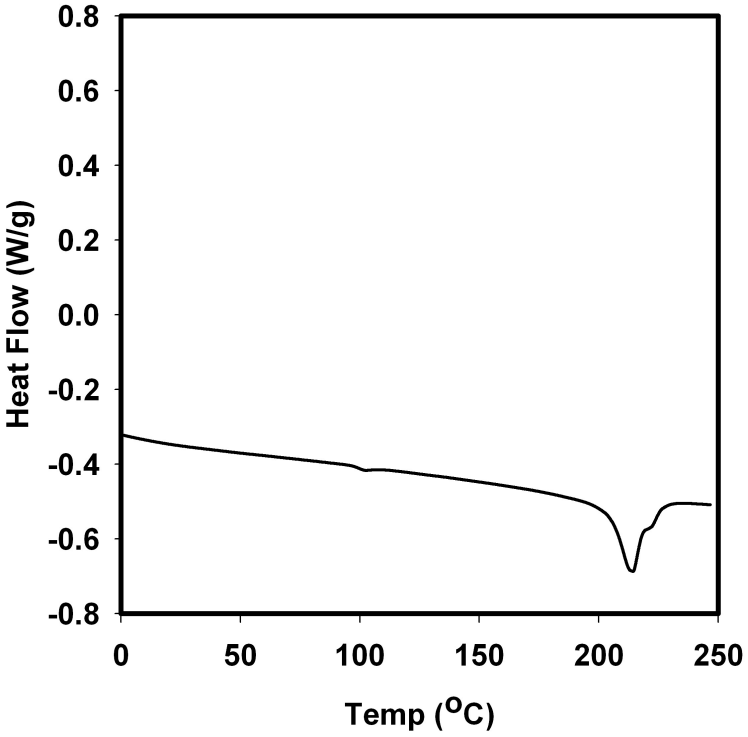

Figure S46. DSC heating curve for **P2**.

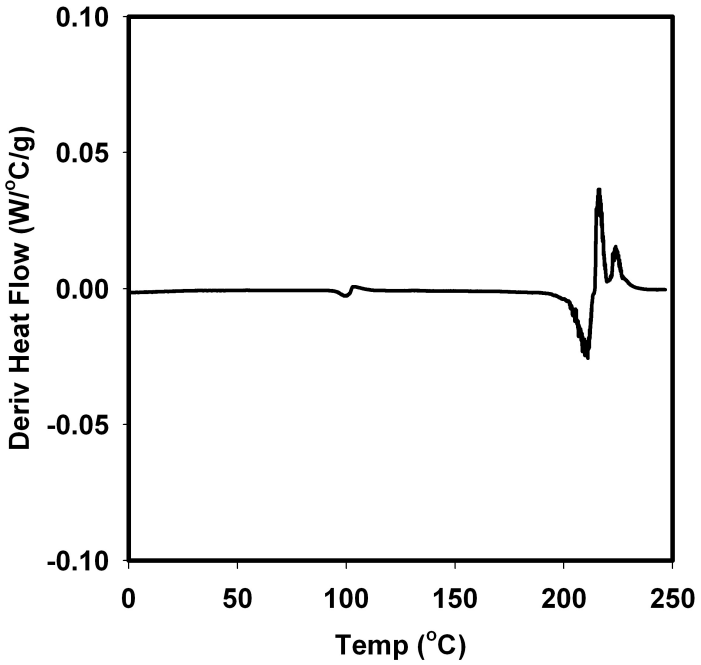

Figure S47. Derivative of the DSC heating curve for **P2**.

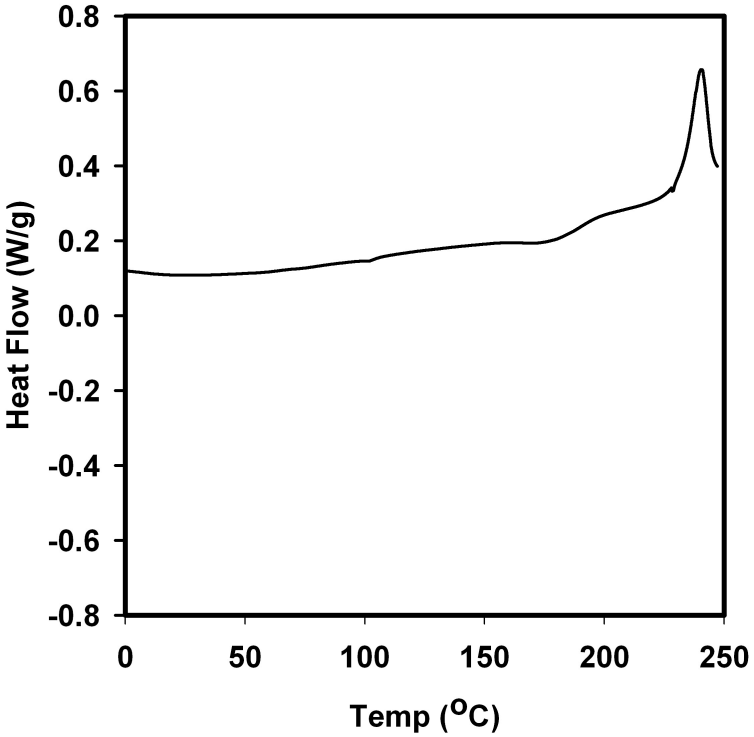

Figure S48. DSC heating curve for **P3**.

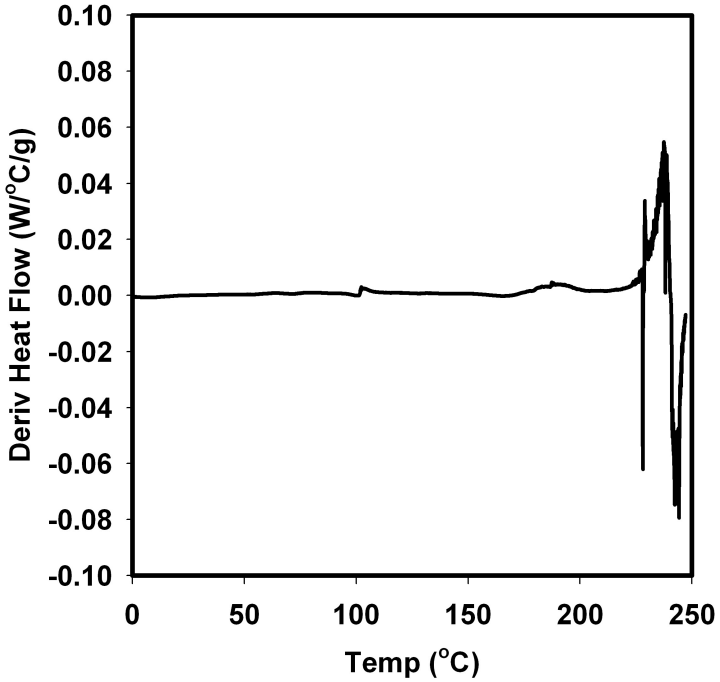

Figure S49. Derivative of the DSC heating curve for **P3**.

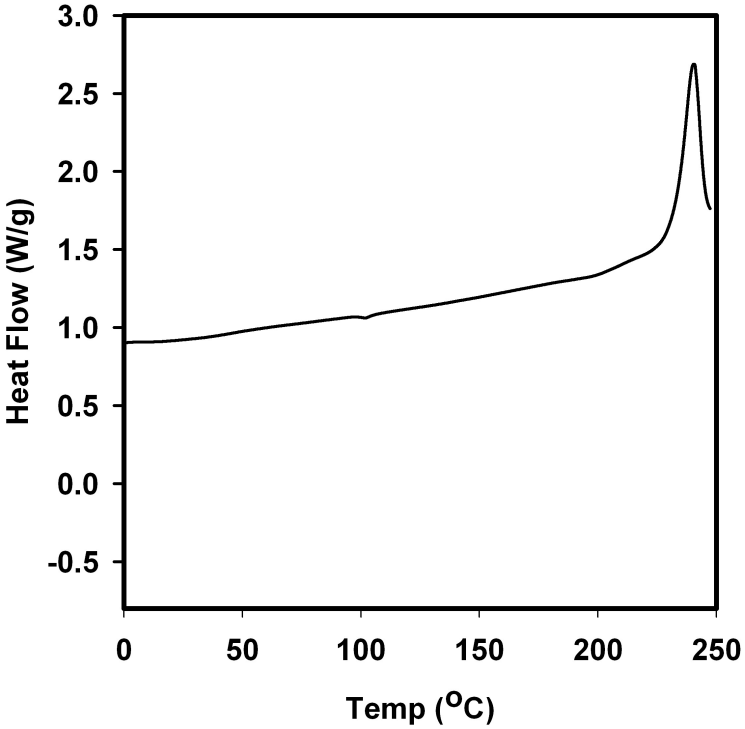

Figure S50. DSC heating curve for **P7**.

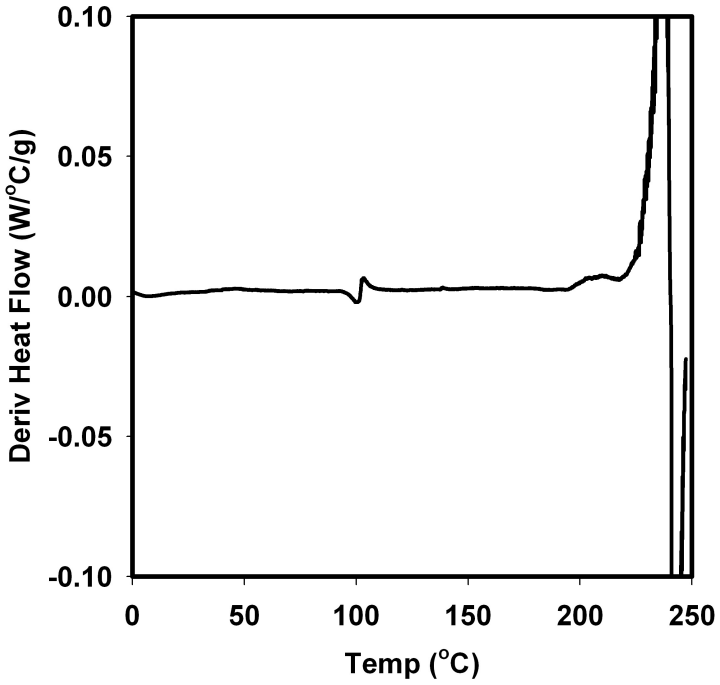

Figure S51. Derivative of the DSC heating curve for **P7**.

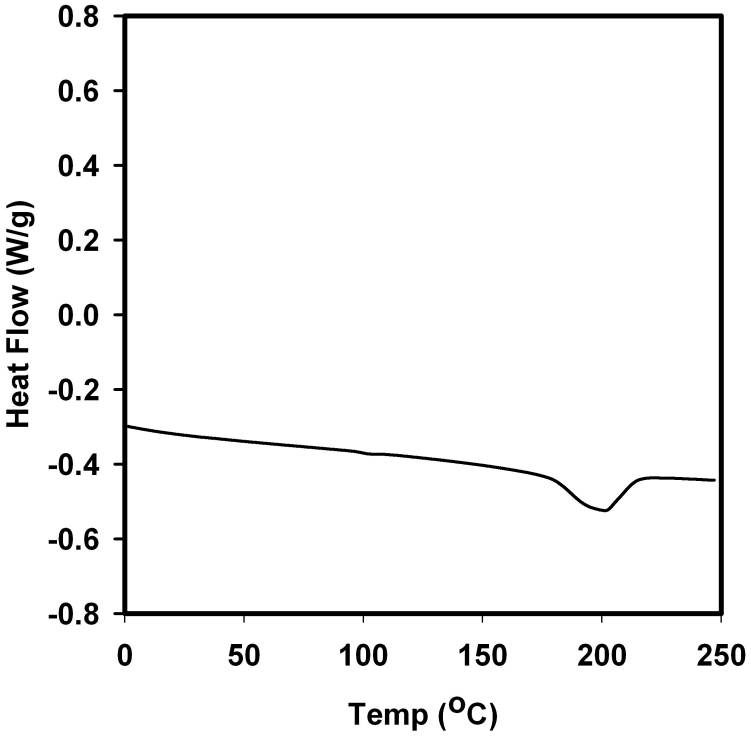

Figure S52. DSC heating curve for **P8**.

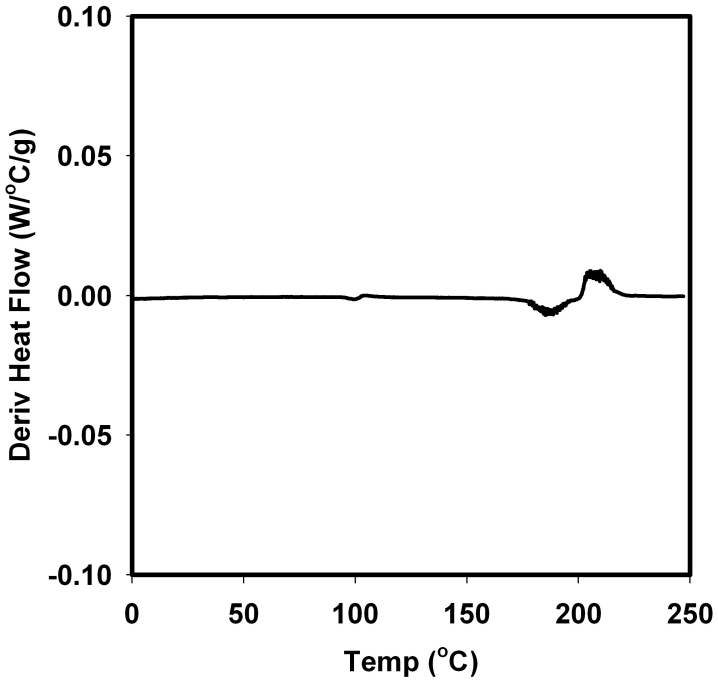

Figure S53. Derivative of the DSC heating curve for **P8**.

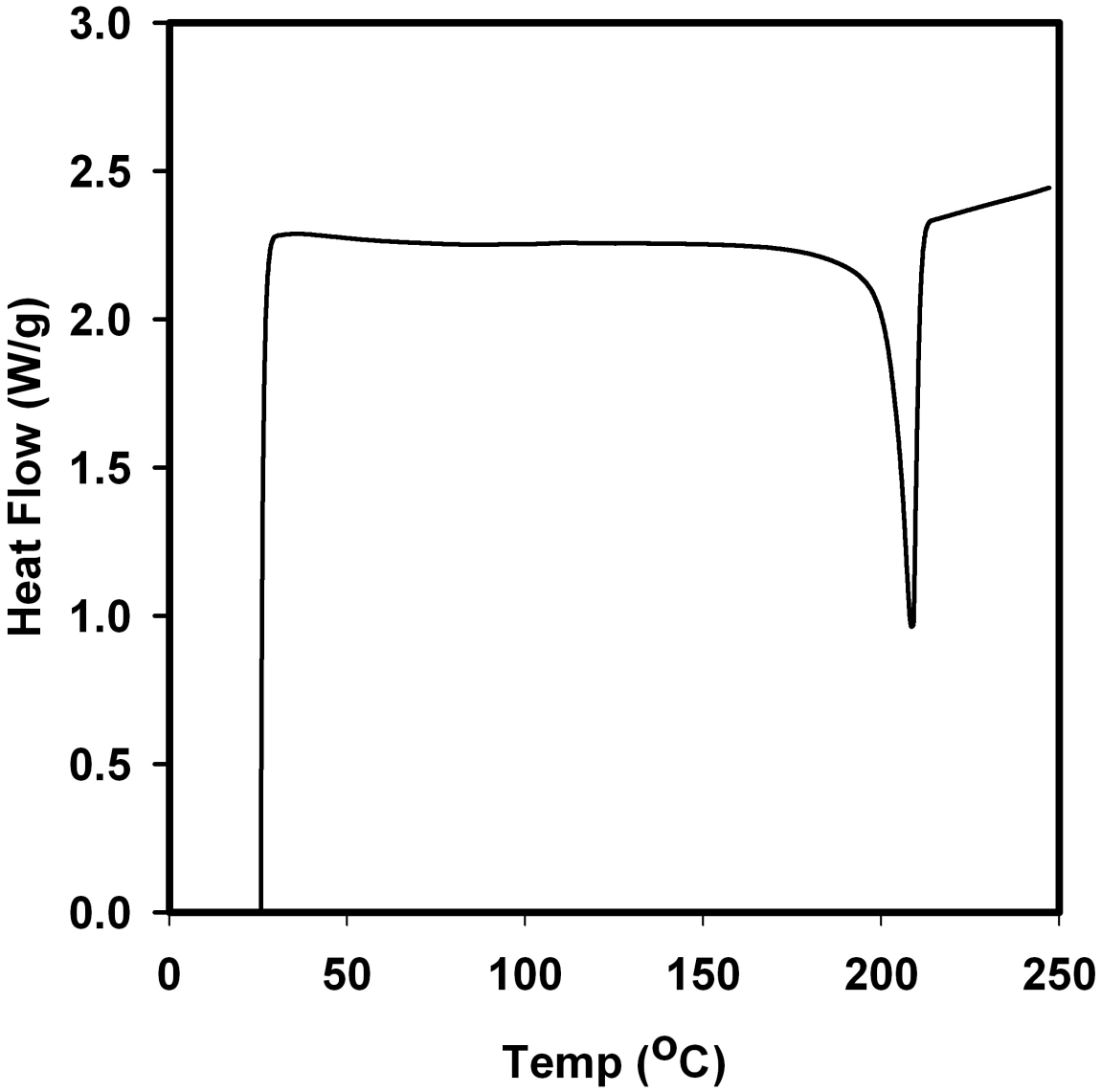

Figure S54 DSC heating curve for block copolymer M_n = 50 kDa, PDI = 1.21

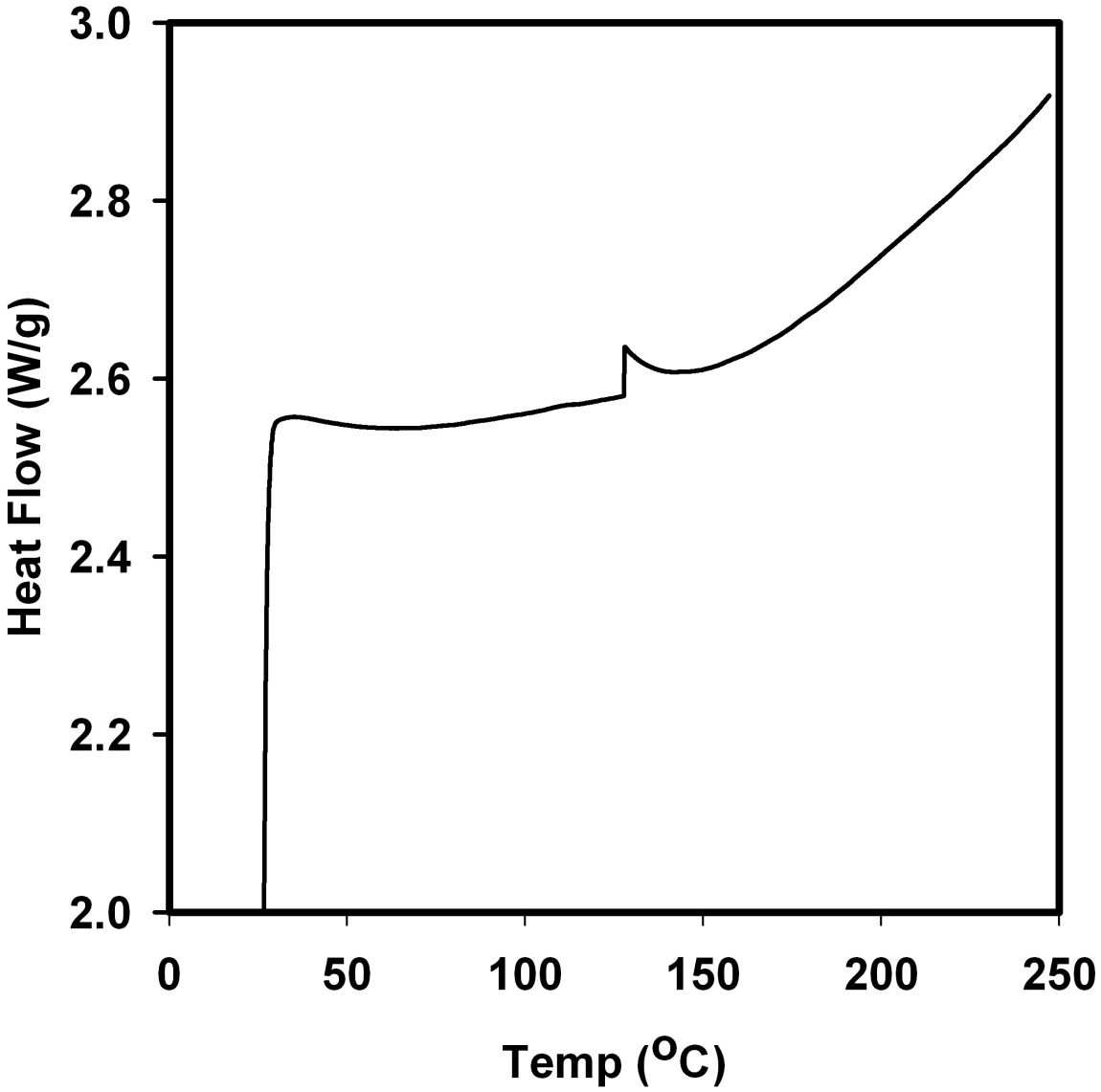

Figure S55 DSC heating curve for random copolymer M_n = 45 kDa, PDI = 1.16

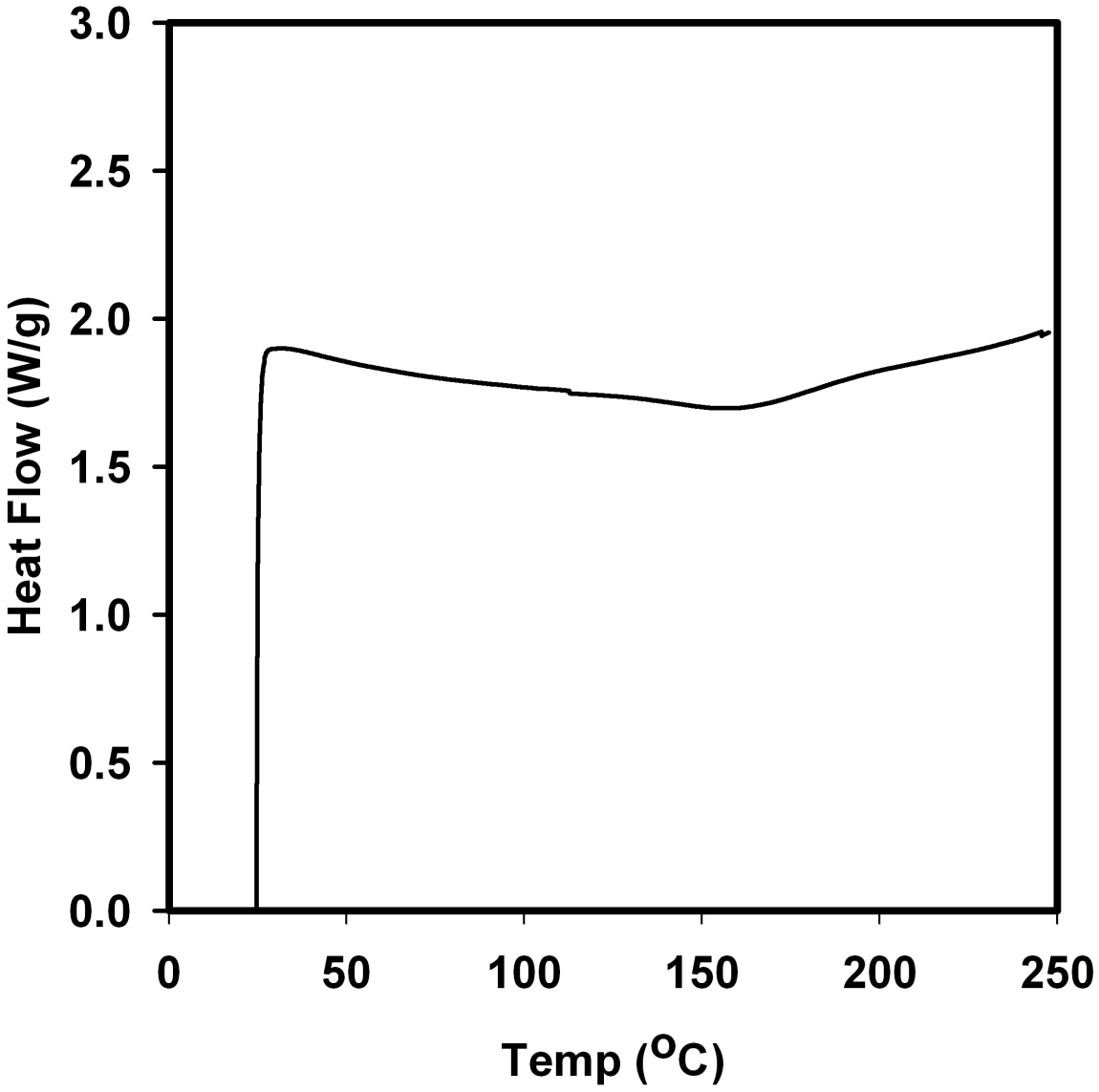

Figure S56 DSC heating curve for gradient copolymer M_n = 47 kDa, PDI = 1.23